PB84-158153

Simulation Model for Watershed Management Planning. Volume 1 Model Theory and Formulation

Colorado State Univ., Fort Collins

Prepared for

Environmental Research Lab., Athens, GA

Feb 84

U.S. Department of Commerce
National Technical Information Service
NTIS

EPA-600/3-84-028a
February 1984
PB84-158153

SIMULATION MODEL FOR WATERSHED MANAGEMENT PLANNING
Volume I: Model Theory and Formulation

by

Daryl B. Simons
Ruh-Ming Li
Kenneth G. Eggert
Jimmy Nan-Hsiung Ho
William T. Fullerton
V. M. Ponce
Nguyen Duong
Civil Engineering Department
Engineering Research Center
Colorado State University
Fort Collins, Colorado 80523

Grant No. 805131-01

Project Officer

Lee A. Mulkey
Technology Development and Applications Branch
Environmental Research Laboratory
Athens, Georgia 30613

ENVIRONMENTAL RESEARCH LABORATORY
OFFICE OF RESEARCH AND DEVELOPMENT
U.S. ENVIRONMENTAL PROTECTION AGENCY
ATHENS, GEORGIA 30613

REPRODUCED BY
NATIONAL TECHNICAL
INFORMATION SERVICE
U.S. DEPARTMENT OF COMMERCE
SPRINGFIELD, VA. 22161

TECHNICAL REPORT DATA
(Please read Instructions on the reverse before completing)

1. REPORT NO.
EPA-600/3-84-028a

2.

3. RECIPIENT'S ACCESSION NO.
PB84 158153

4. TITLE AND SUBTITLE
Simulation Model for Watershed Management Planning,
Volume I: Model Theory and Formulation

5. REPORT DATE
February 1984

6. PERFORMING ORGANIZATION CODE

7. AUTHOR(S)
Daryl B. Simons, Ruh-Ming Li, Kenneth G. Eggert, Richard Miskimins, William T. Fullerton, Jimmy Nan-Hsiung Ho V. M. Ponce, and Nguyen Duong

8. PERFORMING ORGANIZATION REPORT NO.

9. PERFORMING ORGANIZATION NAME AND ADDRESS
Civil Engineering Department
Engineering Research Center
Colorado State University
Fort Collins CO 80523

10. PROGRAM ELEMENT NO.
CARB1A

11. CONTRACT/GRANT NO.
805131

12. SPONSORING AGENCY NAME AND ADDRESS
U.S. Environmental Protection Agency--Athens GA
Office of Research and Development
Environmental Research Laboratory
Athens GA 30613

13. TYPE OF REPORT AND PERIOD COVERED
Final, 4/77-10/80

14. SPONSORING AGENCY CODE
EPA/600/01

15. SUPPLEMENTARY NOTES
Volume II: Model User Manual

16. ABSTRACT

Evaluation of nonpoint source pollution problems requires an understanding of the behavioral response to an ecosystem to the impacts of land use activities on individual components of that ecosystem. By analyzing basic ecosystem processes and impacts of land use activities on specific factors governing production and transport of nonpoint source pollution, it is possible to predict cause-effect relationships between these activities and water quality. To facilitate these predictions, a simulation model for evaluation of alternative agricultural and silvicultural practices as a function of both environmental and management parameters was developed. The generalized planning model may be used to predict watershed response to land use including both planned management practices and unplanned activities associated with catastrophic events. Nonpoint source pollution from these activities and events may include loading of streams by: sediment from surface erosion, mass wasting, channel bottom and bank erosion; thermal energy; biological oxygen demanding contaminants; organic debris; nutrients and dissolved solids; pesticides; and other waste materials either in solution or adsorbed to sediments. The model consists of a soil-plant-atmospheric water component for adjusting soil moisture as a function of evaporation, evapotranspiration, soil-water hydraulics, and snowmelt; a kinematic wave surface water routing component; a hydraulically based sediment yield component; a subsurface flow component; a pollutant routing routine; and streambank erosion and forest litter routing routines.

17. KEY WORDS AND DOCUMENT ANALYSIS

a. DESCRIPTORS	b. IDENTIFIERS/OPEN ENDED TERMS	c. COSATI Field/Group

18. DISTRIBUTION STATEMENT RELEASE TO PUBLIC	19. SECURITY CLASS *(This Report)* UNCLASSIFIED	21. NO. OF PAGES 211
	20. SECURITY CLASS *(This page)* UNCLASSIFIED	22. PRICE

EPA Form 2220-1 (9-73)

DISCLAIMER

Although the research described in this report has been funded wholly or in part by the United States Environmental Protection Agency through Grant No. 805131-01 to Colorado State University, it has not been subjected to the Agency's required peer and policy review and therefore does not necessarily reflect the views of the Agency and no official endorsement should be inferred.

FOREWORD

As environmental controls become more costly to implement and the penalties of judgment errors become more severe, environmental quality management requires more efficient analytical tools based on greater knowledge of the environmental phenomena to be managed. As part of this Laboratory's research on the occurrence, movement, transformation, impact, and control of environmental contaminants, the Technology Development and Applications Branch develops management or engineering tools to help pollution control officials achieve water quality goals.

Evaluation of nonpoint source pollution problems requires an understanding of the behavioral response of an ecosystem to the impacts of land use activities on individual components of that ecosystem. By analyzing basic ecosystem processes and impacts of land use activities on specific factors governing production and transport of nonpoint source pollution, it is possible to predict cause-effect relationships between these activities and water quality. To facilitate these predictions, a simulation model for evaluation of alternative agricultural and silvicultural practices as a function of both environmental and management parameters was developed.

William T. Donaldson
Acting Director
Environmental Research Laboratory
Athens, Georgia

ABSTRACT

Nonpoint source pollution represents an integration of the behavioral response of an ecosystem to the impacts of land use activities on individual components of the ecosystem. By analyzing basic ecosystem processes and the impacts of forest activities on specific processes governing production of nonpoint source pollution, it is possible to predict cause-effect relationships between forest activities and water quality. To predict nonpoint source pollution on upland forested watersheds, a simulation model for evaluation of alterentive forest management practices as a function of both environmental and management parameters is presented. The model also permits the evaluation of alternative agricultural practices.

The simulation may be used to predict watershed response to forestry and farming activities including both planned management practices and unplanned activities associated with catastrophic events. Nonpoint source pollution from these activities and events may include loading of streams by sediment from surface erosion, mass wasting, and channel bottom and bank erosion; thermal energy; biological contaminants, organic debris, nutrients and dissolved solids, and pesticides. The simulation in this report allows estimation of these environmental impacts.

The simulation is composed of seven components: a soil-plant-atmosphere water simulation for adjusting soil moisture as a function of evaporation, evapotranspiration, and soil-water hydraulics; a kinematic wave surface water routing component; a hydraulically based sediment yield model; a subsurface flow component; a temperature and dissolved oxygen component; a nutrient routing for nitrogen and phosphorus compounds; and streambank and forest litter routing routines.

This report was submitted in fulfillment of Grant No. R805131-01 by Colorado State University under the sponsorship of the U.S. Environmental Protection Agency. This report covers the period April 10, 1977, to October 31, 1980, and work was completed as of October 31, 1980.

TABLE OF CONTENTS

Page

Abstract iv

LIST OF FIGURES viii

LIST OF TABLES x

ACKNOWLEDGMENT xi

SECTION 1 - INTRODUCTION 1

SECTION 2 - MODEL STRUCTURE 5
- INTRODUCTION 5
- PROSPER 6
- ENERGY BALANCE 10
- RESISTANCE OF WATER FLOW AND ELECTRICAL ANALOGUE 16
- INFILTRATION AND INTERCEPTION 21
  - Interception 21
  - Infiltration 25
  - Computational Sequence of Infiltration 31
  - Infiltration Parameters 33
- SUMMARY 34
- SYMBOLS FOR SECTION 2 36

SECTION 3 - WATER AND SEDIMENT ROUTING 40
- INTRODUCTION 40
- SUBPROGRAM MULT 44
  - Derivation of Analytial Kinematic Wave Equations 45
  - Sediment Determination 62
    - Overland Sediment Transport Capacity 62
    - Channel Sediment Transport Capacity 69
    - Determination of Sediment Supply 70
    - Determination of Sediment Yield 71
  - SUBPROGRAM SORT 71
  - SUBPROGRAM MCHNL 71
    - Mathematical Derivation of the Numerical Kinematic Routing Procedure 73
    - Channel Infiltration Routine 78
    - Sediment Routing 78
      - Governing Equation for Sediment Routing 80
      - Numerical Procedure for Sediment Routing 80
- SYMBOLS FOR SECTION 3 84

SECTION 4 - NUTRIENT ROUTING 90
- INTRODUCTION 90
- BASIC CONCEPTS FOR NITROGEN AND PHOSPHORUS 92
  - Nitrogen 92
  - Phosphorus 95
- MODEL FORMULATION AND STRUCTURE 96
  - Description of Conceptual Model 96
  - Biological Conversion Processes 99

TABLE OF CONTENTS (continued)

Page

Mineralization 99
Nitrification 101
Denitrification 103
Plant Uptake 104
Adsorption-Desorption 104
Adsorption-Desorption for Ammonium 105
Adsorption-Desorption for Ortho-Phosphorus 106
Sediment as a Pollutant Transport Medium 107
Nutrient Loading Function 110
Mass Balance Equations for Nutrient Model 114
Coupled System of Differential Equations for Phosphorus . 116
Model Structure 117

SECTION 5 - TEMPERATURE AND DISSOLVED OXYGEN ROUTING 119
INTRODUCTION 119
GOVERNING PROCESS FOR TEMPERATURE AND DISSOLVED OXYGEN 120
Concept and Governing Factors for Thermal Loading 120
Concept and Governing Factors for Dissolved Oxygen 121
MODEL FORMULATION AND STRUCTURE 122
Temperature Loading Modeling 123
Canopy-Ground Cover Processes 125
Surface Runoff Processes 126
Dissolved Oxygen Loading Model 128
Model Structure 131
SYMBOLS FOR SECTION 5 134

SECTION 6 - STREAMBANK EROSION 137
INTRODUCTION 137
STREAMBANK EROSION 138
STREAMBANK EROSION BY CHANNEL WIDENING 140
MODELING STREAMBANK EROSION BY CHANNEL WIDENING 142
LIMITATIONS OF THE MODEL 145
SUMMARY 145
SYMBOLS FOR SECTION 6 146

SECTION 7 - THE RILLING PROCESS AND FOREST LITTER 148
INTRODUCTION 148
RILL AND INTERRILL FLOW 149
Rill Development 150
Rill Density 150
FOREST LITTER LOADING 156
SYMBOLS FOR SECTION 7 158

SECTION 8 - A PLANNING MODEL USING INTERACTIVE SEQUENTIAL GOAL PROGRAMMING 160
INTRODUCTION 160
CONCEPTUAL DESIGN OF THE SEQUENTIAL MULTI-LEVEL GOAL PROGRAMMING MODEL 162
An Iterative Approach to Goal Programming 164
Approach to Model Simplification for Practical Use 166

TABLE OF CONTENTS (continued)

Page

CONCLUSIONS AND SUGGESTIONS FOR FUTURE RESEARCH 166
SYMBOLS FOR SECTION 8 172

SECTION 9 - SNOWMELT 173
INTRODUCTION 173
SNOWMELT PROCESSES 174
General 174
THERMAL DIFFUSION MODEL 175
ENERGY BALANCE 179
SHORTWAVE RADIATION 179
LONGWAVE RADIATION 183
WATER BALANCE 184
POTENTIAL EVAPOTRANSPIRATION 184
SOIL MANTLE RECHARGE 185
MELT WATER RUNOFF 186
SYMBOLS FOR SECTION 9 188

REFERENCES 190

LIST OF FIGURES

Figure		Page
1	Schematic of water flux calculation of PROSPER	7
2	Schematic of HYDROL	11
3	General flow chart of subprogram HYDROL	12
4	Transformation of rainfall hyetograph by interception	24
5	Location of wetting front with respect to soil layers	26
6	Average capillary suction head as a function of initial moisture content	35
7	Transformation of topographic map into watershed geometric representation	42
8	Method of characteristics solution domain illustrating calculation of characteristics in downstream direction	49
9	Method of characteristics solution domain illustrating a set of characteristics for an arbitrary excess rainfall histogram	51
10	Definition sketch of triangular channel	54
11	Method of characteristics solution domain illustrating upstream calculation of characteristics between bounding characteristics previously calculated in downstream direction	61
12	Method of characteristics solution domain illustrating effect of negative rainfall excess rates	63
13	Assumed variation of overall resistance with ground cover. . . .	65
14	Spatial to temporal reorganization of runoff events by SORT	72
15	Definition sketch for channel water and sediment finite difference routing scheme	75
16	Flowchart of nitrogen cycle calculation, Program NUTRINT	97
17	Flowchart of phosphorus cycle calculation, Program NUTRINT . . .	98
18	Partition coefficient procedure	112
19	Flow chart for thermal and dissolved oxygen model	133
20	Schematic of rill pattern model	153

LIST OF FIGURES (continued)

Figure Page

21 Overall structure of proposed planning model 163

22 Flow chart for linear goal planning algorithm 167

23 Finite difference grid for snowpack temperature 177

LIST OF TABLES

Table Page

1 VARIOUS SPECIES OF NITROGEN AND THEIR OXIDATION STATE 93

2 TOTAL POLLUTANT IN MIXTURE VOLUME FOR NITROGEN CYCLE 111

3 TOTAL POLLUTANT IN MIXTURE VOLUME FOR PHOSPHATE CYCLE 111

ACKNOWLEDGMENTS

The authors wish to thank the production staff at the Engineering Research Center for their efforts in preparing this report. Annette Ward, Tamra McFall, and Janna Fullerton checked, edited and prepared the report for publication. Lee Mulkey was the Project Officer for this study from the Environmental Protection Agency, Athens, Georgia, Laboratory. The assistance of all these individuals is greatly appreciated with special thanks to the technical typing personnel.

SECTION 1

INTRODUCTION

The theoretical foundation of the watershed simulation component of the generalized planning model for evaluation of alternative management practices is described in this report. The model is a cause-effect simulation based on mathematical descriptions of watershed processes related to non-point source pollution. Non-point source pollution represents an integration of the behavioral response of the ecosystem to the impacts of land use activities on individual components of the ecosystem. Forestry activities include both planned management practices such as timber production and harvest, road construction, watershed management, stream improvement, low head impoundments, application of pesticides and fertilizers, foliage production and grazing, mechanical site preparation, and controlled burning and unplanned activities associated with catastrophic events such as wildfire or large runoff events. Non-point source pollution from these activities and events may include loading of streams by: 1) sediment from surface erosion as well as channel bottom and bank erosion, 2) thermal energy, 3) dissolved oxygen, 4) forest litter, and 5) nitrogen and phosphorus compounds.

Obviously, there are a number of possible formulations for each of the subcomponents of such a model; however, general criteria for the development of a generalized planning model were specified by the U.S. Environmental

Protection Agency. These general criteria were used as guidelines for the selection of all model components and are listed below:

1) Temporal resolution should be both short- and long-term. Forest management for timber production is usually related to tree life. Consequently, any analysis having a time horizon of less than one rotation is inadequate for proper long-range timber management planning, and the temporal resolution for long-range plans should be 20 to 40 years.

2) Specific management plans and activities are very often limited to small watersheds. Most watersheds subject to legal requirements for water quality management are quite large and often encompass complete river basins or sub-basins. As a consequence, spatial resolution should accommodate small watersheds within river systems as a whole.

3) The model should be widely applicable, i.e., regional specificity should be reflected in model parameters, not in the model itself. The only feasible way to develop such a model is to consider the physical significance of the governing processes. Only such a physically-based model can provide an appropriately general cause-effect relationship between forest activities and water quality.

4) The model should be oriented for use by land management personnel. This would require documentation with a user guide.

5) The overall planning model should provide flexibility to managers for treating various multiple resource output and pollution concerns as either goals or constraints.

In addition to the above criteria, some additional guidelines were adapted for model subcomponent development: 1) models should use the simplest approximations of physical processes that provide accurate representation without sacrificing necessary sensitivity to management criteria, and 2) implementation of theory should provide routines that are efficient in computer time and computer memory requirements. To satisfy these guidelines whenever possible, formulations are used that lead to equations having analytical solutions. Usually an analytical solution to a system of equations or a particular differential equation results in a more efficient algorithm than a numerical approach. As will be shown in the case of water routing, however, boundary condition requirements often dictate the circumstances under which an analytical solution may be applied.

The model presented in this report contains the following specific hydrologic components: 1) daily water balance, evapotranspiration, vertical soil water movement, and snowmelt, 2) water routing in watersheds and channels, 3) sediment routing in watersheds and channels, 4) thermal loading, 5) dissolved oxygen routing, 6) forest litter loading, and 7) nitrogen and phosphorus loading. The model will be addressed specifically to forest activities involving timber harvest, timber planting and replacement, grazing, mechanical site preparation, and prescribed fire. Alone or in combination, these activities constitute the substance of many planned management practices in the forest environment. Examples of the application of the model to such activities will be included in a separate user's manual.

This report is subdivided into nine sections. Section 2 discusses the water balance and infiltration subprogram. This section incorporates hydrologic processes of evapotranspiration, evaporation, energy balance, infiltration, interception, and vertical soil water movement. Routing of storm water runoff and the accompanying sediment yield is developed in Section 3. The theory described in this section covers application of the kinematic wave approximation to a system of subwatershed units and methods required for integrating subunits into a large watershed. Sections 4 and 5 concern water quality. In Section 6, routing of various nitrogen and phosphorus compounds is described using first-order kinetic theory. Dissolved oxygen and thermal loading based on a mass and energy balance approach are described in Section 5. Section 6 provides a simple method for estimation of sediment quantities derived from streambank erosion. Forest litter loading resulting from storm water runoff is considered in Section 7. The interface with the goal programming component of a generalized planning model is included with a brief description of the goal programming module in Section 8. Finally, the snowmelt processes are discussed in Section 9.

The theory as presented and implemented in the watershed simulation model represents a balanced approach based upon the physical processes mentioned above. Initial testing indicates that simulation is time and memory efficient and has the sensitivity required to fulfill developmental criteria.

SECTION 2

WATER BALANCE

INTRODUCTION

The amount of rainfall which infiltrates the soil is dependent on moisture content or degree of saturation at the beginning of the storm. Since infiltration exerts a fundamental control on the storm water runoff hydrograph, any long-term hydrologic simulation must have a component for calculating the changes in soil moisture content as a function of time. The primary processes affecting the amount of soil moisture are infiltration, percolation, evaporation, evapotranspiration, and drainage. These interrelated processes involve hydrologic, biologic, atmospheric, and soil specific aspects. Therefore, a physically-based water balance model must simulate all of these aspects and properly account for their interrelation.

After searching the literature for an existing water balance model, it was decided to modify and implement the simulation presented by Goldstein and Mankin (1972). This program known as PROSPER has been widely tested in a variety of locations with generally good results (Swift et al., 1975, and Luxmoore et al., 1977) particularly in the deciduous forest biome. The success of these applications is probably based on the flexibility built into the model. It is possible to adapt model subroutines to a particular watershed environment by modifying the methods used to calculate the resistances to water flux through the soil and plant components. A modification of PROSPER forms about 60 percent of the subprogram HYDROL to be discussed in this section. The remaining 40 percent includes a layered soil infiltration component for more precise determination of storm water runoff and a storm water interception routine. Both infiltration and interception components provide greater sensitivity to management activities in the watershed than the original PROSPER and the infiltration routine provides for the interfacing of HYDROL with water and sediment routing and water quality subprograms.

PROSPER

PROSPER is a plant-atmosphere-soil water flux simulation which implements an energy balance and aerodynamic calculation of evapotranspiration using the Penman method with a multilayer Darcian soil model. The model simulates the fluxes of water through the soil and plants in response to atmospheric and solar conditions. The simulation as presented by Goldstein, Mankin, and Luxmoore (1974) uses a time increment of one day. All hydrologic, plant, and atmospheric processes are averaged on a daily basis. The model as implemented uses an electrical circuit analogue for the soil and plant system. Current in the circuit loop represents water flux through the respective soil, plant, or atmospheric component. A representation of the program concept as presented by Goldstein, Mankin, and Luxmoore (1974) appears in Figure 2. Detailed equations for the variables in Figure 1 will be discussed in subsections below; however, a general overview describing daily water flux calculation follows immediately. This discussion includes the overall modifications to PROSPER that were made to produce HYDROL, the water balance component of the generalized planning model.

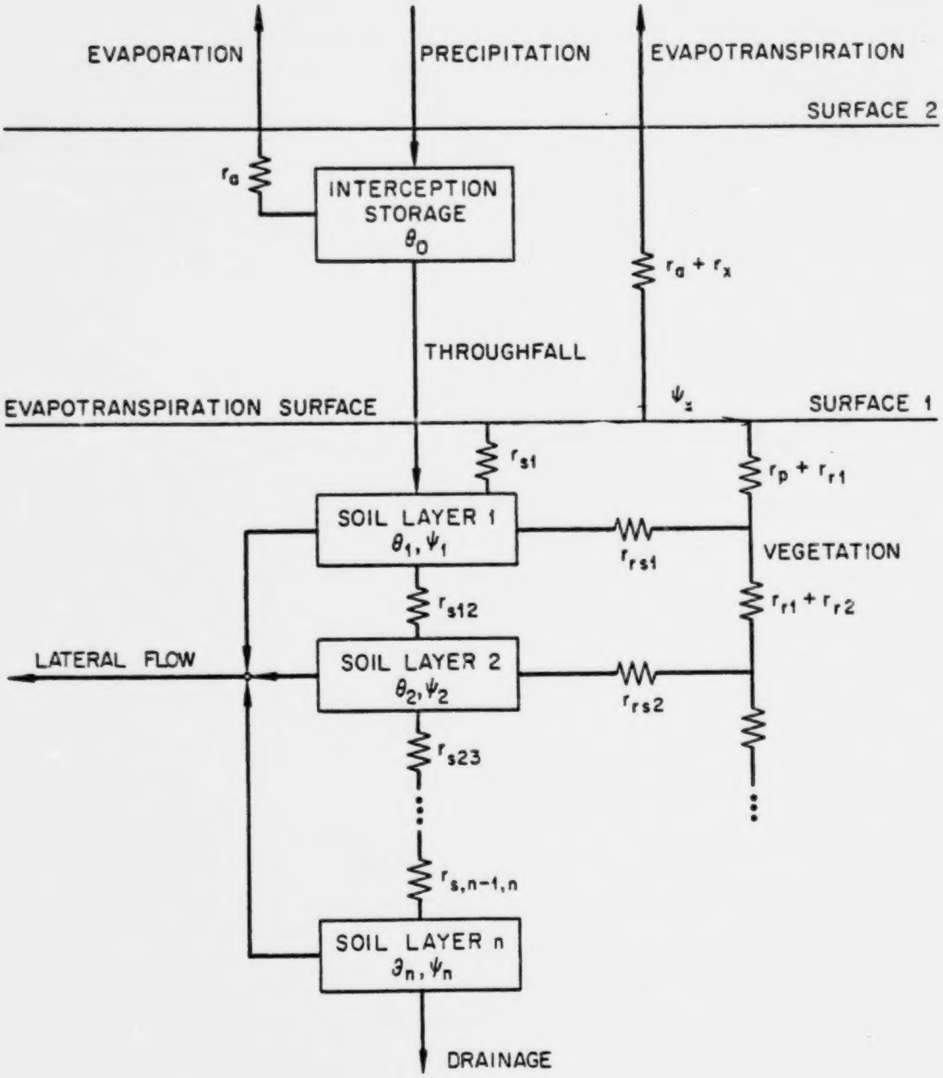
EVAPORATION
PRECIPITATION
EVAPOTRANSPIRATION
SURFACE 2
r_a
INTERCEPTION STORAGE θ_0
$r_a + r_x$
THROUGHFALL
EVAPOTRANSPIRATION SURFACE
ψ_x
SURFACE 1
r_{s1}
$r_p + r_{r1}$
SOIL LAYER 1 θ_1, ψ_1
r_{rs1}
VEGETATION
r_{s12}
$r_{r1} + r_{r2}$
LATERAL FLOW
SOIL LAYER 2 θ_2, ψ_2
r_{rs2}
r_{s23}
$r_{s,n-1,n}$
SOIL LAYER n θ_n, ψ_n
DRAINAGE

Figure 1. Schematic of water flux calculation of PROSPER (from Goldstein, Mankin, and Luxmoore, 1974).

Variables appearing in Figure 1 are as follows:

θ_o = interception storage

θ_i = volumetric water content of soil layer i

ψ_x = hydraulic potential of the evapotranspiration surface

ψ_i = hydraulic potential of soil layer i; $\psi_i = \psi_{mi} + \psi_{gi}$ where ψ_{mi} and ψ_{gi} are the capillary pressure head and the gravitational head of the ith soil layer respectively

r_{si} = resistance to water flux within soil layer i

r_{sij} = resistance to water flux between the ith and jth layers

r_{ri} = resistance to flux within the roots of the ith soil layer

r_{rsi} = resistance to soil water uptake by the roots of layer i

r_ℓ = litter resistance to vapor flux

r_p = resistance to water flux within the above ground portion of the plant

r_a = resistance to water vapor transfer between the evapotranspiration surface and the atmosphere

r_x = resistance to water vapor release by the evapotranspiration surface.

The basis of the electrical analogue is that water moves through the system driven by differences in hydraulic potential. Resistances to water flux are defined in terms of plant, soil, and litter characteristics. If the potentials and resistances are known, then flux of water through any part of the system may be calculated using standard network analysis techniques. The potential of each soil layer is assumed to be a function of the soil water content and is known from previous calculations or initial conditions. Similarly, resistances to flow in soil layers are functions of the soil and plant conductivities which are again functions of soil layer moisture content. Therefore, at any given time hydraulic potentials and resistances throughout the soil column are known from previous calculations.

The central assumption in model formulation is that there is no storage of water at the evapotranspiration surface, i.e., flow of water to the evapotranspiration surface F_w equals flow of water vapor F_v away from the surface. From aerodynamic considerations to be discussed later, flow away from the surface is a function of both atmospheric phenomena and hydraulic potential of the surface ψ_x. Since as previously stated, ψ_x may be related to soil moisture status through network analysis, equating F_v and F_w leads to an equation that may be solved for ψ_x as a function of soil, plant, and atmospheric processes. With ψ_x known, F_v and changes in soil layer moisture content θ_i may be calculated.

There has been considerable discussion concerning applicability of electrical analogues to the plant transpiration process (Cowan, 1965). Cowan points out that the analogy of current to water flux is intuitive but oversimplistic considering the complex geometry and kinetics of plant tissues. This criticism seems more applicable to a detailed representation of plant physiology. On this scale, lumping the internal complexities and physiological processes of the plant into such a model can yield only the most qualitative results; however, if the simulation problem includes a vegetative stand of great heterogeneity, the averaging of processes in such a model is much more likely to produce good representation. This is particularly true when the emphasis is on daily water fluxes. In this situation, a model that provides at least a qualitative representation may be calibrated to accurately provide daily average fluxes while still reflecting physiological plant responses.

The original PROSPER model was not adequate for calculating infiltration response to storms of varying intensity; however, the model is well-suited to determining all other fluxes. Therefore, PROSPER was joined with a storm-wise interception and infiltration model. The infiltration model is an application to a layered soil of an explicit Green-Ampt formulation presented by Eggert (1976). The interception model removes the volume of rainfall which may be stored by the cover on a given day from the beginning of the storm and compensates for daily interception evaporation losses. The modifications are illustrated in Figure 3, which may be regarded as a schematic representation of HYDROL.

The general computational sequence in HYDROL is to determine net energy available for evapotranspiration and soil evaporation. Based on current moisture status of the soil, values of resistance for the electrical analogue and soil layer potentials are calculated. Then on a time increment basis to be discussed later, evapotranspiration surface potential ψ_x, vapor flux, and change in soil layer moisture status are calculated. On days when a storm causes water to be intercepted or to infiltrate into the soil, interception and infiltration volumes are computed and soil moisture is adjusted accordingly. An explanation of the calculation of each of these program steps follows. A general flow chart for HYDROL appears in Figure 4.

ENERGY BALANCE

HYDROL uses a modification of the Penman method of estimating evapotranspiration. This method is based on determining the energy available for evaporation from an energy budget. Energy balance at the evapotranspiration surface is governed by conservation of energy. An expression of the energy conservation law is

$$\text{Input Energy} - \text{Output Energy} = \Delta \text{ Energy Storage}$$

Although a rigorous breakdown of this conservation equation would include mechanical and chemical forms of energy, for the purpose of evaluating flux of

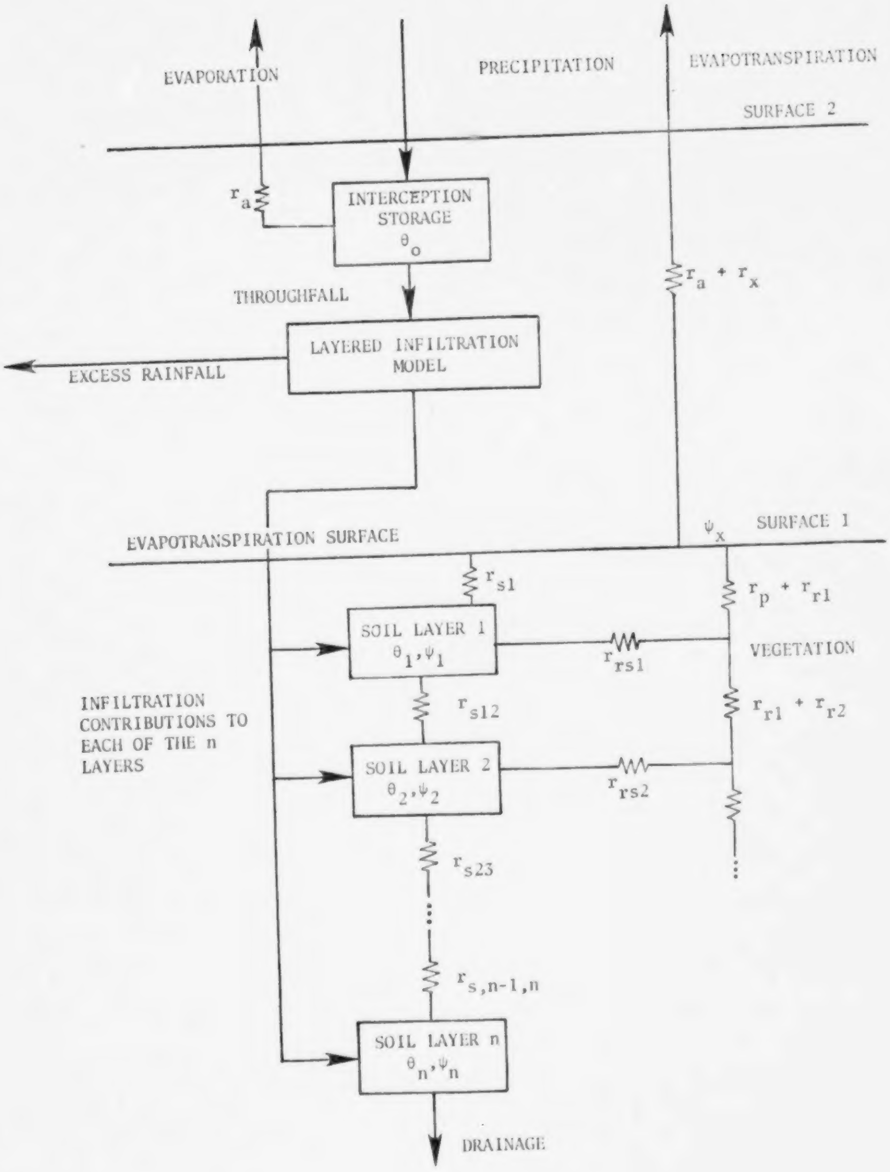
EVAPORATION
PRECIPITATION
EVAPOTRANSPIRATION
SURFACE 2
r_a
INTERCEPTION STORAGE θ_o
$r_a + r_x$
THROUGHFALL
LAYERED INFILTRATION MODEL
EXCESS RAINFALL
EVAPOTRANSPIRATION SURFACE
ψ_x
SURFACE 1
r_{s1}
$r_p + r_{r1}$
SOIL LAYER 1 θ_1, ψ_1
r_{rs1}
VEGETATION
INFILTRATION CONTRIBUTIONS TO EACH OF THE n LAYERS
r_{s12}
$r_{r1} + r_{r2}$
SOIL LAYER 2 θ_2, ψ_2
r_{rs2}
r_{s23}
$r_{s,n-1,n}$
SOIL LAYER n θ_n, ψ_n
DRAINAGE

Figure 2. Schematic of HYDROL.

Reproduced from best available copy.

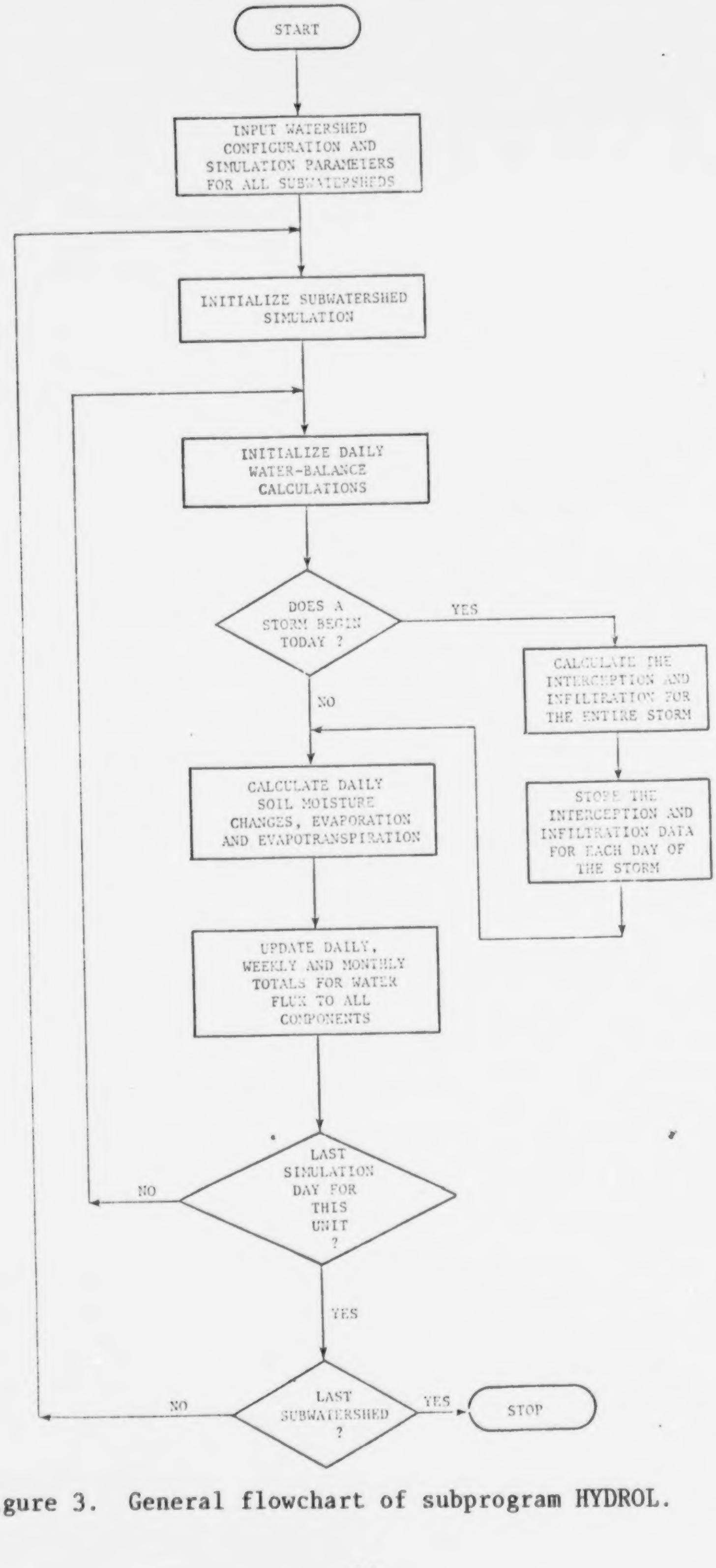

START
INPUT WATERSHED CONFIGURATION AND SIMULATION PARAMETERS FOR ALL SUBWATERSHEDS
INITIALIZE SUBWATERSHED SIMULATION
INITIALIZE DAILY WATER-BALANCE CALCULATIONS
DOES A STORM BEGIN TODAY ?
YES
CALCULATE THE INTERCEPTION AND INFILTRATION FOR THE ENTIRE STORM
STORE THE INTERCEPTION AND INFILTRATION DATA FOR EACH DAY OF THE STORM
NO
CALCULATE DAILY SOIL MOISTURE CHANGES, EVAPORATION AND EVAPOTRANSPIRATION
UPDATE DAILY, WEEKLY AND MONTHLY TOTALS FOR WATER FLUX TO ALL COMPONENTS
LAST SIMULATION DAY FOR THIS UNIT ?
NO
YES
LAST SUBWATERSHED ?
NO
YES
STOP

Figure 3. General flowchart of subprogram HYDROL.

water through the forest system, these energy forms are negligible when compared to the flow of radiant energy and heat. Therefore, the equation of energy conservation may be expressed on a daily basis per unit area for the evapotranspiration surface as follows (Tanner and Pelton, 1960)

$$R_N - A - E - ME = G \qquad (1)$$

where R_N = net daily solar radiation, longwave and shortwave flux

G = daily change in soil heat storage = daily heat flux in or out of the soil

A = sensible heat daily flux

E = latent heat daily flux

ME = all other miscellaneous daily energy fluxes.

Daily sensible heat flux is the flux caused by energy being either conducted or convected away. Daily latent heat flux is the heat flux due to the flow of water vapor evaporated within the system. ME includes miscellaneous heat fluxes such as the chemical energy changes due to photosynthesis that are, in general, negligible in comparison to the other heat fluxes. G is the ground storage energy flux or the daily heat flux in and out of the soil system. Both fluxes R_N and G are usually based on direct measurement. For the present purpose it is assumed that G may be empirically represented as a sinusoidal function whose values and frequency of fluctuation depend on the day of the year and the location of the watershed. The function chosen in this study is fit to data compiled by Van Wijk and De Vries (1966). In this case

$$G = G_m + G_r \sin \left(\frac{2\pi (D - \eta)}{365}\right) \qquad (2)$$

where G_m is the mean value of G for one year, D is the Julian day number, η is a phase shift to compensate for simulation starting time, and G_r is maximum daily heat flux.

Net incoming solar radiation R_N may be estimated by calculation or direct measurement. Direct measurement is preferred because variations in atmospheric conditions introduce large errors into estimates due to changes in transmissivity and optical mass; however, it is possible to estimate solar radiation on the canopy surface as is further discussed in Section 6. For the present discussion R_N is assumed to be directly measured.

Latent heat flux density E may be expressed as the product of latent heat of vaporization and vapor flux $L_v F_v$. As discussed by Goldstein and Mankin (1972), vapor flux F_v may be expressed as a function of vapor density and resistance to flux as

$$F_v = \frac{\rho^*_{w_1} - \rho_{w_2}}{r_a + r_x} = \frac{\rho^*_{w_1} - \rho^*_{w_2}}{r_a + r_x} - \frac{\rho_{w_2} - \rho^*_{w_2}}{r_a + r_x} \tag{3}$$

where $\rho^*_{w_1}$ is saturation water vapor density at evapotranspiration surface 1 which corresponds to the canopy leaf surface, $\rho^*_{w_2}$ is the saturation vapor density at evapotranspiration surface 2, ρ_{w_2} is water vapor density at evapotranspiration surface 2 essentially representing the atmosphere near the canopy, ρ_{w_1} is vapor density at surface 1, r_a is resistance to vapor flux due to diffusion resistance, and r_x is the resistance to vapor flux from the evapotranspiration surface 1. Equation (3) represents a combined aerodynamic and energy balance approach based on work presented by Tanner and Pelton (1960) and Cowan and Milthorpe (1968), and further discussion of the theory may be found in those papers. The overall method is similar to the Penman method, but attempts to include plant physiology with the energy and aerodynamic considerations.

The sensible heat flux to the atmosphere A is given by

$$A = [\sigma c_p \rho_a \ (T_1 - T_2)]/r_a \tag{4}$$

where c_p is the specific heat of air at constant pressure, T_1 is the temperature of evapotranspiration surface 1, T_2 is the temperature of evapotranspiration surface 2, and ρ_a is the density of air. Quantity σ is a correction factor included by Goldstein, Mankin, and Luxmoore (1974) to compensate for the difference in evapotranspiration area and effective convection area. Using Equations (1), (3) and (4), an expression for vapor flux from evapotranspiration surface 1 to evapotranspiration surface 2 may be derived as follows:

$$F_v = \left[\frac{(R_N - G)\,\delta}{\sigma c_p \rho_a} + \frac{\rho_{w_2}{}^{*} - \rho_{w_2}}{r_a}\right] \Bigg/ \left[\frac{r_a + r_x}{r_a} + \frac{L_v\,\delta}{\sigma c_p \rho_a}\right] \qquad (5)$$

where $\delta = (\rho^{*}_{w_1} - \rho^{*}_{w_2})/(T_1 - T_2)$. It is assumed that $\delta \cong d\rho^{*}_{w}/dT$, which may be related to measured vapor pressure by the ideal gas law

$$\delta \cong \frac{d\rho^{*}_{w}}{dT} = \frac{1}{R_v T}\;\frac{de^{*}}{dT} \qquad (6)$$

Here R_v = gas constant for water vapor or $R_v = R/M_{H_2O}$ where R is the universal gas constant and M_{H_2O} is the molecular weight of water, and e^{*} is is the saturation vapor pressure.

The equation for net radiation input R_N based on measurement varies with the type of measuring device used. If incident shortwave energy is measured, then R_N may be calculated as

$$R_N = R_S\,(1 - \alpha) + R_{NL} \qquad (7)$$

where R_S is the measured shortwave energy, α is the albedo or ratio of reflected to incident radiation, and R_{NL} is the net longwave radiation absorbed by the evapotranspiration surface.

RESISTANCE TO WATER FLOW AND ELECTRICAL ANALOGUE

Equation (5) shows vapor flux to be a function of the environmental parameters of temperature, vapor pressure, and net radiation and resistance to vapor flow r_a and r_x. Resistance to vapor flux due to diffusion resistance may be derived from aerodynamics to be of the form

$$r_a = \frac{c_1\ \ell^b}{u^{0.5}} \tag{8}$$

where c_1 is a constant depending on leaf shape, b is an empirically fitted exponent, ℓ is a characteristic length usually taken as the leaf length, and u is wind speed. Cowan and Milthorpe (1968) present a relationship using mean area of individual leaves instead of leaf length

$$r_a \approx \frac{2.6\ A_\ell^{0.25}}{u^{0.5}} \tag{9}$$

where A_ℓ is the average leaf area in cm^2 and u is the average wind speed in cm/sec.

Goldstein, Mankin, and Luxmoore (1974) use

$$r_a \approx \frac{3.3\ \ell^{0.3}}{u^{0.5}} \tag{10}$$

where ℓ is in cm and u is in cm/sec. Resistance to vapor flux from the evapotranspiration surface r_x lumps stomatal control of vapor flux, cell wall diffusion resistance, and substomatal diffusion resistance into one resistance which is a function of the hydraulic potential within the leaf cells. This potential is simulated by the hydraulic potential of evapotranspiration surface 1, ψ_x. Therefore, from Equation (5) the vapor flux F_v from the evapotranspiration surface is a function of the hydraulic potential at the surface ψ_x.

Surface resistance to vapor flux r_x uses the following form suggested by Goldstein, Mankin, and Luxmoore (1974).

$$\begin{aligned} r_x &= R_x + (r_c - R_x)\, e^{h_1(\psi_c - \psi_x)} \quad , \quad |\psi_x| < |\psi_c| \\ r_x &= r_c \quad , \quad |\psi_x| \geq |\psi_c| \end{aligned} \tag{11}$$

This form was suggested by a review of literature regarding the physiology of water movement in plants. Parameter ψ_c is the surface water potential at which the evapotranspiration surface reaches a maximum resistance of r_c. This resistance r_c is analogous to cuticle resistance which dominates under conditions of high water stress. Parameters h_1 and R_x are empirically determined; however, R_x is analogous to the stomatal resistance at full hydration.

The hydraulic potential of evapotranspiration surface 1, ψ_x , however, depends on moisture content of the soil layers. Water balance techniques are used to calculate the mass flow rate of moisture to the evapotranspiration surface. The electrical analogue illustrated by Figure 3 is used to calculate this flow. Here hydraulic potential, mass flow rate and resistance to flow are analogous to voltage, current, and electrical resistance, respectively.

Hydraulic potential of the individual soil layers is taken as a function of moisture content within the layer. Data for the soil layers are assumed to be provided by laboratory or in-field tests of the soil properties. Non-hysteretic curves relating hydraulic potential to moisture content and conductivity K to moisture content θ are generated from a few tensiometer measurements using theory discussed by Green and Corey (1971). This technique allows fitting functions $g(\theta)$ and $h(\theta)$ to the tensiometer data for matric potential and conductivity respectively. Therefore

$$\psi_{m_i} = g_i\ (\theta_i)$$

and (12)

$$K_i = h_i\ (\theta_i)$$

where ψ_{m_i} is matric potential of the $i^{\underline{th}}$ layer, K_i is soil conductivity of the $i^{\underline{th}}$ layer, and θ_i is moisture content of the $i^{\underline{th}}$ layer. Total hydraulic potential in the $i^{\underline{th}}$ layer, ψ_i, is given by

$$\psi_i = \psi_{m_i} + \psi_{g_i} \tag{13}$$

where ψ_{g_i} is the gravitational potential of the $i^{\underline{th}}$ layer given by

$$\psi_{g_i} = \sum_{j=1}^{i-1} d_j + \frac{d_i}{2} \tag{14}$$

where d_i is the thickness of the $i^{\underline{th}}$ layer.

Resistance to flow in soil layers r_{s_i} is calculated from

$$r_{s_i} = \frac{(d_i/2)}{K_i} \tag{15}$$

Between soil layers the resistance $r_{s_{ij}}$ is taken as

$$r_{s_{ij}} = r_{s_i} + r_{s_j} \tag{16}$$

where r_{s_i} and r_{s_j} are the resistances of the $i^{\underline{th}}$ and $j^{\underline{th}}$ adjacent layers respectively. It should be noted that these soil resistances are functions of the soil layer moisture content through the conductivity K.

Before concluding the discussion of soil resistances it is necessary to point out that generally hysteresis occurs in the matric potential-moisture content and conductivity-moisture content curves between the wetting and drying curves. The theory implemented by Green and Corey (1971) does not allow for the calculation of this hysteresis. In a soil where this phenomena is important, measurements of both curves should be made for drying and wetting phenomena. In addition, the interpolation routine for matric potential and conductivity should be modified so that the appropriate curve is used.

Steady-state analysis of plant transpiration can allow an Ohm's law representation of water movement through the plant tissue (Cowan and Milthorpe, 1968). Further, the assumption that there are no changes in water storage allows the plant to be simulated as a hydraulic conduit delivering water to the evapotranspiration surface. Therefore, water which enters the plant through the root system equals the flux of water lost through evapotranspiration. Finally, due to lack of detailed data, Goldstein and Mankin (1972) assume that the velocity of water throughout the plant is constant, allowing the active area of roots to be estimated as equal to the evapotranspiration surface area.

The resistance to flow of the roots in the $i^{\underline{th}}$ layer r_{r_i} is determined by

$$r_{r_i} = \frac{(d_i/2)}{A_{r_i} K_{r_i}} \tag{17}$$

where A_{r_i} is the total root cross-sectional area per unit soil area in the $i^{\underline{th}}$ layer, and K_{r_i} is the conductivity of the roots in the $i^{\underline{th}}$ layer. The resistance to water uptake from the soil into the root is represented as

$$r_{rs_i} = (d_i\ A_{r_i})/(f_i A_I K_i) \tag{18}$$

where r_{rs_i} is the resistance to water uptake in the $i^{\underline{th}}$ layer, f_i is the fraction of active root area in the $i^{\underline{th}}$ layer, and A_I leaf area index defined below. Assumptions leading to the formulation of Equation (18) are justified due to a lack of data; however, should such data become available, modification of the expression is a simple task. The final resistance to flow is the resistance of the above-ground portion of the plant r_p. Plant resistance r_p is empirically determined from field or laboratory experiments. For the purpose of this simulation it is taken as depending only upon the size of the vegetative stand.

In an application to a deciduous forest, in order to insure that a decrease in leaf area below some level of canopy closure would increase the plant resistance to flow, Swift et al. (1975) recommended dividing r_p by an empirical scaling factor to obtain

$$F_e(A_I) = \frac{kA_I^2}{(A_1{}^2 + A_I^2)} \tag{19}$$

where A_I is the leaf area index or ratio of total leaf area to ground area, k is an efficiency factor, and A_1 is the scaling factor for canopy closure. Thus a reduction of transpiration for each unit of ground area is allowed for when canopy cover is greatly reduced. Therefore all plant resistance terms are divided by $F_e(A_I)$ to give a more realistic simulation at low values of A_I.

All necessary information for the calculation of the daily water fluxes through the plant-soil-atmosphere system have been discussed above. The calculation of the water fluxes begins with the determination of ψ_x, the hydraulic potential of the evapotranspiration surface. Using standard linear circuit analysis techniques (Seshu and Belabanian, 1963) it is possible to solve for the flow of water to the evapotranspiration surface as a function of ψ_x. That is,

$$F_w = h_w\ (\psi_x) \tag{20}$$

where F_w is the flow of water to the evapotranspiration surface and h_w is the function derived by circuit analysis. The exact form of h_w depends on the number of soil layers modeled and is left unspecified in this description.

Recalling the earlier assumption that the vapor from the evapotranspiration surface F_v is equal to the rate at which water is supplied to the surface, the right-hand sides of Equations (20) and (5) may be equated yielding an expression that when combined with Equation (11) may be solved for ψ_x. This equation is solved using a linear fractional iteration routine for obtaining the roots of a nonlinear equation.

A single daily calculation of ψ_x was suggested by Goldstein, Mankin, and Luxmoore (1974) to introduce numerical instabilities, particularly when the soil conductivities are high, as is often the case in forest soils. Therefore, the calculation ψ_x is accomplished by dividing the flux calculation into N iterations based on the amount of infiltrated throughfall, soil layer thickness, wetted zone hydraulic conductivity, and the previous day's value of N. The routine calculates $(1/N)^{\underline{th}}$ of the water flux as a function of $(1/N)^{\underline{th}}$ of the infiltrated throughfall and net radiation. After N iterations, the calculation of daily water flux is completed. The simulation then moves on to the next day and so forth through the year.

INFILTRATION AND INTERCEPTION

Interception

A portion of rainfall is intercepted by canopy foliage, ground cover and forest litter. A portion of this water eventually reaches the ground as stem flow or by dripping from vegetation; however, water that is held on these surfaces never reaches the soil and is lost to evaporation. In many situations such as light rainfall or in dense forests, this process cannot be ignored. For the purposes of this simulation, the intercepting area is taken to be equal to the area of evapotranspiration surface 1. Maximum and minimum values of interception storage per unit area are assumed to be provided data.

Therefore, potential interception storage is a volume of water related to evapotranspiration surface size and the amount of water already existing in interception storage.

On a day when rainfall occurs, an amount of water equal to the available interception storage or the volume of rainfall, whichever is smaller, is removed from the storm water available for infiltration. Some or all of this water is evaporated during the day. Any water left in interception storage decreases the amount of interception potential for the next day to the difference between the maximum potential storage and the amount of water left in storage. In addition, since the storage of energy available for evaporation in the forest environment is assumed negligible with respect to the daily energy fluxes, the energy required to evaporate water from interception storage is deducted from the daily influx of solar radiation before evapotranspiration is calculated.

The above discussion describes the approach used to calculate interception in the original PROSPER simulation. This approach works well for determining daily water balance; however, it must be augmented in order to modify the rainfall hyetographs needed for infiltration and subsequent surface water routing calculations, particularly when a storm lasts for more than one day. The following scheme, consistent with the water balance routines of PROSPER, is used to calculate the throughfall intensity histogram for a storm.

On the day the rainfall begins, a volume of water equal to that day's potential interception volume is removed from the beginning of the rainfall hydrograph. Of course, if this volume is greater than the day's precipitation volume, no throughfall will occur on this day, and the remaining interception volume forms a part of the potential interception volume for the next day. The rationale for removing the interception volume from the beginning of the storm on the first day of the event is based on the concept that at the beginning of a storm the potential interception volume represents a reservoir that must be filled before throughfall can reach the ground. Processes of stemflow and dripping are ignored for the purposes of this simulation. If there is insufficient rainfall volume to satisfy the interception volume on the first day of the storm, all of that day's rainfall is intercepted. The remaining unfilled interception volume is added to the day's evaporation loss from interception, and this volume becomes the potential "front-end" interception loss for the next day, and so forth through the storm. The change in the beginning of the storm to reflect front-end interception losses is illustrated in Figure 4a.

If the storm lasts for more than one day, significant changes in potential interception volume may occur as a result of evaporation. Evaporation losses from the interception storage are assumed to be made up by interception on the following day. Since evaporation losses tend to be distributed throughout the day, these losses are not subtracted from the beginning of that day's rainfall. The evaporation losses from the interception volume are assumed to be made up throughout the storm event. The interception storage is assumed to be replenished uniformly throughout the storm period during that day. Distribution of interception storage losses and subsequent modification of rainfall after the initial "front-end" storage is satisfied are illustrated by Figure 4b.

Equations (21a) and (21b) below are used to calculate the "front-end" and distributed evaporation interception volumes, respectively.

$$V_I = \left[\left(\frac{A_{T\ell}}{A_{\ell max}}\right)\left(V_{I_{max}} - V_{I_{min}}\right) + V_{I_{min}}\right] - V_{I_c} \qquad (21a)$$

and

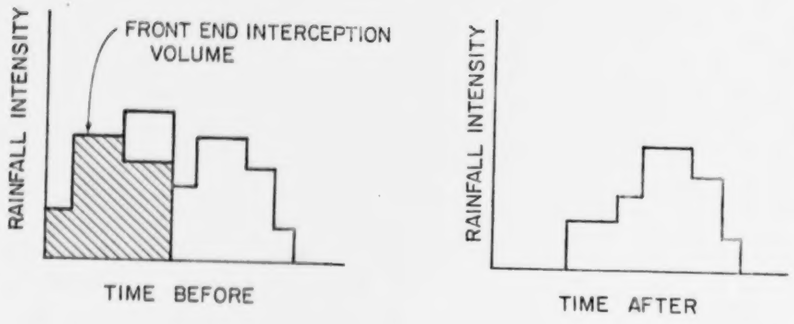

4a. "Front end" interception.

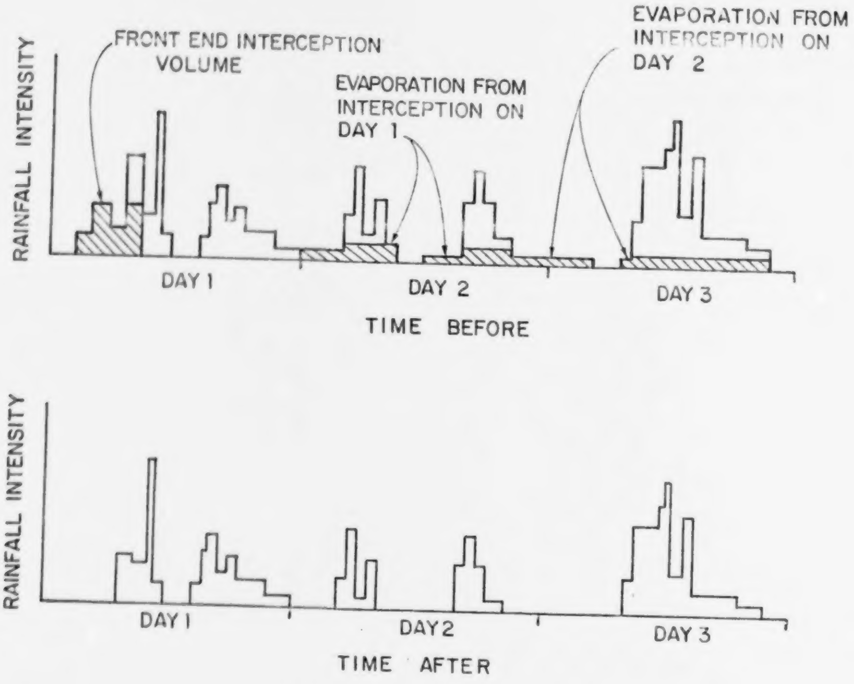

4b. Multiple day storms.

Figure 4. Transformation of rainfall hyetograph by interception.

$$V_I = \left(\frac{E_I}{D_s}\right) D_s \qquad (21b)$$

where E_I is the daily evaporation loss from interception storage and D_s is the duration of the nonzero portion of a storm on a given day. Equation (21b) appears unsimplified to illustrate that the intensity (E_I/D_s) is subtracted from the hyetograph intensities to provide for a uniform distribution of the evaporation losses from interception.

Infiltration

Moisture reaching the ground as throughfall will either run off or infiltrate into the soil. In previous implementations of the PROSPER model, the entire volume of throughfall was added to the first soil layer. After the daily water balance calculation, any water in excess of the saturation water content for each layer was added together as lateral runoff. If only daily balances are required, this approach is probably sufficient; however, in order to correctly predict the runoff hydrograph, the time history of the infiltration event must be known. Therefore, an infiltration model must be coupled to the water balance routines.

The infiltration scheme chosen for this simulation is an extension to layered soils of the time-explicit Green-Ampt formulation as presented for homogeneous soils by Eggert (1976). Derivation of the infiltration scheme for layered soils parallels that for a homogeneous soil. For clarity, the derivation will be briefly described. The Green-Ampt (1911) formulation assumes that as rainfall infiltrates into the soil a wetting front advances like a piston so that the rate of change of volume behind the wetting front equals the infiltration rate at the surface. The situation is illustrated by Figure 6. Here the location of the wetting front at time t is shown by the dashed line at depth z from the surface. At the beginning of the storm the

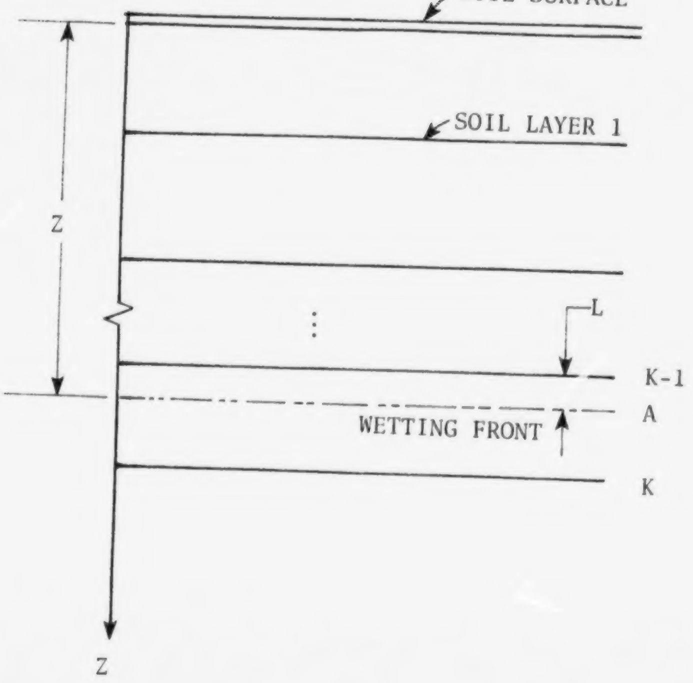

SOIL SURFACE
SOIL LAYER 1
Z
L
K-1
A
WETTING FRONT
K
Z

Figure 5. Location of wetting front with respect to soil layers.

wetting front is assumed to be at the surface. It moves downward through the soil column as water infiltrates, filling the volume of pore space not already occupied by water initially in the layers at the beginning of throughfall.

To formulate the equation of infiltration it is assumed that the wetting front as mentioned before is already at depth z as shown in Figure 5. The total hydraulic head h_T at depth z is

$$h_T = \sum_{i=1}^{k-1} \Delta h_i + h_k \tag{22}$$

where Δh_i is the increase in head in the $i^{\underline{th}}$ fully wetted layer, and h_k is the head in the $k^{\underline{th}}$ layer containing the wetting front. For flow above the wetting front, Darcy's law for the $i^{\underline{th}}$ layer may be written

$$\frac{Q}{A_G} = q = K_i \frac{\Delta h_i}{\Delta z_i} \tag{23}$$

where Q is the total volume inflow of water per unit area, A_G is the ground area, q is the Darcian velocity, K_i is the hydraulic conductivity in the wetted zone of the $i^{\underline{th}}$ layer, Δh_i is the change in head in the $i^{\underline{th}}$ layer and Δz_i is the thickness of the $i^{\underline{th}}$ layer. Solving Equation (23) for Δh_i for all $i = 1, k$ and substituting the result into Equation (22) yields an expression for the total hydraulic head at z as a function of the Darcian flux q

$$h_T = q \left(\sum_{i=1}^{k-1} \frac{\Delta z_i}{K_i} + \frac{\ell}{K_k} \right) \tag{24}$$

where ℓ is the distance that the wetting front has penetrated the $k^{\underline{th}}$ layer; however, total hydraulic head may also be written as the sum of the gravitational and capillary suction heads such that

$$h_T = \underbrace{\sum_{i=1}^{k-1} \Delta z_i + \ell}_{\text{gravitational head}} + \underbrace{\bar{\psi}_k}_{\text{capillary pressure head}} \tag{25}$$

where $\bar{\psi}_k$ is the capillary suction head in the k^{th} layer. Therefore, Equation (25) may be substituted into Equation (24) yielding an expression for q, that is

$$q = \frac{\sum_{i=1}^{k-1} \Delta z_i + \ell + \bar{\psi}_k}{\sum_{i=1}^{k-1} \frac{\Delta z_i}{K_i} + \frac{\ell}{K_k}} \tag{26}$$

If F is allowed to be the total infiltrated water volume above the wetting front at z, it may be expressed as

$$F = \sum_{i=1}^{k-1} \phi_i \, \Delta S_i \, \Delta z_i + \phi_k \, \Delta S_k \ell \tag{27}$$

where ϕ_i is the porosity of the i^{th} layers, and ΔS_i is the difference between the percent of pore space in the i^{th} layer filled with water at saturation and the percent of pore space filled with water initially, or the initial degree of saturation deficit of the i^{th} layer. The product of porosity and degree of saturation deficit is the potential change of dimensionless water content, or for the i^{th} layer, $\Delta\tilde{\theta}_i = \phi_i \, \Delta S_i$. Allowing the summation term of Equation (27) to be represented as F_{k-1}, the length ℓ may be expressed as

$$\ell = \frac{F - F_{k-1}}{\Delta\tilde{\theta}_k} \tag{28}$$

Using Equations (27) and (28) and noting that $q = \frac{dF}{dt}$ by continuity, Equation (26) may be rewritten as

$$\frac{dF}{dt} = \frac{z_{k-1}\,\widetilde{\Delta\theta}_k + F - F_{k-1} + \bar{\psi}_k\,\widetilde{\Delta\theta}_k}{W_{k-1}\,\widetilde{\Delta\theta}_k + \dfrac{F - F_{k-1}}{K_k}} \tag{29}$$

where $z_{k-1} = \sum_{i=1}^{k-1} \Delta z_i$ and $W_{k-1} = \sum_{i=1}^{k-1} \frac{\Delta z_i}{K_i}$. In order to simplify algebra it may be noticed that for flow in the $k^{\underline{th}}$ layer

$$\left.\begin{aligned} \widetilde{\Delta\theta}_k\,(z_{k-1} + \psi_k) - F_{k-1} &= c_k = \text{constant} \\ W_{k-1}\,\widetilde{\Delta\theta}_k - \frac{F_{k-1}}{K_k} &= d_k = \text{constant} \end{aligned}\right\} \tag{30}$$

Therefore, for flow in the $k^{\underline{th}}$ layer, Equation (29) may be written as

$$\frac{dF}{dt} = \frac{c_k + F}{d_k + \dfrac{F}{K_k}} \tag{31}$$

Suitable rearrangement of Equation (31) and integration within the $k^{\underline{th}}$ layer yields the following nonlinear expression for F,

$$\left(d_k - \frac{c_k}{K_k}\right) \ln\left(1 + \frac{F}{c_k}\right) - \left(d_k - \frac{c_k}{K_k}\right) \ln\left(1 + \frac{F_{k-1}}{c_k}\right) + \frac{F - F_{k-1}}{K_k} = t - t_{k-1} \tag{32}$$

where t is the time after the beginning of the event when the total infiltrated volume equals F , and t_{k-1} is the time when the total infiltrated volume was F_{k-1} (or when the wetting front was at $z = z_{k-1}$). In order to obtain an approximate solution to Equation (32) it is noted that within the $k^{\underline{th}}$ layer the infiltrated volume at some time $t + \Delta t$ may be expressed as

$$F(t + \Delta t) = F(t) + \Delta F \tag{33}$$

where ΔF is the change in F occurring between t and $t + \Delta t$. If Equation (32) is written for $F(t + \Delta t)$ and $F(t)$ and a subtraction is performed, an expression for ΔF as a function of $F(t)$ results. That is,

$$\left(d_k - \frac{c_k}{K_k}\right) \ln \left(1 + \frac{\Delta F}{c_k + F(t)}\right) + \frac{\Delta F}{K_k} = \Delta t \tag{34}$$

The logarithmic term may be expressed using a standard series expansion for $\ln(a + x)$,

$$\ln (a + x) = \ln a + 2\left[\frac{x}{2a + x} + \frac{1}{3}\left(\frac{x}{2a + x}\right)^3 + \ldots\right] \tag{35}$$

If only the first two terms of Equation (35) are used, insignificant error results (Li, Simons, and Stevens, 1975). Noting that $a = 1$, Equation (34) may be approximately rewritten and simplified to become

$$\begin{gathered} \Delta F^2 + (2K_k d_k + 2F(t) - K_k \Delta t)\, \Delta F \\ - 2K_k \Delta t\, (c_k + F(t)) = 0 \end{gathered} \tag{36}$$

Equation (36) may be immediately recognized as a quadratic equation for ΔF. All other quantities in Equation (36) are known at time $t + \Delta t$. Therefore the change in infiltrated volume between time t and $t + \Delta t$ may be calculated from

$$\Delta F = \frac{-\beta \pm \sqrt{\beta^2 - 4\gamma}}{2} \tag{37}$$

where $\beta = 2K_k d_k + 2F(t) - K_k \Delta t$

$\gamma = -2K_k \Delta t\, (c_k + F(t))$

and only the positive root is physically meaningful.

Equation (37) provides a time-explicit formulation for the change in infiltrated volume occurring between t and $t + \Delta t$. The formulation is written for flow in the $k^{\underline{th}}$ layer. However, this presents no computational problems since initially $F = 0$ and the flow is in the first layer. As the event proceeds in time, water enters the upper soil surface of the soil and the wetting front travels down through the soil. One need only keep track of the location of the wetting front at any time and appropriately update the values of $F(t)$, W_{k-1}, Z_{k-1}, $\widetilde{\Delta\theta}_k$, $\bar{\psi}_k$, F_{k-1}, and K_k depending on the location of the wetting front. The only apparent difficulty is the implicit nature of the problem, since depth of the wetting front at any time is directly related to infiltrated volume. However, the problem is easily solved due to the explicit nature of Equation (37). The change in infiltrated volume ΔF given by Equation (37) represents a potential volume that will infiltrate if there is sufficient supply of water at the surface. If there is insufficient throughfall during Δt to satisfy the potential volume, then the infiltration is controlled by rainfall and

$$\Delta F = i\ \Delta t \tag{38}$$

Computational Sequence of Infiltration

The computation of infiltration proceeds as follows:

1. Initially the infiltrated volume is zero, that is F_{k-1} for $k = 1$, or $F_o = 0$. All infiltration parameters are set equal to the first layer values. The depth of the wetting front z is zero.
2. Based on the current values of W_{k-1}, F_{k-1}, z_{k-1}, $\widetilde{\Delta\theta}_k$, $\bar{\psi}_k$, $F(t)$, and a new time increment, Δt^* , a value of ΔF is estimated. From this value of ΔF , the potential depth of the wetting front is calculated based on the current layer parameters; that is,

$$z = z_{old} + \frac{\Delta F}{\widetilde{\Delta\theta}_k} \tag{39}$$

3. If z is greater than the depth of the base of the current layer, all of the layer parameters must be updated to those of the next layer. Before updating, a new Δt must be calculated. This calculation is necessary since part of the original time increment Δt^* will be spent in the upper layer and part in the lower layer. The amount of time required to wet the remainder of the current layer at the potential rate may be calculated using Equation (34) for Δt as a function of ΔF. With $\Delta F = \widetilde{\Delta\theta}_k(z_k - z_{old})$, the time

necessary to fill the remainder of the current layer $\Delta t'$ is calculated directly from Equation (34). New Δt for the next layer is therefore $\Delta t_{new} = \Delta t_{old} - \Delta t'$. Now all of the layer parameters are updated and the calculation returns to step 2. If z is less than the depth of the current layer, an average potential infiltration rate is calculated based on total potential volume of infiltration during the original Δt^*.

$$\bar{f} = \frac{\Delta F}{\Delta t^*} \tag{40}$$

4. The potential infiltration rate $\bar{f}$ for time period Δt^* is compared to rainfall intensity for Δt^*. If $\bar{f}$ is less than the rainfall rate, then $\Delta F + F$ is the new infiltrated volume at time $t + \Delta t^*$ and location of the wetting front is known from the tests of steps 2 and 3. Since supply has exceeded infiltration capacity for this Δt^*, an excess intensity for this time period is calculated as

$$e = i - \bar{f} \tag{41}$$

where e is the excess intensity during Δt^*. If the event is not over, the calculation returns to step 2. If $\bar{f}$ is greater than i, the calculation proceeds to step 5.

5. Since the rainfall rate is less than the infiltration rate, the current estimates of ΔF and z are too high. The change in infiltrated volume during this time period is

$$\Delta F = i \, \Delta t^* \tag{42}$$

and the new value of F at time $t + \Delta t^*$ is

$$F(t + \Delta t^*) = F(t) + i\Delta t^* \tag{43}$$

Based on this value of $F(t + \Delta t^*)$ and $z(t)$, the value of $z(t + \Delta t^*)$ is calculated and the soil layer parameters are reset accordingly. No excess rainfall is generated during this time period Δt^* and the calculation returns to step 2 unless the event is over.

When the whole event is over, a new histogram representing the time history of excess rainfall has been calculated. This record is stored on a file for later use by the water and sediment routing and litter loading routines. Total infiltrated volume for the event is stored on a file for the phosphorus and nitrogen loading routines.

Storms lasting more than one day have been redefined into a continuous event by the interception routine. Therefore, calculation of infiltration requires no special logic for events lasting more than one day. Volumes of water that infiltrate the soil layers each day during the rain storm are stored for later use by the water balance routine.

Infiltration Parameters

The Green-Ampt layered infiltration model described above is essentially a two parameter model: 1) K_i the hydraulic conductivity in the wetted zone of the $i^{\underline{th}}$ layer and 2) $\bar{\psi}_i$ the average capillary suction head of the $i^{\underline{th}}$ layer. A possible third parameter is the porosity of the $i^{\underline{th}}$ soil layer ϕ_i but this parameter is bound to the initial saturation deficit ΔS_i which is discussed below, and is assumed not to change as a function of moisture content. Hydraulic conductivity of the soil layer is a function of the layer moisture content. However, the Green-Ampt formulation is based on the saturated conductivity of the wetted zone K_s. This parameter does not appreciably vary with moisture content. Average suction head, however, is a direct function of initial degree of saturation. This parameter is evaluated by taking the weighted mean of the capillary suction between the initial degree of saturation and the final degree of saturation using the relative conductivity as a weighting function. The approach was suggested by Mein and Larson (1973). The equation for average head takes the form

$$\bar{\psi}_k = \int_{k_k(S_i)}^{k_k(S_w)} \psi dk_k \tag{44}$$

where k is the relative hydraulic conductivity of the $k^{\underline{th}}$ layer, that is, $k_k(S) = \frac{K_k(S)}{K_{s_k}}$ where K_{s_k} is the saturated hydraulic conductivity of the $k^{\underline{th}}$ layer and $K_k(S)$ is hydraulic conductivity of the $k^{\underline{th}}$ layer at saturation S, S_w is the final or wetted soil degree of saturation usually taken as 1.0, and S_i is the initial degree of saturation. Graphs of $\bar{\psi}$ as a function of S_i are shown in Figure 6. For degrees of saturation near 1.0, $\bar{\psi}$ is obviously a sensitive function of S_i. For this reason the value of $\bar{\psi}_i$ is updated based on the value of S_i on the day prior to the storm by re-evaluating Equation (44). Therefore, the initial degree of saturation serves as an initial condition affecting the saturation deficit ΔS_i and the average suction head. All of the parameters mentioned above are determined by the soil routine of the daily water flux model or are supplied as changing inputs from daily moisture content calculations.

SUMMARY

The hydrological water balance model has been described and its major subcomponents explained. It should be noted that great flexibility is built into the model since implementation of the model to widely varying forest and agricultural watershed types may be accomplished by reformulating the manner of calculations of the various component resistances. This subprogram creates a large number of scratch files for use by various other subprograms.

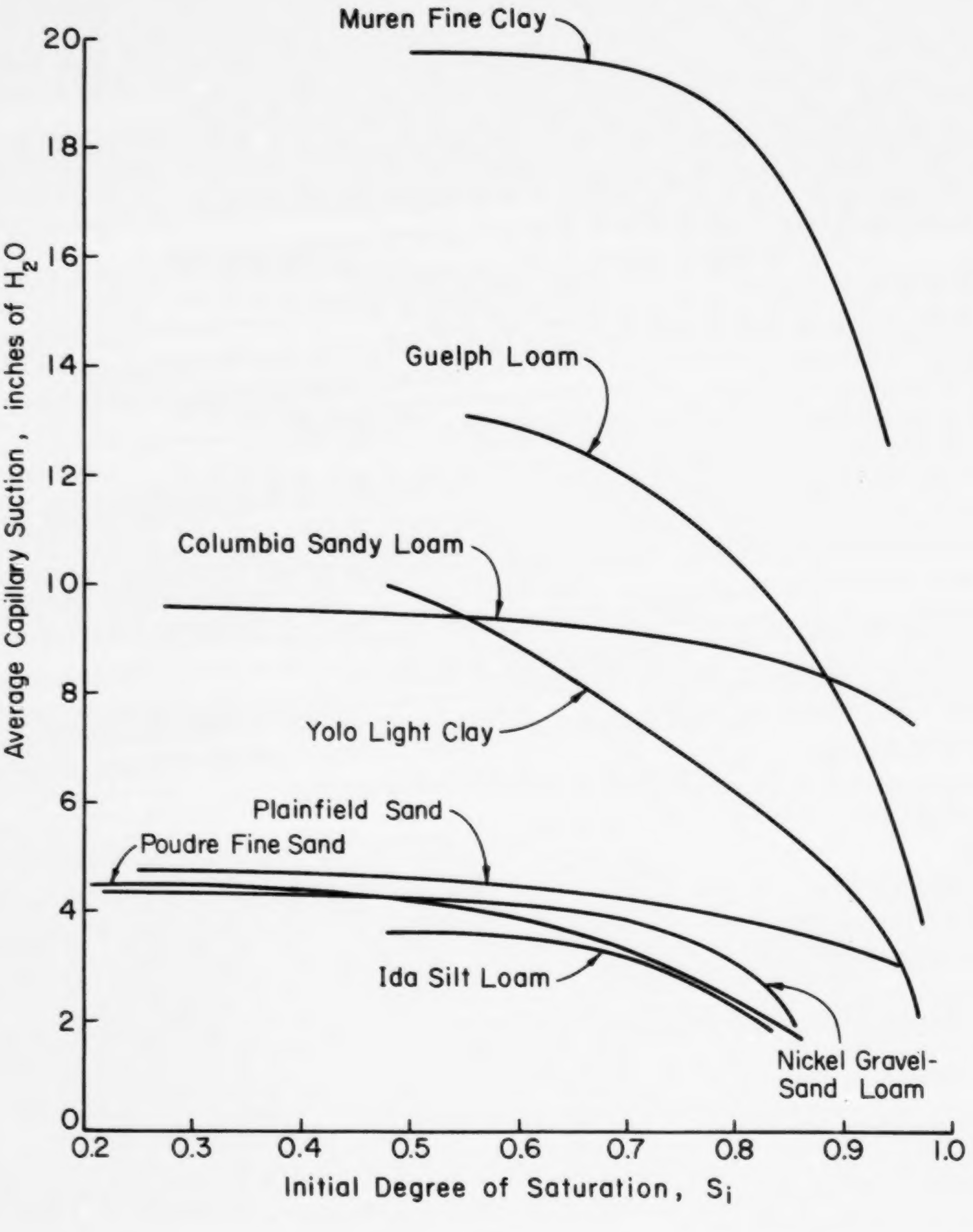

Figure 6. Average capillary suction head as a function of initial moisture content.

SYMBOLS FOR SECTION 2

Symbol	Description
A	Daily sensible heat transfer to atmosphere
A_1	Scaling factor for canopy closure
A_G	Ground area
A_I	Leaf area index
A_ℓ	Leaf area of individual leaves
$A_{\ell max}$	Maximum total leaf area
A_r	Total root cross-sectional area in a soil layer
$A_{T\ell}$	Total watershed leaf area
b	Fitted exponent in r_a expression
c_1	Leaf shape constant in r_a expression
c_p	Specific heat of air at constant pressure
D	Day of the year $0 \leq T \leq 366$
D_s	Duration of storm on a given day
d	Thickness of soil layer
E	Daily latent heat leaving the evapotranspiration surface
E_I	Daily evaporation from interception storage
e	Excess intensity
e^*	Saturation water vapor pressure

Symbol	Description
F	Infiltrated volume
F_e	Evapotranspiration area scaling factor
F_w	Flow of water to the evapotranspiration surface
F_v	Daily water vapor flux from evapotranspiration surface
$\bar{f}$	Average infiltration rate
f	Fraction of active root area
G	Net daily change in soil heat storage
G_m	Annual average baseline changes in soil heat storage
G_r	Maximum daily heat flux from soil
h	Hydraulic head
h_1	Fitted parameter in expression for r_x
h_T	Total hydraulic head
i	Rainfall intensity
K	Soil hydraulic conductivity; a function of moisture content
K_r	Hydraulic conductivity of root
K_s	Saturated hydraulic conductivity
k	Efficiency factor in evapotranspiration area index expression
k_r	Relative conductivity; $k_r = \frac{K}{K_s}$
L	Leaf length
L_v	Latent heat of vaporization of water
ℓ	Distance from top of current soil layer to wetting front
M	Molecular weight
ME	Miscellaneous daily heat transfer
Q	Volumetric flow rate

Symbol	Description
q	Darcian water flux
R	Universal gas constant
R_N	Net daily solar radiation including both short- and long-wave
R_{NL}	Measured longwave radiation
R_S	Measured direct beam shortwave solar radiation
R_v	Water vapor gas constant
R_x	Empirical constant analogous to stomatal resistance
r_a	Resistance to vapor flux due to diffusion resistance
r_c	Macroscopic resistance analogous to crucial resistance
r_ℓ	Resistance to vapor flux through litter
r_p	Resistance to water flow in above-ground portion of plant
r_r	Resistance to root water flow
r_{rs}	Resistance to soil water uptake by roots
r_s	Resistance to soil water movement
r_x	Resistance to vapor flux from the evapotranspiration surface
S	Degree of saturation
S_i	Initial degree of saturation
S_w	Degree of saturation in the wetted zone
T	Temperature
t	Time
u	Wind speed
V_I	Total interception volume
V_{I_c}	Current interception storage
$V_{I_{max}}$	Maximum interception storage

Symbol	Description
$V_{I_{min}}$	Minimum interception storage
z	Depth from the soil surface
α	Albedo
ΔS	Saturation deficit
$\Delta\tilde{\theta}$	Dimensionless soil water content deficit
δ	Slope of saturation vapor density temperature function
θ	Volumetric water content of soil
θ_o	Interception storage
ρ_a	Density of air
ρ_w	Water vapor density
ρ_w^*	Saturation water vapor density
σ	Correction factor for difference in evapotranspiration and convection area
ϕ	Soil porosity
ψ	Hydraulic potential
$\bar{\psi}$	Average suction head
ψ_c	Critical surface water potential of evapotranspiration surface at which surface attains maximum resistance, r_c
ψ_m	Matric capillary pressure head
ψ_g	Gravitational hydraulic potential
ψ_x	Hydraulic potential at evapotranspiration surface
η	Phase shift in ground energy flux equation

SECTION 3

WATER AND SEDIMENT ROUTING

INTRODUCTION

This section describes the water and sediment routing subprogram. In the overall model structure, as illustrated by Figure 1, this subprogram occupies the program block labeled RUNOFF. However, RUNOFF consists of three separate subprograms. As will be explained, these subprograms follow a computational sequence based on gravity.

Subprogram RUNOFF is designed to route storm water and sediment runoff from watersheds of complex geometry. In order to accomplish this task, the complex watershed geometry must be simplified into a representation suitable for computer simulation. The geometric approximation used in RUNOFF consists of an arbitrary number of two-plane and one-channel ("open book") watersheds linked together by channels. The open book approximation was first proposed by Wooding (1965) and represents a hydraulically sound method for subdividing a large watershed. All subwatershed units, planes, and open books have no upstream inflows and are routed using the method of characteristics solution to the kinematic wave problem for overland and channel flow. The channel in this case is the intersection of the two planes of the open book. These primary channels also have no upstream inflow and are routed using the method of characteristics solution. Channels that join subwatersheds have upstream inputs and require a numerical solution to the kinematic wave approximation. The necessity for numerical channel routing rather than the method of characteristics arises from the occurrence of kinematic shock as discussed by Kibler and Woolhiser (1970). The analytical solution cannot be applied in situations where kinematic shock occurs.

For simplicity the numerical solution to the kinematic wave problem could have been used for both the subwatershed units and the linking channels. However, an analytical solution such as the method of characteristics approach allows more efficient use of computer storage and usually more rapid calculation of the runoff hydrograph. Therefore, whenever possible analytical solutions are employed. To be consistent, in the portions of the watershed where the analytical method is used to route the water, the sediment yield is also computed by an analytical method. Likewise, in the portions where water is routed numerically, the sediment yield is computed by a numerical routing scheme.

Figure 7 illustrates the transformation of a watershed into the geometrical representation used in the simulation. A detailed example of the transformation will be included in the User's Manual for the generalized planning model. However, the basic technique follows. Figure 7a depicts a topographic map of a small watershed suitable for open book representation. Length of the primary channel L_c is determined and the channel is extended to the watershed divide on a path normal to the topography contours. The channel and its extension serve to divide the watershed into two areas, A_1 and A_2. Using L_c as the length of the intersection of the planes, areas A_1 and A_2 define the length of the overland flow units. Slopes of the planes are determined by length weighted averages of flow paths on each plane. Primary channel slopes are determined by rise divided by length. This process

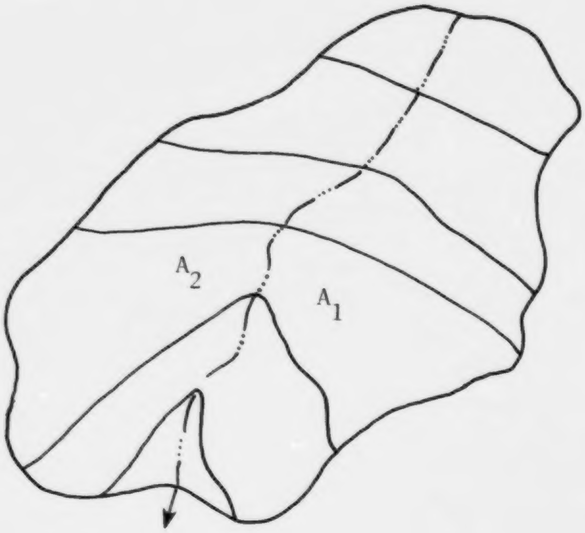

a) Original subwatershed topographic map

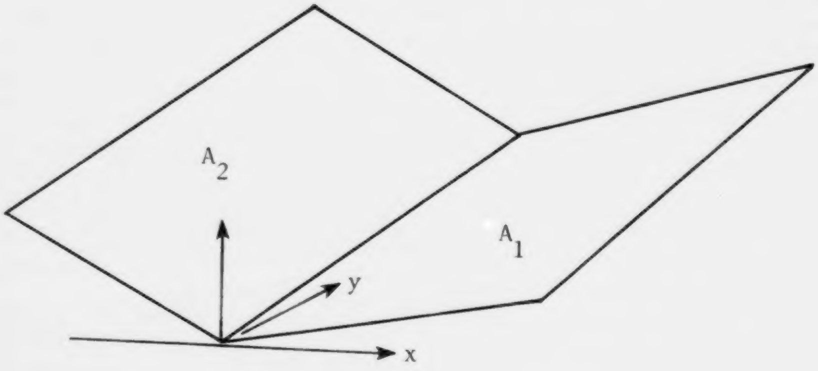

b) Wooding plane representation

Figure 7. Transformation of topographic map into watershed geometric representation.

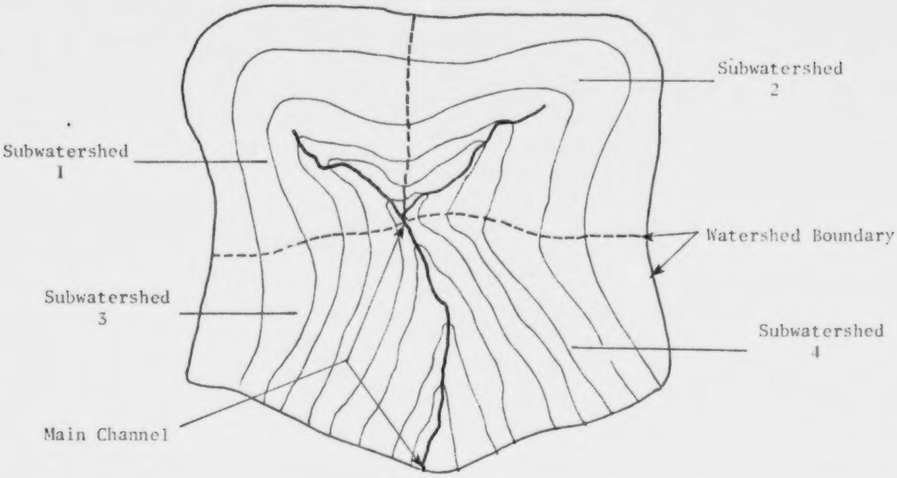
Subwatershed
2
Subwatershed
1
Watershed Boundary
Subwatershed
3
Subwatershed
4
Main Channel

c) Original complex watershed topographic map

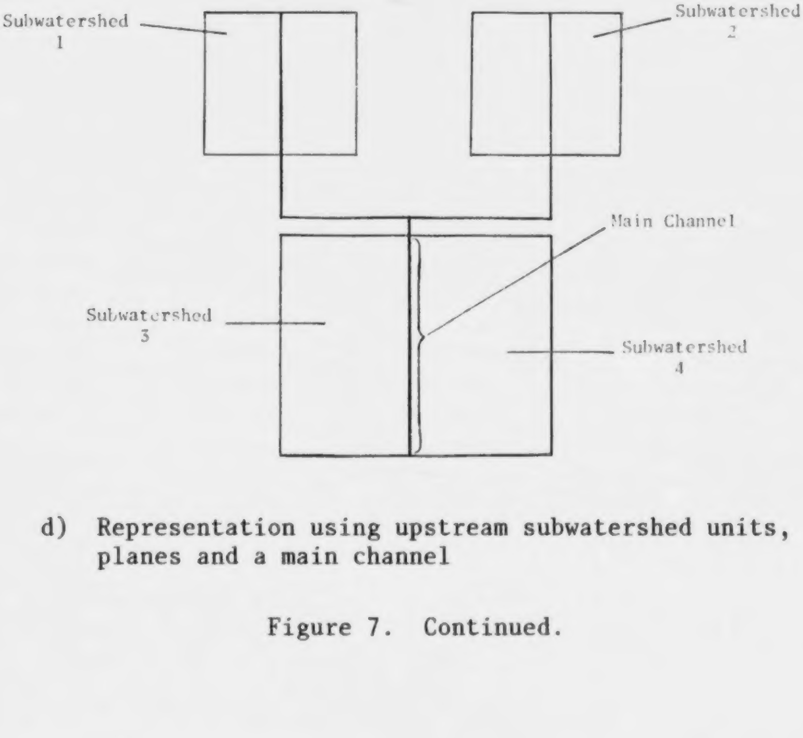
Subwatershed
1
Subwatershed
2
Main Channel
Subwatershed
3
Subwatershed
4

d) Representation using upstream subwatershed units, planes and a main channel

Figure 7. Continued.

results in a representation of the watershed in Figure 8a by the open book shown in Figure 8b.

Figure 8c depicts a more complex watershed map. In this case the watershed is subdivided into subwatersheds that are best represented by either a single plane or an open book watershed representation. Once this subdivision has been finished the geometries of the subwatershed representations are determined in the same manner as before. The resulting approximation has a form illustrated by Figure 8d.

The computational sequence in calculating storm water runoff and the attendant sediment runoff follows gravity. Overland flow and primary channel routines are contained in program MULT. This program performs the water and sediment routing for all of the subwatersheds in the system. Order of calculation of the subwatersheds is in the downstream direction of the main channel. Hydrographs calculated by MULT must be reordered and a common time grid for the numerical routing program used in the main channel system, MCHNL. This sorting is carried out by program SORT. Sorted data is then routed by MCHNL for the whole system on a time increment by time increment basis. This procedure allows overland and primary channel flow hydrographs to be stored on permanent files rather than in central memory, and therefore, the size of the complex watershed modeled is not unduly restricted by the necessity of storing all of the inflow hydrographs to the main channel. Component programs of RUNOFF are discussed in greater detail below.

SUBPROGRAM MULT

The two tasks performed in MULT are determination of sediment yield by size fractions and routing of water for all plane and upstream subwatershed units that form the entire watershed. Water routing is performed analytically by applying the method of characteristics to the kinematic wave approximation of the momentum and continuity equations. The sediment yield is calculated by comparing the supply due to detachment by both rainfall and runoff, and potential transporting capacity.

Derivation of Analytical Kinematic Wave Equations

This portion of the section clarifies the analytical kinematic routing component of the watershed model. This is essentially the same derivation given by Harley, Perkins, and Eagleson (1970), and Simons, Li, and Eggert (1976). This routing procedure is used by the plane and subwatershed units of MULT to determine upstream and lateral inflows into the channel units of MCHNL.

A simple routing procedure is presented to compute both overland flow (used by the plane and subwatershed units), and channel flow (used only by the subwatershed units). Other than a few minor changes needed to switch the procedure between overland and channel flow, derivations are identical.

The analytical solution to the kinematic wave approximation is based on the continuity and momentum equations in the absence of all dynamic interaction. The continuity equation for overland flow is

$$\frac{\partial q}{\partial x} + \frac{\partial y}{\partial t} = e \qquad (45)$$

where q is the discharge per unit width, x is the downstream dimension, y is the depth, t is time and e is the lateral inflow. In this case, e is the excess rainfall function provided by the subprogram HYDROL.

The Darcy-Weisbach resistance equation for overland flow is

$$S_f = f \frac{q^2}{8gy^3} \qquad (46)$$

where S_f is the friction slope, f is the Darcy-Weisbach friction factor, and g is the acceleration due to gravity. By neglecting dynamic effects, the momentum equation for a kinematic wave becomes

$$S_f = S_o \tag{47}$$

Substituting Equation (46) into Equation (47) and rearranging, the following expression for discharge as a function of depth is

$$q^2 = \frac{8gS_o}{f} y^3 \tag{48}$$

Many researchers, most recently Chen (1976), have shown that f may be represented as

$$f = \frac{K}{N_r} \tag{49}$$

where N_r is the Reynolds number and K is a constant directly dependent on resistance. The Reynolds number may be expressed as

$$N_r = \frac{q}{\nu} \tag{50}$$

where ν is the kinematic viscosity of water. Equations (49) and (50) may be substituted into Equation (48) to give

$$q = \frac{8gS_o}{K\nu} \quad y^3 \tag{51}$$

Discharge is often assumed to be a power function of depth

$$q = \alpha y^{\beta} \tag{52}$$

Therefore, in the case of overland flow $\beta = 3$ and α is expressed as

$$\alpha = \frac{8gS_o}{K\nu} \tag{53}$$

Substituting Equation (52) into Equation (45) yields

$$\alpha\beta y^{\beta-1} \frac{\partial y}{\partial x} + \frac{\partial y}{\partial t} = e \tag{54}$$

This partial differential equation may be solved by the method of characteristics. The total differential of y(x,t) is given by

$$dy = \frac{\partial y}{\partial t}\,dt + \frac{\partial y}{\partial x}\,dx \tag{55}$$

Equations (54) and (55) form a system of two equations in two unknowns, and may be written in matrix form as

$$\begin{bmatrix} \alpha\beta y^{\beta-1} & 1 \\ dx & dt \end{bmatrix} \begin{bmatrix} \frac{\partial y}{\partial x} \\ \frac{\partial y}{\partial t} \end{bmatrix} = \begin{bmatrix} e \\ dy \end{bmatrix} \tag{56}$$

Characteristic paths along which the solution is valid are found by determining the loci of indeterminancy of the solution. These loci are obtained by equating the determinant of the coefficient matrix with zero. The resulting characteristic equation is

$$\frac{dx}{dt} = \alpha\beta y^{\beta-1} \tag{57}$$

Integrating Equation (57) with respect to time yields

$$x - x_o = \alpha\beta \int_{t_o}^{t} y^{\beta-1}\,dt' \tag{58}$$

Invariants of this solution are found by substituting the right-hand side of Equation (56) for each column of the coefficient matrix and equating the determinant of the resulting matrix equal to zero. The invariants are

$$\frac{dy}{dt} = \frac{dq}{dx} = e \tag{59}$$

or by integrating Equations (59)

$$y - y_o = \int_{t_o}^{t} e\,dt' \tag{60}$$

or

$$q - q_o = \int_{x_o}^{x} edx' \tag{61}$$

By substituting Equation (60) into Equation (58), the following expression for the characteristic path is obtained

$$x - x_o = \alpha\beta \int_{t_o}^{t} \left[\int_{t_o}^{t'} ed\sigma + y_o \right] dt' \tag{62}$$

Theoretically, if the functional form of e(t) is known, then Equation (62) will give the characteristics in the x-t plane. When e(t) is a histogram, then with reference to Equation (60), Equation (62) may be evaluated in pieces.

The procedure that calculates characteristic paths is illustrated in Figure 8. From any point (x_i, t_i) on characteristic C , the value of x_{i+1} on C corresponding to time t_{i+1} may be calculated by Equation (62) expressed as

$$x_{i+1} = x_i + \alpha\beta \int_{t_i}^{t_{i+1}} [e_{i+1}(t' - t_i) + y_i]^{\beta-1} dt' \tag{63}$$

From Equation (60) it may be seen that

$$y_{i+1} = y_i + e_{i+1}(t_{i+1} - t_i) \tag{64}$$

Integrating Equation (63) yields

$$x_{i+1} = x_i + \frac{\alpha}{e_{i+1}} [(y_i + e_{i+1}(t_{i+1} - t_i))^{\beta} - y_i^{\beta}] \tag{65}$$

For a given plane of length L , values of x_{i+1} are calculated until $x_{i+1} \geq L$. Time of arrival of the characteristic at the downstream boundary t_L is found by solving Equation (65) for t_L in terms of t_j and x_j.

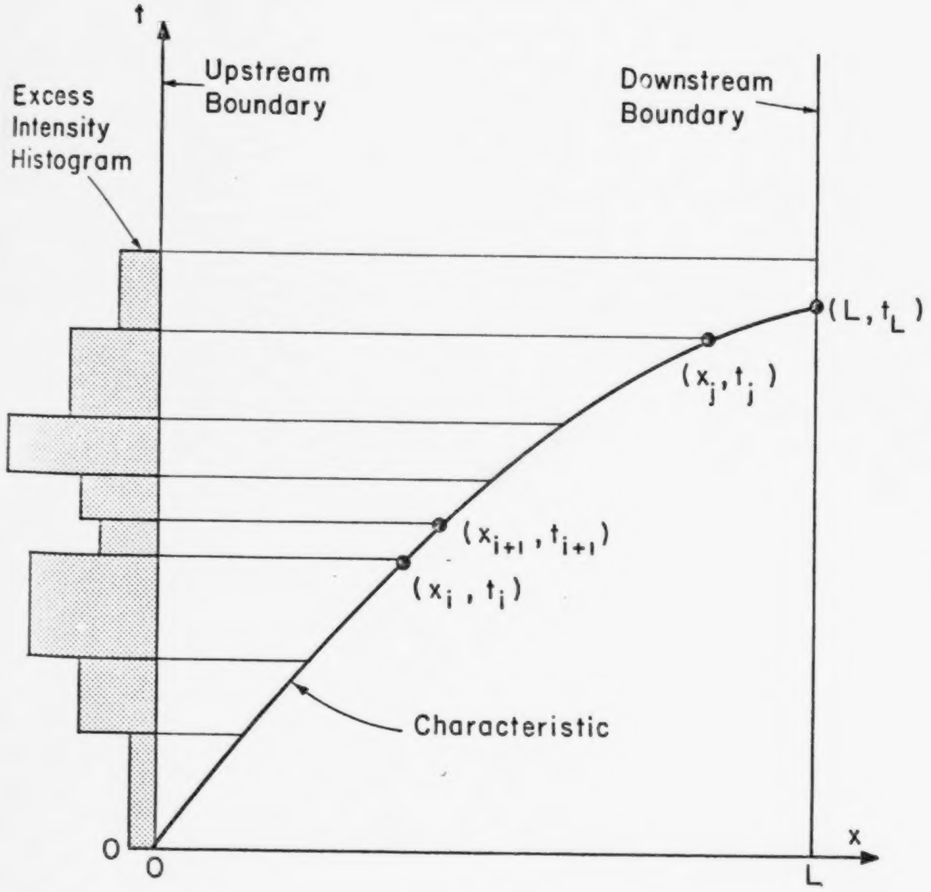
t
Upstream Boundary
Excess Intensity Histogram
Downstream Boundary
(L, t_L)
(x_j, t_j)
(x_{i+1}, t_{i+1})
(x_i, t_i)
Characteristic
0
0
x
L

Figure 8. Method of characteristics solution domain illustrating calculation of characteristics in downstream direction.

$$t_L = t_j + \frac{1}{e_{j+1}}\left\{\left[\frac{e_{j+1}(L-x_j)}{\alpha} + y_i{}^{\beta}\right]^{\frac{1}{\beta}} - y_j\right\} \tag{66}$$

For cases where $e_{j+1} = 0$, Equation (65) and (66) may be rederived from Equation (62) yielding

$$t_L = \frac{L - x_j}{\alpha\beta y_j{}^{\beta-1}} + t_j \tag{67}$$

and

$$x_{i+1} = x_i + \alpha\beta y_i{}^{\beta-1}(t_{i+1} - t_i) \tag{68}$$

Equations (65) through (68) are used serially, until the storm ends and the discharge is arbitrarily small, to calculate the characteristic lines beginning at the starting time of each block of excess rainfall (Figure 9).

As previously stated, the channel routing scheme is nearly identical to the overland flow routing. The continuity equation for channel flow is

$$\frac{\partial Q}{\partial x} + \frac{\partial A}{\partial t} = q_{\ell} \tag{69}$$

where Q is the total discharge, A is the cross-sectional area of the channel and q_{ℓ} is the lateral inflow to the channel.

When using the Darcy-Weisbach friction factor, kinematic wave approximation to the momentum equation can be written as

$$S_o \cong S_f = f\,\frac{Q^2}{8gRA^2} \tag{70}$$

in which S_o is bed slope, S_f is energy slope, f is the Darcy-Weisbach friction factor, g is the gravitational acceleration, and R is the hydraulic radius. By definition the hydraulic radius is

$$R = \frac{A}{P} \tag{71}$$

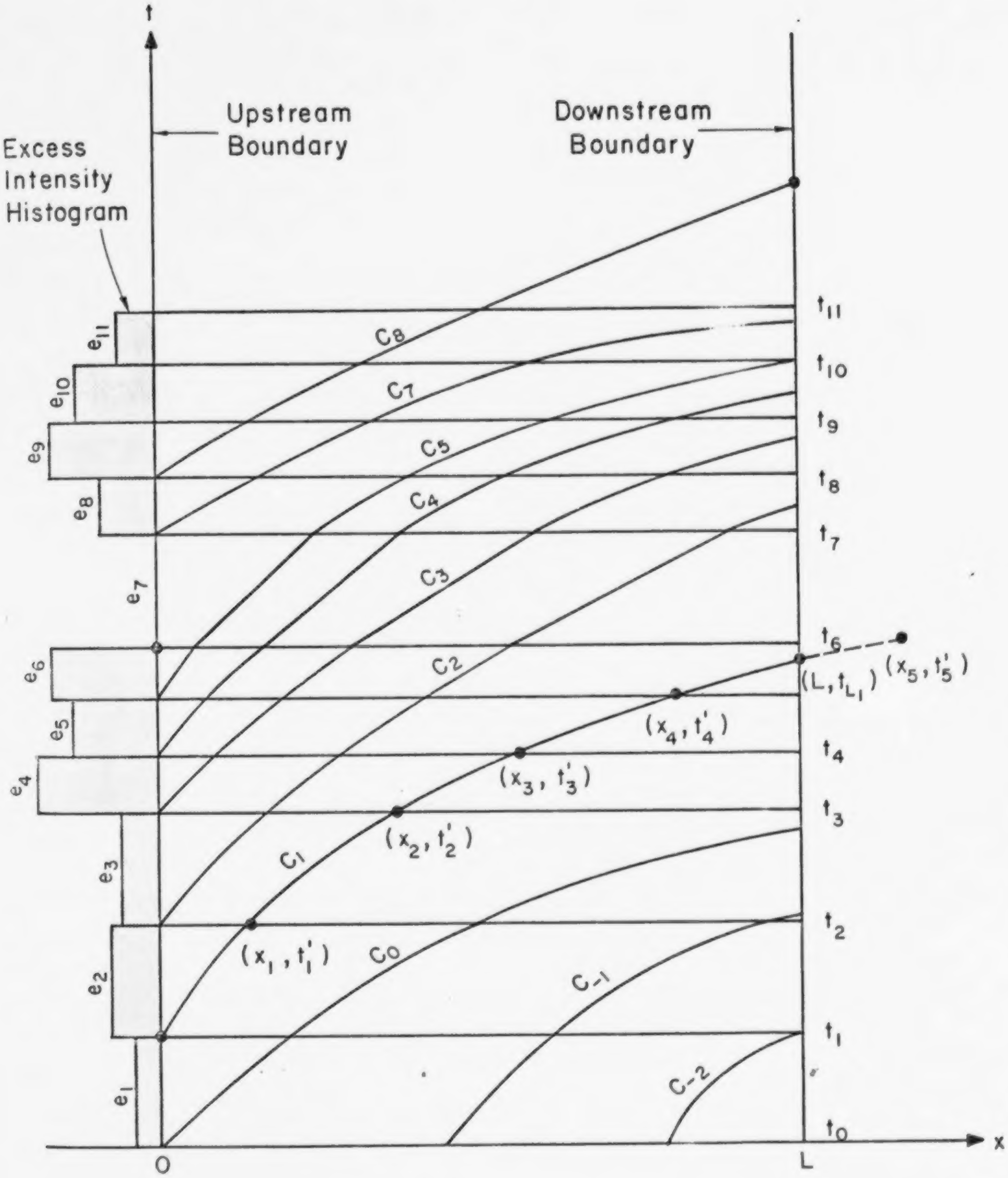
t
Upstream Boundary
Downstream Boundary
Excess Intensity Histogram
e1
e2
e3
e4
e5
e6
e7
e8
e9
e10
e11
t0
t1
t2
t3
t4
t6
t7
t8
t9
t10
t11
C8
C7
C5
C4
C3
C2
C1
C0
C-1
C-2
(x1, t'1)
(x2, t'2)
(x3, t'3)
(x4, t'4)
(L, tL1)
(x5, t'5)
O
L
x

Figure 9. Method of characteristics solution domain illustrating a set of characteristics for an arbitrary excess rainfall histogram.

in which P is the wetted perimeter and usually can be represented as a power function of flow area or

$$P = a_1 A^{b_1} \tag{72}$$

in which a_1 and b_1 are constants that vary with the shape of a cross-sectional area. Simons, Li, and Ward (1977) devised a computer program to estimate a_1 and b_1 providing the cross section of the channel is known.

If Manning's equation is used, the momentum equation is

$$S_o \simeq S_f = \frac{n^2 Q^2}{2.21 R^{4/3} A^2} \tag{73}$$

in which n is Manning's roughness coefficient that represents overall resistance.

Manning's equation is frequently used in hydraulic engineering to describe flow in open channels. The Manning roughness coefficient is usually determined by measurement and can be expressed as a power function of flow discharge. In this study, only a constant value is assumed for a particular response unit.

If the Chezy relationship is employed, the momentum equation becomes

$$S_o \simeq S_f = \frac{Q^2}{A^2 C^2 R} \tag{74}$$

in which C is the Chezy coefficient and can be related to f as

$$C = \sqrt{\frac{8g}{f}} \tag{75}$$

The flow cross-sectional area can be expressed as a power function of discharge

$$Q = \alpha A^{\beta} \tag{76}$$

in which α and β are coefficients with values dependent on channel shape, roughness, and slope.

If Manning's equation is applied, the corresponding α and β are determined by using Equations (71), (72), and (76). The values are

$$\alpha = \left[\frac{S_o(2.21)}{n^2 \ a_1^{4/3}}\right]^{1/2} \tag{77}$$

and

$$\beta = \frac{5 - 2b_1}{3} \tag{78}$$

If the Chezy relationship is used, the α and β values are determined using Equations (71), (72), (74) and (76). The values are

$$\alpha = \left[\frac{S_o C^2}{a_1}\right]^{1/2} \tag{79}$$

and

$$\beta = \frac{3 - b_1}{2} \tag{80}$$

The user may also assume that the two planes of the Wooding watershed model meet to form a triangular channel. The wetted perimeter of that channel P (Figure 10), may be expressed as

$$P = \frac{A}{R} = r_1 + r_2 = [y^2 + t_1^2]^{1/2} + [y^2 + t_2^2]^{1/2} \tag{81}$$

where the subscripts refer to planes 1 and 2. Since t_1 and t_2 may be expressed as

$$t_1 = \frac{y}{S_1} \ ; \ t_2 = \frac{y}{S_2} \tag{82}$$

Equation (81) may be written

$$P = y\left[\left(1 + \frac{1}{S_1^2}\right)^{1/2} + \left(1 + \frac{1}{S_2^2}\right)\right]^{1/2} \tag{83}$$

Referring to Figure 10, the cross-section area of the channel may be expressed as

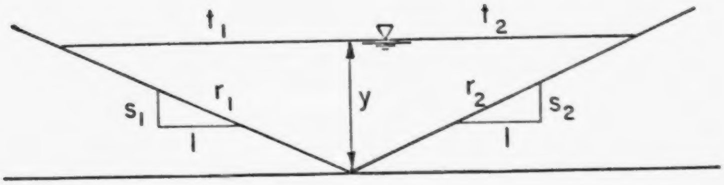
t_1
t_2
y
r_1
r_2
s_1
s_2
1
1

Figure 10. Definition sketch of triangular channel.

$$A = \frac{1}{2} y \; [t_1 + t_2] \tag{84}$$

or

$$A = \frac{1}{2} y^2 \; [\frac{1}{S_1} + \frac{1}{S_2}] \tag{85}$$

Solving Equation (85) for y and substituting the result into Equation (83) yields the following expression for P in terms of A,

$$P = a_1 \; A^{1/2} \tag{86}$$

allowing

$$a_1 = \left[\frac{2}{\left(\frac{1}{S_1} + \frac{1}{S_2}\right)}\right]^{1/2} \left[\left(1 + \frac{1}{S_1{}^2}\right)^{1/2} + \left(1 + \frac{1}{S_2{}^2}\right)^{1/2}\right] \tag{87}$$

$$b_1 = 1/2 \tag{88}$$

The a_1 and b_1 calculated in this manner may then be used to obtain α and β by substitution into either Equations (77) and (78) or (79) and (80). If a_1 and b_1 are not input to the program, it will calculate them as in Equations (87) and (88).

Equations for water routing are again Equations (65) through (68). Excess e is replaced by lateral inflow or discharge per unit width q_ℓ. Parameters α and β are defined above, and y and q are replaced by A and Q, respectively. Since there are two planes, lateral inflow to the channel consists of the sum of the two overland flow discharge hydrographs.

A problem in constructing an open-book catchment simulation using the method of characteristics solution for kinematic wave routing lies in the timing of the overland flow feeding the channel. In order to preserve as much generality as possible, the two planes must be allowed to differ in geometric and hydraulic properties. When using the method of calculating characteristics, one selects a time on the upstream boundary of the solution domain, t_o (Figure 9) and proceeds to determine points on the characteristic until the downstream boundary is reached. Time of arrival of that characteristic at the downstream boundary t_L is a function of the lateral inflow and the hydraulic and geometric properties of the plane. Therefore, for the selection of the same set of t_o's , different planes produce different sets of t_L's.

This situation poses no particular difficulty until it is desired to combine the overland flow discharges to produce the lateral inflow for channel routing. It might be suggested that the difficulty may be easily handled by simply interpolating each onto a common time line. This solution is valid though an unknown amount of error in each discharge occurs due to interpolation. If, on the other hand, it is possible to pick the time on the downstream boundary and then calculate t_o on the upstream boundary, the two overland flow hydrographs could simply be added time by time to obtain the desired lateral inflow to the channel. Further, in this case, there would be no error included in forming the inflow hydrograph. A subroutine was developed to find the t_o corresponding to a selected t_L , and it is based on the theory presented below.

The equation for a general characteristic path is

$$\frac{L}{\alpha\beta} = \int_{t_o}^{t_L} \left[\int_{t_o}^{t'} [q_\ell\ (\sigma)\ d\sigma]^{\beta-1} \right] dt' \tag{89}$$

where L is the length of the slope being routed and t' and σ are dummy variables of integration. The problem here is to solve Equation (89) for t_o when everything else is known. Lateral inflow q_ℓ is generalized. Therefore, Equation (89) may be used for both overland and channel flow. For simplicity of discussion, the method will continue to be developed for overland flow. However, it will be directly applicable to channel flow simply by specifying the appropriate α, β, and q_ℓ. For overland flow, the lateral inflow q_ℓ is defined as the excess rainfall after satisfying infiltration and interception e. This function is assumed to exist in the form of a histogram and is displayed vertically along the upstream boundary in Figure 9.

Since $e(t)$ has the form of a histogram, excess rainfall during the j^{th} time increment $t_j - t_{j-1}$ is constant. In addition, the form of Equation (89) may be simplified by noticing the inner integration, i.e., the integration of σ is simply the difference between the cumulative excess at time t_L and the cumulative excess at time t_o. That is

$$\int_{t_o}^{t_L} e(\sigma)\, d\sigma = E(t_L) - E(t_o) \tag{90}$$

where E represents the cumulative excess.

With this notation in mind and taking advantage of the histogram form of $e(t)$, Equation (89) may be rewritten as

$$\begin{aligned} \frac{L}{\alpha\beta} &= \int_{t_k}^{t_L} [e_{k+1}\, t' - e_{k+1}\, t_k + E_k - e_{j+1}\, t_o + e_{j+1}\, t_j - E_j]^{\beta-1}\, dt' \\ &+ \sum_{i=j+2}^{k} \int_{t_{i-1}}^{t_i} [e_i\, t' - e_i\, t_{i-1} + E_{i-1} - e_{j+1}\, t_o + e_{j+1}\, t_j - E_j]^{\beta-1}\, dt' \\ &+ \int_{t_o}^{t_{j+1}} [e_{j+1}\, t' - e_{j+1}\, t_j + E_j - e_{j+1}\, t_o + e_{j+1}\, t_j - E_j]^{\beta-1}\, dt' \end{aligned} \tag{91}$$

Equation (91) consists of nothing more than a series of simple integrations of the form

$$\int (at' + b)^{\beta-1}\, dt' = \frac{1}{\alpha\beta} (at' + b)^{\beta} \qquad (92)$$

Integrating as in Equation (92) and introducing A_i as defined below

$$A_i = -e_i\, t_{i-1} + E_{i-1} + e_{j+1}\, t_j - E_j \qquad (93)$$

Equation (91) may be written as

$$\frac{L}{\alpha\beta} = \frac{1}{e_{k+1}\beta} [e_{k+1}\, t' + A_{k+1} - e_{j+1}\, t_o]^{\beta} \Big|_{t_k}^{t_L}$$

$$+ \sum_{i=j+2}^{k_1} \frac{1}{e_i\beta} [e_i\, t' + A_i - e_{j+1}\, t_o]^{\beta} \Big|_{t_{i-1}}^{t_i}$$

$$+ \frac{1}{e_{j+1}\beta} [e_{j+1}\, t' - e_{j+1}\, t_o]^{\beta} \Big|_{t_o}^{t_{j+1}} \qquad (94)$$

Since Equation (94) may be explicitly differentiated with respect to t_o, a Newton-Rapson technique provides a simple solution. The subroutine developed uses a second-order routine to speed convergence. The routine proceeds by rewriting Equation (94) as

$$f(t_o) = -\frac{L}{\alpha\beta} + \frac{1}{e_{k+1}\beta} [e_{k+1}\, t' + A_{k+1} - e_{j+1}\, t_o]^{\beta} \Bigg|_{t_k}^{t_L}$$

$$+ \sum_{i=j+2}^{k} \frac{1}{e_i\beta} [e_i t' + A_i - e_{j+1}\, t_o]^{\beta} \Bigg|_{t_{i-1}}^{t_i}$$

$$+ \frac{1}{e_{j+1}\beta} [e_{j+1}\, t' - e_{j+1}\, t_o]^{\beta} \Bigg|_{t_o}^{t_{j+1}} \qquad (95)$$

The first and second derivatives of $f(t_o)$ with respect to t_o are respectively,

$$f'(t_o) = \frac{e_{j+1}}{e_{k+1}} \left\{ [e_{k+1}\, t_L + A_{k+1} - e_{j+1}\, t_o]^{\beta-1} - [e_{k+1}\, t_k + A_{k+1} - e_{j+1}\, t_o]^{\beta-1} \right\}$$

$$+ \sum_{i=j+2}^{k} \frac{e_{j+1}}{e_i} \left\{ [e_i\, t_o + A_i - e_{j+1}\, t_o]^{\beta-1} - [e_i\, t_{i-1} + A_i - e_{j+1}\, t_o]^{\beta-1} \right\}$$

$$- [e_{j+1}\, t_{j+1} - e_{j+1}\, t_o]^{\beta-1} \qquad (96)$$

and

$$f''(t_o) = \frac{e_{j+1}^{2}}{e_{k+1}} (\beta-1) \left\{ [e_{k+1}\, t_L + A_{k+1} - e_{j+1}\, t_o]^{\beta-2} - [e_{k+1}\, t_k + A_{k+1} - e_{j+1}\, t_o]^{\beta-2} \right\}$$

$$+ \sum_{i=j+2}^{k} \frac{e_{j+1}^{2}}{e_i} (\beta-2) \left\{ [e_i\, t_i + A_i - e_{j+1}\, t_o]^{\beta-2} - [e_i t_{i-1} + A_i - e_{j+1}\, t_o]^{\beta-2} \right\}$$

$$+ (\beta-1)\, (e_{j+1})\, [e_{j+1}\, t_{j+1} - e_{j+1}\, t_o]^{\beta-2} \qquad (97)$$

The second-order Newton's method is based on truncating a Taylor's series expansion of $f(t_o)$ about a trial value of t_o, defined as t_o^{*}, after the third term. Thus, $f(t_o)$ is written as

$$f(t_o) \simeq f(t_o^{*}) - (t_o - t_o^{*})\, f'(t_o^{*}) + \frac{(t_o - t_o^{*})^2}{2}\, f''(t_o^{*}) \qquad (98)$$

Roots of $f(t_o)$ are then obtained by setting $f(t_o) = 0$ in Equation (98) and solving the resulting quadratic for t_o. This value of t_o becomes the new estimate of the root and interations continue until

$$\left| \frac{f(t_o^{*})}{\frac{L}{\alpha\beta}} \right| < \eta \qquad (99)$$

where η is some arbitrarily small convergence increment.

In this manner, t_o's can be calculated corresponding to selected t_L's. Values of t_o contain some error due to the Newton's method approximation. However, this error, unlike the error due to interpolation, may be precisely controlled by the specification of η.

The number of terms in the summation appearing in Equations (95), (96), and (97) are determined by using the histogram of the lateral inflow to subdivide the solution domain. This subdivision is accomplished by calculating the characteristics arising at the beginning of each new histogram element (Figure 12). Since applications for which these routines are intended never exhibit kinematic shock, no characteristics in the solution domain intersect. Therefore, the characteristics calculated serve as a minimum set of bounds for those to be calculated by Equation (99). The number of terms in Equations (95) through (97) are immediately known by simply counting the number of histogram units crossed by the regions that are bounded by the characteristics having t_L's on either side of the t_L selected (Figure 11). Thus, the values of k and j for a given t_L in Equations (95) through (97) are known.

This technique provides a rapid means of findings t_o's corresponding to a given t_L. Three iterations of Newton's method have seemed sufficient for $\eta = 0.0001$. Knowing t_o and t_L, depth may be evaluated at the downstream boundary at time t_L by using Equation (60). This depth is used to determine the discharge at the downstream boundary at time t_L by using Equation (52).

There is one final point that should be covered. The routines described will operate satisfactorily for either positive or negative excess rainfall rates but the following condition must hold.

$$y > 0 \tag{100}$$

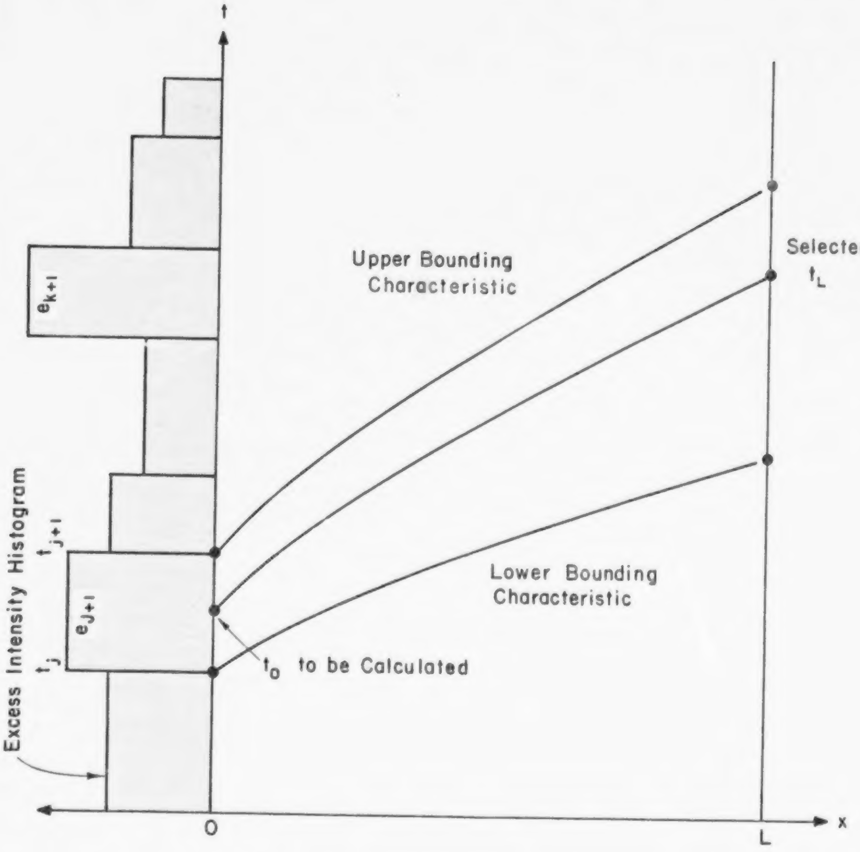
t
Upper Bounding Characteristic
Selected t_L
e_{k+1}
Excess Intensity Histogram
t_{j+1}
e_{J+1}
t_j
t_0 to be Calculated
Lower Bounding Characteristic
0
L
x

Figure 11. Method of characteristics solution domain illustrating upstream calculation of characteristics between bounding characteristics previously calculated in downstream direction.

From Equation (60) with $y_o = 0$, y can be expressed as

$$y = \int_{t_o}^{t} e(t')\, dt' \qquad (101)$$

where $e(t')$ is the function representing the excess rainfall histogram. Thus, the mandatory condition can be written as

$$\int_{t_o}^{t} e(t')\, dt' > 0 \qquad (102)$$

Physically, this situation occurs when rainfall stops or the intensity becomes quite small. When this occurs, runoff produced on the upper end of a plane due to the previous excess rainfall continues to flow down the plane until it reaches the downstream boundary or until it is completely infiltrated. This situation is illustrated in Figure 12. If the runoff is completely infiltrated, depth of flow becomes zero and the flow and routing are stopped. After the flow is stopped, depth at the downstream boundary will remain zero.

Sediment Determination

Erosion and sediment yields are processes of balancing soil erosion rates and transporting rates of the transporting medium. Generally, sediment yield from a watershed can be divided into processes related to the flow conditions, such as overland flow and channel flow. The following is a discussion of sediment supply due to erosion by both rainfall and runoff, and the transporting rate by overland flow and channel flow in upstream subwatersheds.

Overland Sediment Transport Capacity--

After the runoff rate q is known, the overland sediment transport capacity rate can be calculated. This is accomplished after determination of

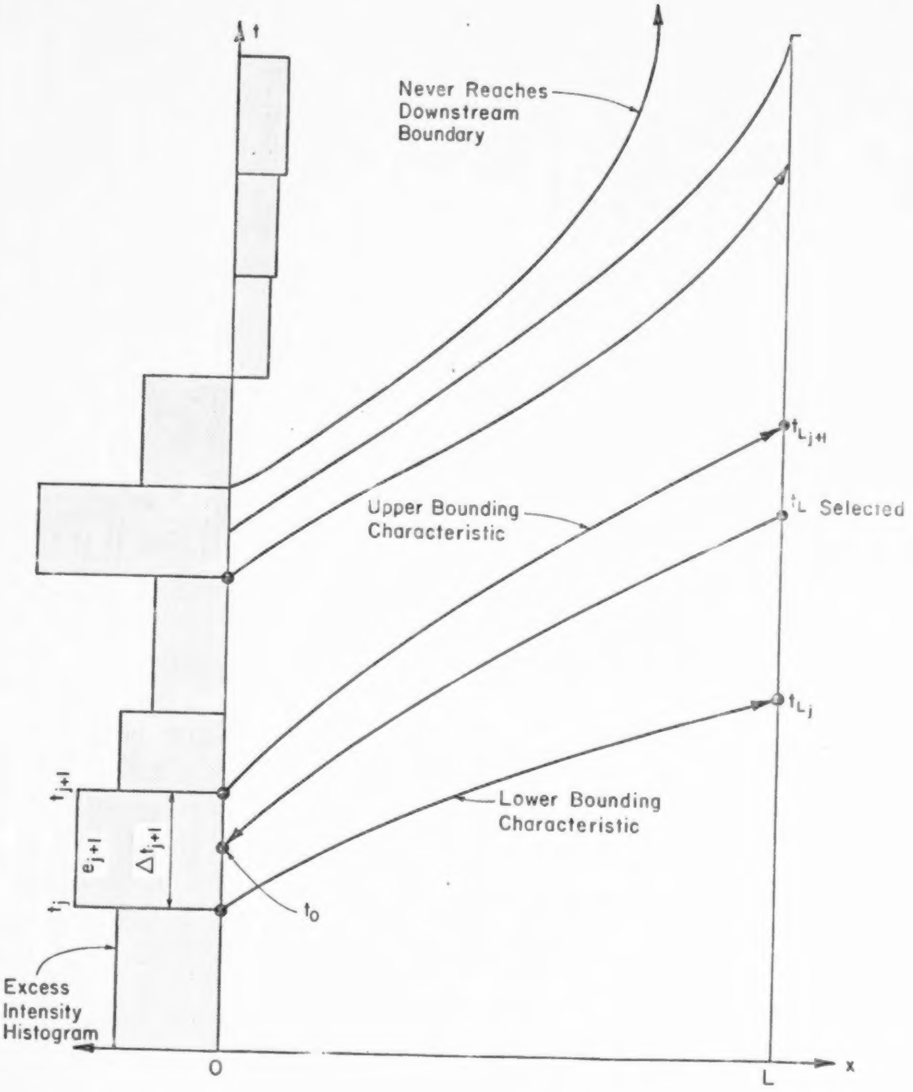
t
Never Reaches
Downstream
Boundary
$t_{L_{j+1}}$
Upper Bounding
Characteristic
t_L Selected
t_{L_j}
t_{j+1}
e_{j+1}
Δt_{j+1}
t_j
Lower Bounding
Characteristic
t_0
Excess
Intensity
Histogram
0
L
x

Figure 12. Method of characteristics solution domain illustrating effect of negative rainfall excess rates.

several intermediate steps. First, the overall flow resistance is assumed to be

$$K_g = K_\ell + (K_h - K_\ell)\, C_g^{\,2} \tag{103}$$

where K_g is the parameter describing the overall flow resistance associated with ground cover effects, K_ℓ is the parameter describing the minimum resistance for the area $(C_g = 0)$, K_h is the parameter describing the maximum resistance for the area $(C_g = 1.0)$, and C_g is the percent of ground cover. An increase in C_g produces a rapid increase in K_g as seen in Figure 13. These values closely agree with those found in Woolhiser's (1975) work in unsteady overland flow modeling.

Both q and K_g are then used to find the average flow depth as

$$y = \left(\frac{qK_g \nu}{8gS}\right)^{1/3} \tag{104}$$

where y is the flow depth, ν is the kinematic viscosity of water, g is the acceleration of gravity, and S_o is the slope of the ground surface.

The mean flow velocity is

$$V = \frac{q}{y} \tag{105}$$

The flow parameters calculated above are then used to determine sediment transport capacity. The procedure for determining sediment transport capacity given by Simons, Li, and Stevens (1975) is used in this report.

The first sediment transport parameter that should be determined is the tractive force or boundary shear stress. Effective boundary shear stress acting on a grain can be determined by

$$\tau = \frac{1}{8}\, f\rho\, V^2 = \frac{1}{8}\, \frac{K_o}{q}\, \nu\rho\, V^2 \tag{106}$$

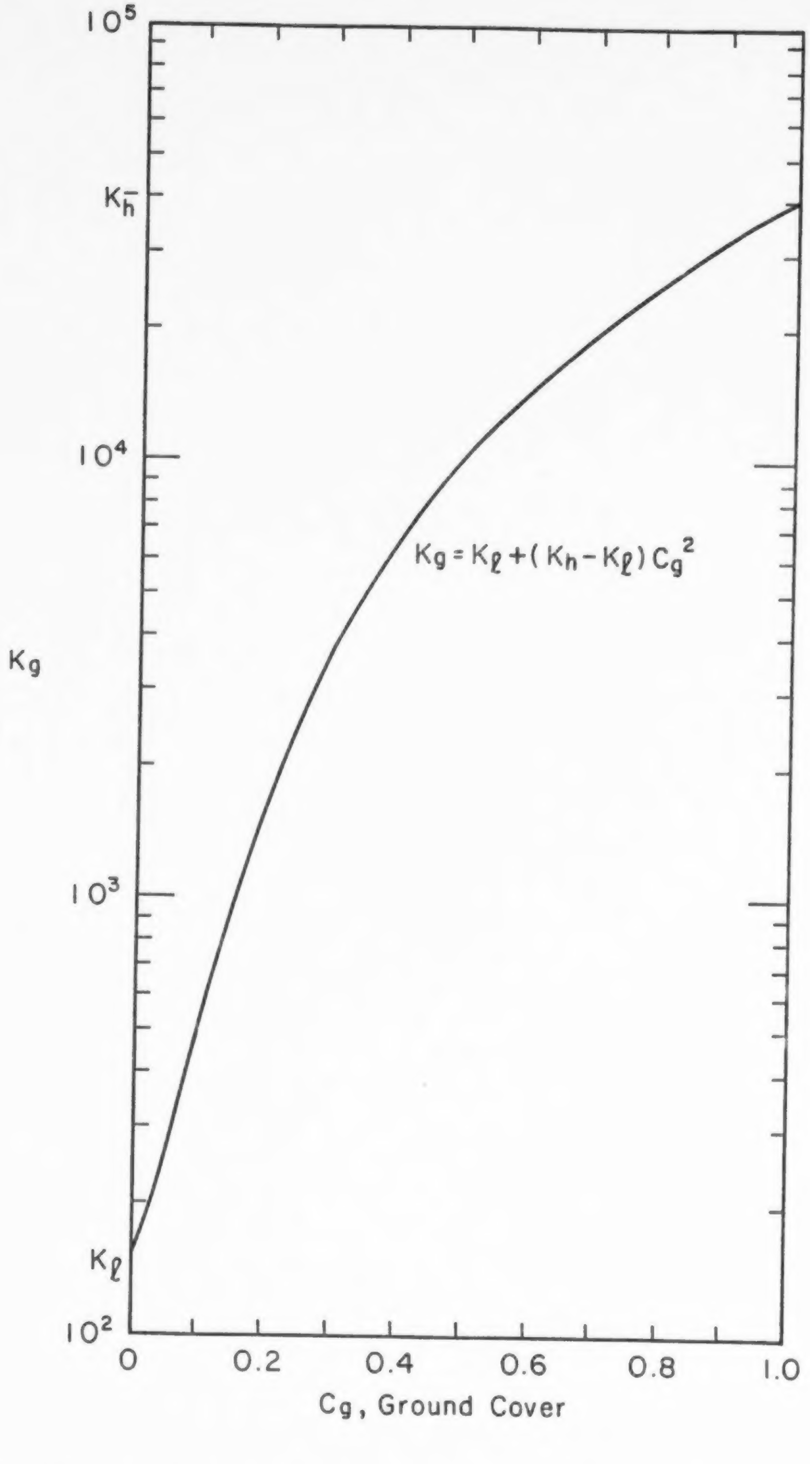

Figure 13. Assumed variation of overall resistance with ground cover.

where τ is the effective boundary shear stress, f is the Darcy-Weisbach friction factor for grain resistance, ρ is the density of water, and K_o is the parameter describing grain resistance.

The boundary shear stress τ', considering total resistance (form and grain resistance) is

$$\tau' = \gamma y S_o \tag{107}$$

where γ is the specific weight of water. It should be noted that τ' is usually much larger than τ. The shear velocity U_* is then

$$U_* = \frac{\tau'}{\rho} \tag{108}$$

The sediment transport capacity rate is an integral of all the individual sediment size transport rates or in discrete form

$$q_t = \sum_{i=1}^{N} (q_{ti} i_s) \tag{109}$$

where q_t is the total transport capacity rate, q_{ti} is the potential transport rate for each size, i_s is the percentage of each sediment size of bed material, and N is the total number of sizes considered. Each individual size transport q_{ti} is composed of bed load transport q_{bi} and suspended load transport q_{si} or

$$q_{ti} = q_{bi} + q_{si} \tag{110}$$

Bed load transport rate can be calculated using the Meyer-Peter, Muller formulation (USBR, 1960) as

$$q_{bi} = \frac{12.85}{\sqrt{\rho}} (\tau - \tau_c)^{1.5} \tag{111}$$

where τ_c is the critical shear force for the given particle size. Though the Meyer-Peter, Müller equation was used here, other suitable bed load formulations could be easily substituted into the model. Critical shear force for particle movement is determined by the Shields criteria of

$$\tau_c = \delta\gamma(S_s - 1)\ d_{si} \tag{112}$$

where δ is a parameter depending on flow conditions, S_s is the specific gravity of the sediment, and d_{si} is the sediment size in question. The value of S_s usually ranges from 2.60 to 2.70, but δ is dependent on flow conditions and should be adjusted to the actual field situation. If τ_c is greater than τ there is no sediment movement.

The suspended load is determined using the Einstein method (1950), or

$$q_{si} = C_a U_* a \frac{S^{w-1}}{(1-S)^w} [(\frac{V}{U_*} + 2.5)\ J_1 + 2.5\ J_2] \tag{113}$$

where C_a is the sediment concentration at distance a above the land surface, and S, A, a, J_1, and J_2 are given below.

The concentration term is related to the bed load transport as

$$q_{bi} = 11.6\ C_a U_* a \tag{114}$$

The distance a is assumed to be

$$a = 2\ d_{si} \tag{115}$$

The dimensionless parameters relate flow depth to sediment size as

$$S = \frac{a}{y} \tag{116}$$

The dimensionless parameter w relates the in-water settling velocity of the sediment to the shear velocity or

$$w = \frac{V_s}{\kappa U_*} \tag{117}$$

where V_s is the settling velocity of the sediment and κ is von Karman's number taken as 0.40.

Settling velocities are a function of particle size and water properties and can be formulated (ASCE, 1975) as

$$V_s = \frac{2.9517\ d_{si}^{\ 2}}{v} \quad \text{when} \quad d_{si} < 0.0002 \text{ feet} \tag{118}$$

or

$$V_s = \frac{(36.064\ d_{si}^{\ 3} + 36v^2)^{1/2} - 6v}{d_{si}} \quad \text{when } d_{si} \geq 0.0002 \text{ feet}$$

Terms J_1 and J_2 are integrals resulting from integration of the equation describing the vertical concentration of sediment in the flow. The first integral J_1 is given as

$$J_1 = \int_S^1 \left(\frac{1 - \sigma}{\sigma}\right)^w d\sigma \tag{119}$$

where σ is a dimensionless relative position

$$\sigma = \frac{\varepsilon}{Y} \tag{120}$$

and ε is the distance above the land surface in the flow. The other integral is similar and is given as

$$J_2 = \int_S^1 \ell n\sigma \left(\frac{1 - \sigma}{\sigma}\right)^w d\sigma \tag{121}$$

These two integrals can be evaluated by successive integrations of a power series expansion given by Li (1974). Rearranging Equation (114) and substituting into Equation (113) gives a simpler form or

$$q_{si} = \frac{q_{bi}}{11.6} \frac{S^{w-1}}{(1-S)^w} \left[\left(\frac{V}{U_*} + 2.5\right) J_1 + 2.5\ J_2\right] \tag{122}$$

The total potential transport rate, Equation (110) becomes

$$q_t = \sum_{i=1}^{N} (q_{si} + q_{bi})\ i_s \tag{123}$$

Potential transport capacity can be found as

$$V_t = \frac{W}{\gamma S_s} \int_0^{D_e - t_p} q_t \, dt \qquad (124)$$

where W is the width of the plane, D_e is the duration of runoff, t_p is the time of ponding, and V_t is the nonporous volume of potential transport.

Channel Sediment Transport Capacity--

After overland flow runoff is known, the sediment transporting capacity of the channel can be calculated. Although the physics of sediment transport for the channel are much the same as those for overland flow, relations describing channel sediment capacity are altered. In the channel, as described earlier, both the discharge and wetted perimeter can be expressed as a power relation of area (Equations (72) and (76)). Since $Q = VA$, Equations (72), (76), and (106) can be combined to solve for τ as

$$\tau = \frac{\rho f}{8\alpha^2} Q^{(2-2\beta)} \qquad (125)$$

Variables α and β are given in Equations (77) and (78) or (79) and (80) as earlier derived. With solutions for α and β, Equation (125) can be solved for τ.

The grain friction factor f for open channel flow is found differently from that for overland flow. For overland flow it was assumed that low Reynolds numbers prevailed and the friction factor was only a function of Reynolds number. Generally, in channel flow it can be assumed that the flow is well into the turbulent region. If the approximate flow values are known, a constant value for f can be used over the range of flows. Usually, for small sediment sizes, sediment supply is the controlling factor and not the sediment transport capacity. Therefore, small differences in the estimation of the f factor are seldom seen in the sediment yield results.

Determination of Sediment Supply--

Potential sediment transport represents the capacity of the system. Supply of sediment comes from two mechanisms: detachment by raindrop splash and detachment by overland and channel flow. For a plane of width and length L , raindrop splash detachment can be formulated as a simple power function of rainfall intensity (Meyer, 1971)

$$V_r = a_1 i^2 LW (1 - \phi) A_b \tag{126}$$

where V_r is the nonporous volume of detached material by raindrop splash, a_1 is an empirically determined constant describing erodibility of the soil, and A_b is an area reduction factor.

The variable A_b represents the fraction of unprotected or bare soil in the area and is given as

$$A_b = 1 - C_g - C_c + (C_g C_c) \tag{127}$$

where $(C_g C_c)$ accounts for areas of cover overlap. Sediment supply by overland flow detachment is determined by

$$V_f = D_f (V_t - V_r) \tag{128}$$

where V_f is detachment by overland flow and D_f is the flow detachment coefficient. An equation similar to that used in overland flow detachment is used for channel flow detachment. For many cases, however, the flow detachment coefficient for channels is assumed to be zero due to natural armoring, riprap, or other forms of bed and bank protection. This is especially true for man-made channels.

If $V_t < V_r$ there is no flow detachment because the transport rate is limited by the transporting capacity. Total available sediment supply is then

$$V_a = V_r + V_f \tag{129}$$

Determination of Sediment Yield--

Once supply and capacity for each size fraction have been calculated and summed over the entire event, actual sediment yield can be determined. This is done by comparing transporting capacity and supply for each size fraction. If the transporting capacity is greater than the total available sediment supply $V_f > V_a$ then sediment yield for that size fraction is equal to V_a. However if $V_f < V_a$, then yield for that size fraction is equal to V_f.

SUBPROGRAM SORT

SORT acts as an interface between the MULT and MCHNL components of RUNOFF and is necessary to make efficient use of computer time and storage. MULT uses an analytical routing method which calls for the results of each unit (plane or subwatershed) to be calculated for the whole event before calculating any results for the next unit in the computational sequence. However, MCHNL uses a numerical procedure which works most efficiently when the results for a single time increment of the event are calculated for all units before proceeding to the next time increment. Since MULT provides the lateral and upstream inflows for MCHNL the space time orientation of the results must be switched. SORT reads the files created in MULT and then executes the switch (Figure 14). In addition, SORT separates the discharge hydrograph from the sediment yield results.

SUBPROGRAM MCHNL

MCHNL uses a numerical scheme to route both water and sediment in the downstream channels. It uses discharges and sediment yields calculated in MULT and rearranged in SORT as upstream and lateral inflows into the channel units. In addition, an infiltration routine calculates the amount of water which infiltrates in the channel units and subtracts it from the lateral inflow.

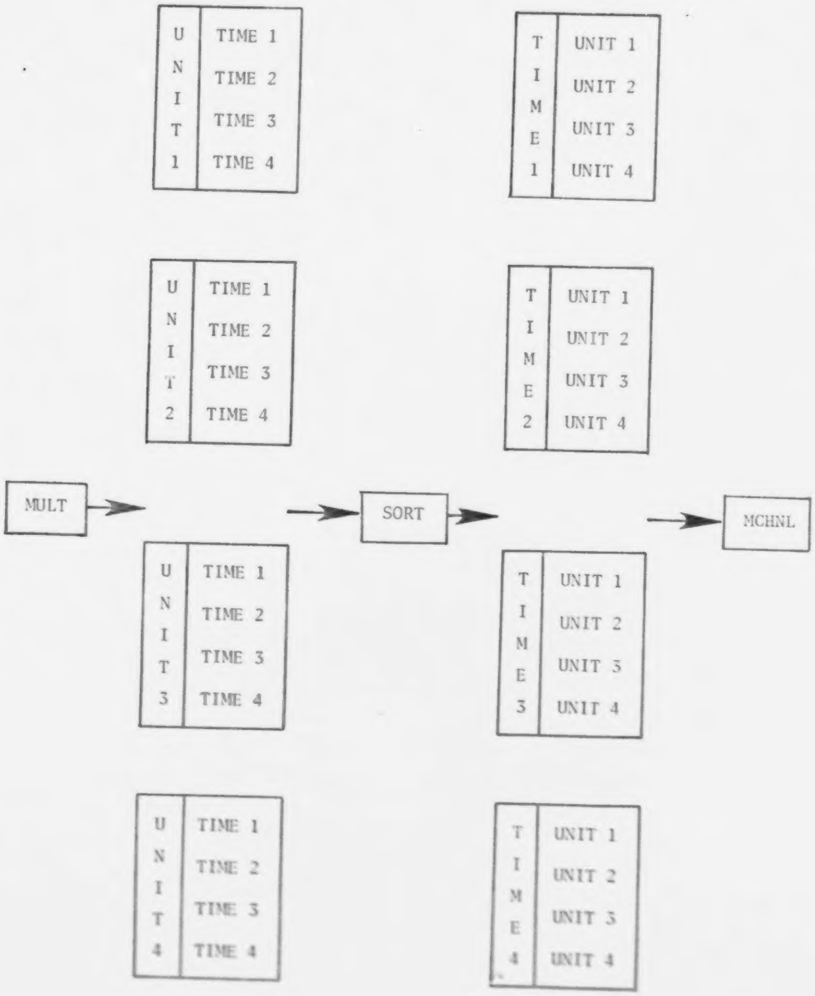
MULT
SORT
MCHNL
UNIT 1
UNIT 2
UNIT 3
UNIT 4
TIME 1
TIME 2
TIME 3
TIME 4

Figure 14. Spatial to temporal reorganization of runoff events by SORT.

Mathematical Derivation of the Numerical Kinematic Routing Procedure

Numerical and analytical kinematic wave routing schemes are governed by the same equations: the equation of continuity, the momentum equation, and equations describing channel geometry and flow resistance. The following numerical kinematic routing procedure is used by MCHNL for the channel units.

Derivation for the discharge-area relationship is slightly different. In MCHNL the relationship is expressed as

$$A = \alpha' \, Q^{\beta'} \tag{130}$$

instead of

$$Q = \alpha \, A^{\beta} \tag{131}$$

as in MULT. This is due to the use of the numerical method in MCHNL. Usually β' is less than 1.0 and has a value of one-third for Reynolds numbers less than 900. Consequently, if discharge is computed incorrectly, the relative error in the flow area is smaller than the relative error in the discharge. On the other hand, the error in the discharge estimation is magnified if the numerical computations are performed on the flow area (Li, Simons, and Stevens, 1975). In the case of MULT, it is more convenient to compute discharge as a function of flow area.

If Manning's equation is applied, the corresponding α' and β' are

$$\alpha = \left(\frac{a_1^{4/3} n^2}{2.21 \, S_o}\right)^{\left(\frac{3}{10-4b_1}\right)} \tag{132}$$

and

$$\beta' = \frac{3}{5-2b_1} \tag{133}$$

If the Chezy relationship is used, the α' and β' values are

$$\alpha' = \left(\frac{a_1}{C^2 S_o}\right)^{[1/(3-b_1)]} \tag{134}$$

and

$$\beta' = \frac{2}{3-b_1} \tag{135}$$

The water continuity equation for the channel can be expressed as

$$\frac{\partial Q}{\partial x} + \frac{\partial A}{\partial t} = q_\ell \tag{136}$$

in which Q is water discharge, x is the downslope distance, A is the flow area, t is time, and q_ℓ is the lateral inflow. Lateral inflow rate q_ℓ for the channel units is obtained from the overland flow in the adjacent plane units calculated in MULT.

The problem of water routing becomes a matter of solving Equations (130) and (136). A nonlinear scheme with an iterative procedure was used in this study. A linear scheme was used to obtain the initial estimate of the unknown discharge for the nonlinear scheme. The linear scheme may be used as is with no iterations to solve for the unknown discharge if the accuracy is satisfied.

The finite difference form of Equation (136) can be represented as

$$\frac{Q_{j+1}^{n+1} - Q_j^{n+1}}{\Delta x} + \frac{A_{j+1}^{n+1} - A_{j+1}^{n}}{\Delta t} = \frac{1}{2}\left(q_{\ell_{j+1}}^{\ n+1} + q_{\ell_{j+1}}^{\ n}\right) \tag{137}$$

in which Q_j^n is the quantity Q at grid point $x = j\Delta x$ and $t = n\Delta t$, Δx is the space increment, and Δt is the time increment. The rectangular network shown in Figure 15 illustrates the x-t grid system.

Unknowns in Equation (137) are Q_{j+1}^{n+1} and A_{j+1}^{n+1}, but the discharge bears a definite relation with the flow area as indicated by Equation (130). With these two equations, the values of the two unknowns can be obtained.

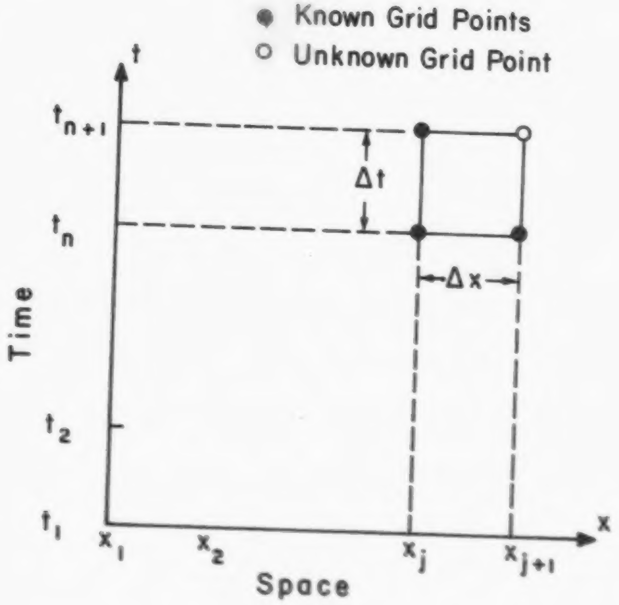
● Known Grid Points
○ Unknown Grid Point
t
t_{n+1}
Δt
t_n
Δx
Time
t_2
t_1
x_1
x_2
x_j
x_{j+1}
x
Space

Figure 15. Definition sketch for channel water and sediment finite difference routing scheme.

Substitution of Equation (130) into Equation (137) yields

$$\frac{\Delta t}{\Delta x} Q^{n+1}_{j+1} + \alpha'(Q^{n+1}_{j+1})^{\beta'} = \frac{\Delta t}{\Delta x} Q^{n+1}_{j} + A^{n}_{j+1} + \frac{\Delta t}{2} (q_{\ell}{}^{n+1}_{j+1} + q_{\ell}{}^{n}_{j+1}) \tag{138}$$

The right side of Equation (138) contains known quantities and is denoted by Ω which can be expressed as

$$\Omega = \frac{\Delta t}{\Delta x} Q^{n+1}_{j} + A^{n}_{j+1} + \frac{\Delta t}{2} (q_{\ell}{}^{n+1}_{j+1} + q_{\ell}{}^{n}_{j+1}) \tag{139}$$

If $r = Q^{n+1}_{j+1}$ and $\theta = \frac{\Delta t}{\Delta x}$, then the left side of Equation (138) is expressed as

$$f(r) = \theta r + \alpha' r^{\beta'} \tag{140}$$

The solution of Equation (138) satisfies the condition

$$f(r) = \theta r + \alpha' r^{\beta'} = \Omega \tag{141}$$

An approximate solution to this nonlinear equation is obtained by the following iterative scheme.

If r^k is the value of r at the k^{th} iteration, Taylor Series expansion of the function $f(r)$ around r^k is

$$\begin{aligned} f(r) = {} & f(r^k) + (r - r^k)\, f'(r^k) + \frac{1}{2}(r - r^k)^2 f''(r^k) \\ & + \frac{1}{6}(r - r^k)^3 f'''(r^k) + \ldots \end{aligned} \tag{142}$$

in which $f'(r^k)$ and $f''(r^k)$ are values of the first and second derivatives of the function at r^k. Dropping the terms higher than the second order, one obtains

$$f(r) \cong f(r^k) + (r - r^k)\, f'(r^k) + \frac{1}{2}(r - r^k)^2 f''(r^k) \tag{143}$$

The purpose of iteration is to force $f(r^{k+1})$ to approach the value of Ω or

$$\Omega \cong f(r^k) + (r^{k+1} - r^k)\, f'(r^k) + \frac{1}{2}(r^{k+1} - r^k)^2 f''(r^k) \tag{144}$$

The solution of Equation (144) is

$$r^{k+1} = r^k - \frac{f'(r^k)}{f''(r^k)} \pm \sqrt{\left(\frac{f'(r^k)^2}{f''(r^k)}\right) - \frac{2(f(r^k) - \Omega)}{f''(r^k)}} \tag{145}$$

in which

$$f(r^k) = \theta r^k + \alpha'(r^k)^{\beta'} \tag{146}$$

$$f(r^k) = \theta + \alpha'\beta'(r^k)^{\beta'-1} \tag{147}$$

and

$$f''(r^k) = \alpha'\beta'(\beta'-1)\ (r^k)^{\beta'-2} \tag{148}$$

There are two solutions to Equation (145). It is advisable to choose the solution that gives the smaller value of $\left|f(r^{k+1})-\Omega\right|$. The above iteration is continued until the absolute error $\left|f(r^{k+1})-\Omega\right|$ is less than a preassigned tolerance η. The termination criteria can be written as

$$\left|f(r^{k+1}) - \Omega\right| \leq \eta \tag{149}$$

An appropriate value for η is 0.01 Ω. However, it may be changed according to the purpose of individual problems.

The scheme represented by Equation (137) has proved to be unconditionally stable and can be used with a wide range of time to space increment ratios without loss of significant accuracy (Li, Simons, and Stevens, 1975). However, the initial guess r° is the key to the speed of convergence to the correct numerical solution. The best way of determining r° is to use a linear scheme.

The term $\frac{\partial A}{\partial t}$ in Equation (136) can be expressed as

$$\frac{\partial A}{\partial t} = \frac{\partial A}{\partial Q}\frac{\partial Q}{\partial t} \tag{150}$$

Also, from Equation (130)

$$\frac{\partial A}{\partial Q} = \alpha'\beta'Q^{\beta'-1} \tag{151}$$

Substitution of Equations (150) and (151) into Equation (136) yields

$$\frac{\partial Q}{\partial x} + \alpha'\beta' Q^{\beta'-1}\frac{\partial Q}{\partial t} = q_\ell \tag{152}$$

The finite difference form of Equation (152) is given by the expression

$$\frac{Q_{j+1}^{n+1} - Q_j^{n+1}}{\Delta x} + \alpha'\beta'\left(\frac{Q_{j+1}^{n} + Q_j^{n+1}}{2}\right)^{\beta'-1}\frac{Q_{j+1}^{n+1} - Q_{j+1}^{n}}{\Delta t} = \frac{1}{2}\left({q_\ell}_{j+1}^{n+1} + {q_\ell}_{j+1}^{n}\right) \tag{153}$$

so that

$$r^\circ = Q_{j+1}^{n+1} = \frac{\theta Q_j^{n+1} + \alpha'\beta' Q_{j+1}^{n}\left(\frac{Q_{j+1}^{n} + Q_j^{n+1}}{2}\right)^{\beta'-1} + \frac{\Delta t}{2}\left({q_\ell}_{j+1}^{n+1} + {q_\ell}_{j+1}^{n}\right)}{\theta + \alpha'\beta'\left(\frac{Q_{j+1}^{n} + Q_j^{n+1}}{2}\right)^{\beta'-1}} \tag{154}$$

Equation (154) uses a linear scheme to provide the best initial estimate of r° for the nonlinear scheme. However, Equation (154) is not applicable if both Q_{j+1}^{n} and Q_j^{n+1} are zero. When both Q_{j+1}^{n} and Q_j^{n+1} are zero, $\beta' = 1$ is used in Equation (141) and then

$$r^\circ = \frac{\Omega}{\theta + \alpha'} \tag{155}$$

Channel Infiltration Routine

The channel infiltration routine is similar to the layered infiltration scheme described earlier in the report, but with two differences. First, the channel infiltration routine is not a layered model. Only one homogeneous layer of soil is assumed to exist in the channel. Second, since the depths of flow in the channels are normally much greater than those for overland flow, depth of the water is not ignored. Thus, the equations are the same except for the addition of head due to depth of flow and use of only one layer.

Sediment Routing

Sediment routing in MCHNL uses the same principle as the sediment yield calculations in MULT--the process of balancing supply and capacity for each sediment size. In addition, MCHNL includes the effect of armoring on the sediment transport rate. The process of armoring occurs because of the difference in sediment transport capacity between the different sizes, resulting in a layer of larger size fraction formed on the surface. If the erosion processes continue, this layer of larger size fraction will protect the smaller one from detaching or dislodging.

Sediment calculations in MCHNL are also different in that the numerical method used allows for the sediment to be routed through the channels at each time increment and then integrated over the time increments to arrive at a total yield for each size fraction. The method used in MULT can only provide a total yield for each size fraction, but cannot truly route the sediment through the channel. MCHNL is able to route the sediment because the balancing of transporting capacity and supply can be compared at each time and space increment along the channel due to the use of the numerical scheme. The method used in MULT does not allow for this, since only conditions at the downstream end of the channel are calculated.

Since MCHNL uses the numerical method which requires actual transport rates at each time increment, and it needs to use the yields calculated in MULT as upstream and lateral inflows, the yields in MULT must be transformed into sediment hydrographs. This is accomplished by distributing the yields from MULT in proportion to the water discharge at each time increment. MCHNL could easily be modified to distribute the yields from MULT by various other schemes.

The remainder of this section will be devoted to the governing equations for sediment routing and the development of the numerical routing technique.

Governing Equation for Sediment Routing--

In the channel units the processes which govern sediment routing are the continuity for sediment, the transport capacity, sediment flow detachment and armoring. The continuity equation for sediment size i is

$$\frac{\partial G_{si}}{\partial x} + \frac{\partial C_i A}{\partial t} + (1 - \lambda) \frac{\partial PZ_i}{\partial t} = g_{si} \tag{156}$$

in which i is the size fraction index, G_{si} is total sediment transport rate by volume per unit time, C_i is sediment concentration by volume, Z_i is depth of loose soil, λ is channel bed porosity, and g_{si} is lateral sediment inflow.

Concentration of sediment for a sediment size i is

$$C_i = \frac{G_{si}}{Q} \tag{157}$$

Total concentration of sediment at a cross section is

$$C_T = \sum_{i=1}^{N} C_i \tag{158}$$

and the total loose soil availble is

$$Z_T = \sum_{i=1}^{N} Z_i \tag{159}$$

Sediment transport capacty equations are the same as those used for the channel in MULT and descibed earlier. The only difference is that the transport capacity is calculaed at segments along the channel at each time increment instead of at the downstream end of the channel.

The amount of soil detachment by surface runoff is determined by comparing the total sediment transport capacity to the total available amount of loose soil. Total sediment transport capacity is

$$G_c = \sum_{i=1}^{N} G_{ci} \tag{160}$$

Assuming total sediment transport capacity G_c is equal to the transport rate, the total potential change in loose soil can be determined from Equation (157) as

$$\Delta Z^P = \frac{\partial Z}{\partial t} \Delta t \tag{161}$$

If $\Delta Z^P \geq -Z$, the loose soil storage is enough for transport and there is no detachment of soil by surface runoff. Soil is detached if $\Delta Z^P < -Z$. The amount of detachment can be computed by

$$D = D_f [\Delta Z^P + Z] \tag{162}$$

in which D is the total amount of detached soil and D_f is a detachment coefficient which varies from 0.0 to 1.0 depending on soil erodibility. If the ground surface is completely paved with gravel, D_f is equal to zero. In a river (where the riverbed is always loose) the value for D_f is one.

The new amount of loose soil is then

$$Z_i = Z_i + D\,F_i \tag{163}$$

in which Z_i is calculated for each size fraction of sediment.

Percentage in each size fraction changes over time due to armoring. Water transports the sediment that has a smaller size more easily and leaves the larger size fractions behind. Thus, the percentages of sediment size on the surface need adjustment at each time step. An armoring sediment size D_{AR} which always remains on the ground surface for a given flow condition was selected. If total loose soil depth is greater than armoring size, the adjusted percentages F_{ai} can be written as

$$F_{ai} = \frac{Z_i}{Z_T} \tag{164}$$

If the total loose soil depth Z_T is less than D_{AR}, the adjusted percentages must account for the layer of undisturbed soil which is distributed according to the original percentages plus the loose soil which covers it or

$$F_{ai} = \frac{1}{D_{AR}} [Z_i + F_i (D_{AR} - Z_i)] \tag{165}$$

Numerical Procedure for Sediment Routing--

A numerical procedure for sediment routing is developed to solve equations governing sediment and water movement. Sediment transport capacity is determined by Equation (124) for a given sediment size for the flow conditions obtained by water routing. Potential sediment load concentration for a given sediment size i is then

$$C_i^p = \frac{G_{ci}}{Q} \tag{166}$$

Using the same finite-difference approximation as that in the water routing procedure (Figure 15), potential change in loose soil storage for a given sediment size is determined by utilizing Equations (156) and (166). That is

$$\Delta Z_i^p = \frac{1}{(1-\lambda)p} [(G_{si_j}^{n+1} - C_i^p Q_{j+1}^{n+1})\theta - C_i^p A_{j+1}^{n+1}$$

$$+ C_{i_{j+1}}^{n} A_{j+1}^{n} + \frac{\Delta x}{2} (g_{si_{j+1}}^{n+1} + g_{si_{j+1}}^{n})] \tag{167}$$

Sediment transport rate is dependent on both the available supply of sediment and the transporting capacity of the flow. If $\Delta Z_i^p \geq -Z$, the availability is greater than the transporting capacity. Thus, bed material load transport rate is equal to its transporting capacity or

$$C_{i_{j+1}}^{n+1} = C_i^p \tag{168}$$

and the actual change in Z_i is

$$\Delta Z_i = \Delta Z_i^P \tag{169}$$

If $\Delta Z_i^P < -Z_i$, availability of material is less than the transporting capacity and the transport rate is limited by the availability of loose soil. Bed material is therefore

$$C_{i_{j+1}}^{n+1} = \frac{(1-\lambda)\rho_w Z_i + \frac{\Delta t}{2} (g_{si_{j+1}}^{n+1} + g_{si_j}^{n}) + C_{i_{j+1}}^{n} A_{j+1}^{n} + G_{si_j}^{n+1} \theta}{A_{j+1}^{n+1} + \theta Q_{j+1}^{n+1}} \tag{170}$$

and

$$\Delta Z_i = -Z_i \tag{171}$$

Sediment transport rate G_{si} is determined by

$$G_{si_{j+1}}^{n+1} = C_{i_{j+1}}^{n+1} Q_{j+1}^{n+1} \tag{172}$$

and the amount of loose soil available at the next time increment is

$$Z_i = Z_i + \Delta Z_i \tag{173}$$

SYMBOLS FOR SECTION 3

Symbol	Description
A	Cross-sectional flow area of stream
$A_{1,2}$	Area of plane 1 or 2
A_b	Fraction of unprotected or bare soil
A_{j+1}^{n}	Flow area at location $(j+1)\ \Delta x$ and time step $n\Delta t$
A_{j+1}^{n+1}	Flow area at location $(j+1)\ \Delta x$ and time step $(n+1)\ \Delta t$
A_o	Sediment yield at an upstream station
a	Distance above channel or land surface
a_1	Coefficient in wetted perimeter-stream cross-sectional area relation, or coefficient in raindrop splash sediment detachment equation
a_2	Coefficient in top width-stream cross-sectional area relation
b	Constant describing the influence of runoff to erosion
b_1	Exponent in wetted perimeter-stream cross-sectional area relation
b_2	Exponent in top width-stream cross-sectional area relation
C	Chezy's friction factor
C_a	Sediment concentration at distance a above bed
C_c	Percent of canopy cover
C_g	Percent of ground cover

Symbol	Description
C_i	Sediment concentration for size fraction i
C_{ij+1}^{n}	Sediment concentration at location (j+1) Δx at time step n Δt
C_{ij}^{n+1}	Sediment concentration at location jΔx at time step (n+1) Δt
C_{ij+1}^{n+1}	Sediment concentration at location (j+1) Δx at time step (n+1) Δt
C_i^p	Potential change in sediment concentration
D	Total amount of soil detachment
D_{AR}	Armor size
D_F	Soil detachment by runoff
D_e	Duration of runoff
D_f	Runoff detachment coefficient
d_s	Representative sediment size
E	Cumulative excess rainfall volume
e	Excess rainfall intensity
F_{ai}	Adjusted fraction of the $i^{\underline{th}}$ size sediment
F_i	Initial size fraction of the $i^{\underline{th}}$ size sediment
f	Infiltration rate, or Darcy-Weisbach friction factor
G_c	Total sediment transport capacity
G_{oi}	Sediment transport capacity for $i^{\underline{th}}$ size fraction
G_{si}	Total sediment transport rate for sediment size i
G_{sij}^{n}	Sediment transport rate at location j Δx at time step n Δt for $i^{\underline{th}}$ size fraction
$G_{si\ j+1}^{\ n}$	Sediment transport rate at location (j+1) Δx at time step n Δt for $i^{\underline{th}}$ size fraction
$G_{si\ j}^{\ n+1}$	Sediment transport rate at location j Δx at time step (n+1) Δt for $i^{\underline{th}}$ size fraction

Symbol	Description
$G_{si\,j+1}^{\;\;n+1}$	Sediment transport rate at location (j+1) Δx at time step (n+1) Δt for ith size fraction
g	Acceleration due to gravity
$g_{si\,j}^{\;\;n}$	Lateral sediment inflow rate at location j Δx at time step n Δt for ith size fraction
$g_{si\,j+1}^{\;\;n+1}$	Lateral sediment inflow rate at location (j+1) Δx at time step (n+1) Δt for ith size fraction
i	Average rainfall intensity
J_1, J_2	Integrals in Einstein's suspended sediment load expression
K	Numerator in Darcy-Weisbach resistance to flow equation
K_g	Overall resistance parameter associated with cover effects
K_h	Highest resistance parameter associated with cover effects
K_ℓ	Lowest resistance parameter associated with cover effects
K_o	Grain resistance parameter
L	Length of slope; plane or channel
L_c	Length of channel reach
n	Manning's friction factor
N_r	Reynolds number
P	Wetted perimeter
Q	Water discharge
Q_j^{n+1}	Discharge at location j Δx at time step (n+1) Δt
Q_{j+1}^{n+1}	Discharge at location (j+1) Δx at time step (n+1) Δt
q	Discharge per unit width
q_b	Bed load sediment discharge per unit width
q_ℓ	Lateral inflow to stream channel per unit width

Symbol	Description
q_L	Discharge per unit width at downstream boundary
q_o	Discharge at x_o
q_s	Suspended sediment discharge per unit width
q_t	Total sediment discharge per unit width
R	Hydraulic radius
r	Rainfall intensity
S	Ratio of sediment size to flow depth
S_f	Friction slope
S_o	Bed slope; channel or plane
S_s	Specific gravity of sediment
S_1	Slope of plane 1
S_2	Slope of plane 2
T	Top width of channel
t	Time
t_L	Time of arrival of characteristic at downstream boundary
t_o	Time of characteristic's origin at upstream boundary
t_p	Time of ponding
U_*	Shear velocity
V	Mean flow velocity
V_a	Total available sediment supply (nonporous)
V_f	Sediment supply volume by flow detachment (nonporous)
V_r	Sediment volume detached by raindrop impact (nonporous)
V_s	Particle settling velocity
V_t	Potential transport sediment volume (nonporous)
W	Width of stream on plane
w	Particle fall velocity

Symbol	Description
x	Distance in downslope direction
x_o	Origin of a given characteristic path, usually the upstream boundary
Y_s	Sediment yield
y	Depth of flow
y_L	Depth of flow at the downstream boundary
y_o	Depth of flow at the upstream boundary
Z_i	Depth of loose soil for sediment size i
Z_T	Total loose soil
z	Distance in vertical direction
α	Coefficient in depth-discharge or area-discharge relation
α'	Coefficient in discharge-area relation
β	Exponent in depth-discharge or area-discharge relation
β'	Exponent in discharge-area relation
γ	Specific weight of water
δ	Coefficient in Shield's diagram
η	Convergence increment
ε	Distance above bed in the flow
θ	Slope angle
κ	von Karman constant
μ	Dynamic viscosity
ν	Kinematic viscosity of water
τ	Effective shear stress
τ'	Boundary shear stress

Symbol	Description
τ_c	Critical shear stress
ϕ	Soil porosity
λ	Channel bed porosity
ρ	Density of water

SECTION 4

NUTRIENT ROUTING

INTRODUCTION

Nutrient elements are a source of non-point pollutants affecting water quality. Two of these elements, nitrogen and phosphorus, are pollutants of concern because of their role in eutrophication processes. A physical process simulation model was developed for predicting nutrient losses from forest and agricultural watersheds associated with surface runoff and sediment transport.

Development of pollution control mechanisms calls for an understanding of nutrient processes as they exist in natural ecosystems. Several questions need to be answered before this understanding is achieved. What are their basic characteristics? How do they interact with their natural environment? How do nutrients such as nitrogen and phosphorus act as pollutants to affect water quality?

The primary sources of nitrogen input into the ecosystem are fertilizer, litter fall, and precipitation. Nitrogen may exist in solution principally as nitrate-nitrogen (NO_3-N) and ammonium (NH_4-N). It can also be adsorbed by sediment as ammonium and organic compounds. Therefore, nitrogen can be easily moved with runoff water or sediment to increase the nutrient loading by mechanisms such as dissolving and cation-exchange which are significant in the soil. Under anaerobic conditions, nitrate can be reduced to a volatile gas such as N_2, N_2O, or NH_3. These gases may be oxidized into nitrate in the atmosphere by lightning or photochemical reaction and returned to the soil by precipitation.

Phosphorus primarily comes from the weathering of rock, fertilizer, and decaying organic matter. In general, it exists in organic or inorganic form. It has low solubility and is transported primarily by erosion and thus tends to be moved with sediment into rivers and lakes. Increased phosphorus loading may accelerate eutrophication and aging of a lake.

Surface runoff and subsurface flow may increase the nutrient load in the stream, both in solution and particulate form. Nutrients adsorbed to the suspended solids or settled sediment may go into solution. The extent to which this process occurs is dependent on many factors, such as water temperature and chemical quality of the water. The exchange process occurring between soil particles and soil water is quite similar to that found in streams.

In general, nutrient losses within a watershed may have a direct impact on the quality of water within that watershed. Fertilizers, manure, or other organic matter added to the soil as part of agricultural and silvicultural activities often result in significant nutrient losses through soil erosion and runoff water. Concentrations of nitrogen, in the form of nitrate in drinking water may interact with components in the blood to interfere with oxygen transport and cause methomoglobinemia in infants. Ammonia (NH_3) is toxic to aquatic life even at low concentrations. Eutrophication, the enrichment of waters by nutrients and the ensuing luxuriant growth of plants, has become a widespread problem in the United States. It causes taste and odor problems, kills fish populations, and adversely impinges on recreation usage of lakes and ponds.

Use of this nutrient cycling model allows for prediction of the level of nutrients that will be moved into rivers and streams. This model can serve as a valuable source of management information. Information generated by the model will aid in determining the most suitable control mechanisms for regulating nutrient losses from a watershed. Influx of large amounts of nutrients into a river changes its nutrient content greatly affecting water quality. A nutrient model can guide in the development of the most suitable treatment of watersheds and rivers to improve the river's water quality.

BASIC CONCEPTS FOR NITROGEN AND PHOSPHORUS

In general, the nutrient cycles of nitrogen and phosphorus are quite complex. Several nutrient species for nitrogen and phosphorus may be present in the cycles and change state from one species to another. This change may affect their concentration in the soil. They also interact with soil water and soil particles. This directly affects the nutrient losses during storm events. To better understand the whole nutrient cycle, basic concepts about nitrogen and phosphorus are presented. This should improve the understanding of the processes occurring in the cycle.

Nitrogen

Nitrogen exists in many different species and in many different oxidation states, ranging from +5 to -3. A valence +5 represents the most oxidized state and -3 the most reduced state. As reduction occurs, the more highly oxidized forms become unstable and transform into more reduced forms. Various important nitrogen species and their oxidation states are listed in Table 1.

The atmosphere contains about 78 percent N_2 gas. This element, however, is often in short supply to organisms. Certain microorganisms are capable of assimilating molecular nitrogen and converting it into forms which then become

TABLE 1. VARIOUS SPECIES OF NITROGEN AND THEIR OXIDATION STATE

Chemical Formula	Name	Valence
NO_3^-	nitrate ion	+5
NO_2	nitrogen dioxide	+4
N_2O_4	dinitrogen tetroxide	+4
N_2O_3	dinitrogen trioxide	+3
NO_2^-	nitrite ion	+3
NO	nitric oxide	+2
N_2O	nitrous oxide	+1
N_2	nitrogen	0
NH_3	ammonia	-3
NH_4	ammonium ion	-3

available to plants. These are symbiotic microorganisms which are living in the roots of certain plants, free-living heterotrophic soil bacteria, photosynthetic bacteria, and photosynthetic blue-green algae.

Nitrogen is almost totally absent in the bedrock from which many soils are formed. The presence of nitrogen in soil is therefore due almost entirely to biological action, fertilization, and atmospheric fixation. Plants adsorb nitrogen from the soil in two important forms: nitrate ions and ammonium ions (Lindsay, 1978). Two soil bacteria, nitrosomonas and nitrobacter derive their energy by oxidizing ammonium with the formation of nitrite and nitrate, respectively. These organisms are extremely abundant and active in the soil. Thus, nearly all ammonium reaching the soil will ultimately be oxidized to nitrate in a well-aerated soil condition. These reactions represent oxidation from ammonium to nitrate. Through nitrification, nitrate becomes the end product. It becomes not only the most important form, but also the most important source, of nitrogen available to plants.

The reverse reaction of nitrification, denitrification, may occur in reduced soils. During denitrification, nitrate is dissimilated by bacteria into nitrite, nitrous oxide, nitric oxide, ammonia, and nitrogen gas. Both nitrification and denitrification are concerned with the concentration of microorganisms in the soil. Thus, these processes are of a biochemical nature. Nitrogen may exist in relatively unavailable forms in the soil, since most organic nitrogen compounds are not directly available for plant uptake when they are confined in the decaying organic residue or exist in soil humus; however, these organic compounds may be broken down by soil organisms. Some of the products of decomposition do become directly available to plants. The process of ammonification represents the transformation of organic nitrogen to ammonium ions. These ammonium ions can easily be absorbed by plants.

Organic nitrogen, ammonium, and nitrate are easily subject to losses in streams and lakes through runoff or soil erosion. They can also be moved to groundwater by infiltration or subsurface flow. Losses of nitrate and ammonium are caused primarily by surface runoff, interflow, and deep leaching because the solubility of these nutrient components is high in the water (Sharma and Ghosh, 1976); however, losses of organic nitrogen are predominantly by soil erosion rather than by leaching and interflow, as the solubility of organic nitrogen in water is quite low and its adsorption capability to soil particles is high (Haith, 1973).

In general, nitrogen in the water flow and on sediment is closely related to the biochemical activity of microorganisms in the soil and the geochemical characteristics of soil itself. In other words, nutrient content in overland flow or percolated water will vary regionally and seasonally depending on variation in rates of decomposition of organic matter, differences in exchanging processes, and changes in concentration of nitrogen in the soil by plant uptake.

Phosphorus

Phosphorus, like nitrogen, is one of the basic elements required by all living organisms. It is a constituent of nucleic acids and is utilized in biochemical energy transformations. Total phosphorus content of a soil may vary over a wide range depending upon organic matter content, parent material, and degree of weathering. A correlation exists between total phosphorus and organic matter in the soil. A soil high in total phosphorus is generally high in organic matter. For convenience, soil phosphorus is usually classified as organic or inorganic.

Plants utilize free inorganic phosphate, primarily as orthophosphate, as a nutrient. Inorganic phosphate, after being utilized in biological processes, is converted to organic phosphate. This is an unavailable form; however, organic phosphate may be made available as inorganic phosphate by mineralization processes which are analogous to ammonification in the nitrogen cycle.

The average concentration of water-soluble phosphorus in soil is quite low and thus, soil phosphorus is rarely leached from soils. Loss of phosphorus from a site is primarily through soil erosion rather than subsurface flow or deep seepage. Phosphorus losses, measured as total phosphorus, are primarily associated with transport of sediment (Burwell, Timmons, and Holt, 1975). Most of the solid phase phosphorus is an insoluble phosphate compound such as Ca, Mg, Fe, or Al phosphate, and organic phosphate.

Thus, total phosphorus in solution form represents a much smaller part of phosphorus losses than solid phase phosphorus. Johnson et al. (1976) found that 80 percent of the total phosphorus losses were associated with suspended solids rather than with the water in the stream.

MODEL FORMULATION AND STRUCTURE

Mass balance and loading function concepts were the basic principles utilized in formulating this model. The model was developed to predict loadings of organic nutrients, nitrate, ammonium, and inorganic ortho-phosphorus to streams and rivers. The conceptual models for nitrogen and phosphorus are depicted in Figures 16 and 17. Each figure contains four partitions: atmosphere, litter, soil, and stream flow.

Description of Conceptual Model

Natural nutrient input to the ecosystem comes mainly from precipitation, litter fall, and geologic weathering. By comparison, the amount of input from geologic weathering is insignificant. As a result, precipitation and litter fall were considered the primary external inputs of nutrients from the atmosphere. These average inputs were routed into the litter layer where microbial degradation occurred. The products of degradation were then routed to the stream and into the soil layer. Within the soil layer, these products were again evaluated along with plant uptake and soil adsorption. The products of these processes occurring within the soil were then routed to the stream. Generally, nutrient constituents cannot move unless transported by soil and water and therefore, water and sediment are the major carriers of nutrients through the ecosystem. An evaluation of the amount of these carriers is necessary for predicting nutrient losses from the watershed.

Vegetation in the watershed not only adsorbs nutrients dissolved in soil water but also returns nutrients to the soil through decay. Nutrients

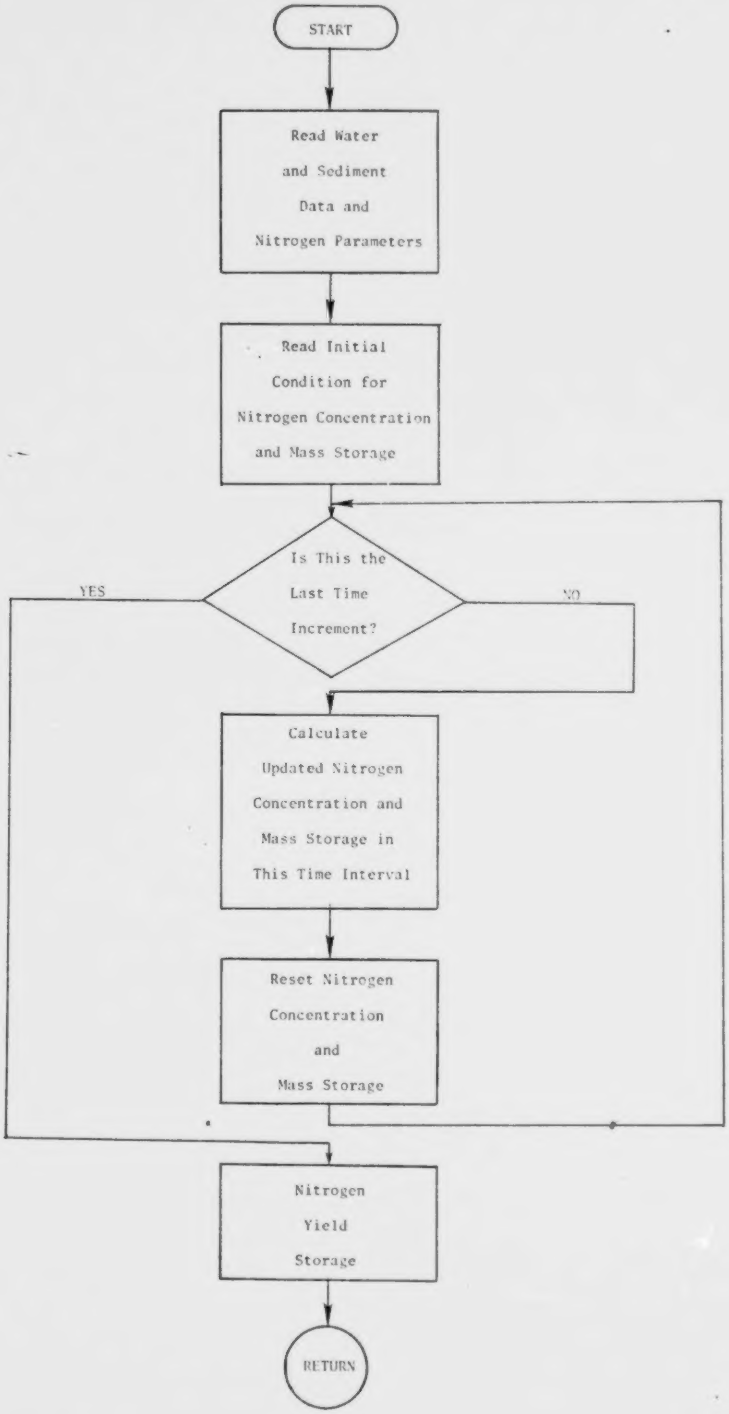
START
Read Water and Sediment Data and Nitrogen Parameters
Read Initial Condition for Nitrogen Concentration and Mass Storage
Is This the Last Time Increment?
YES
NO
Calculate Updated Nitrogen Concentration and Mass Storage in This Time Interval
Reset Nitrogen Concentration and Mass Storage
Nitrogen Yield Storage
RETURN

Figure 16. Flowchart of nitrogen cycle calculation, Program NUTRINT.

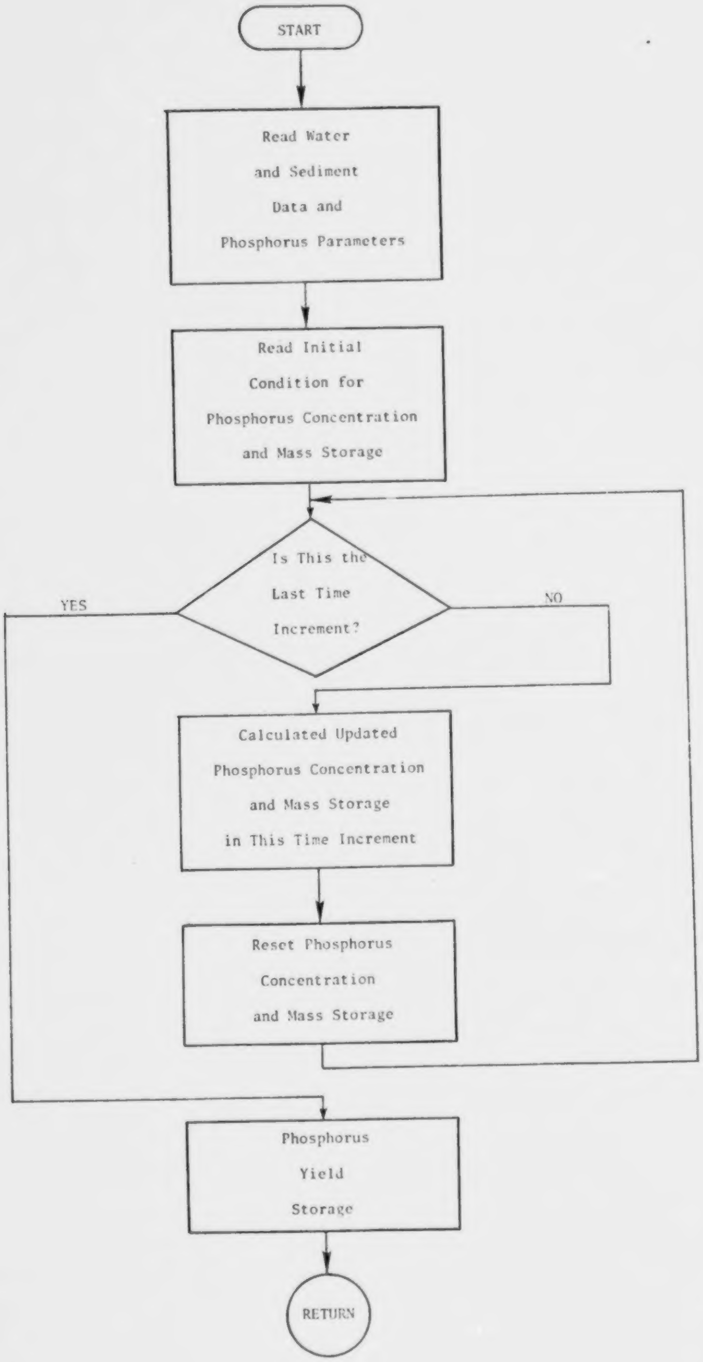
START
Read Water
and Sediment
Data and
Phosphorus Parameters
Read Initial
Condition for
Phosphorus Concentration
and Mass Storage
Is This the
Last Time
Increment?
YES
NO
Calculated Updated
Phosphorus Concentration
and Mass Storage
in This Time Increment
Reset Phosphorus
Concentration
and Mass Storage
Phosphorus
Yield
Storage
RETURN

Figure 17. Flowchart of phosphorus cycle calculation, Program NUTRINT.

dissolved in soil water might be adsorbed on soil particles by ion-exchange. Biological conversion in the soil includes the processes of mineralization, nitrification, reduction, and immobilization. However, Kissel et al. (1977) noted that immobilization did not become significant until the soil temperature remained at 22°C or above for more than two weeks following fertilizer application. Such a situation usually occurs only in tropical areas. Thus, this process is less important than other biological processes in predicting average nutrient concentration in the soil.

The nutrient simulator proposed here is basically a nutrient budget model. All of the processes mentioned above were considered when simulating average nutrient concentrations in the soil except the immobilization process. Quantities of nutrient losses to streams during storms were predicted by the incorporation of the loading function concept. Processes and theories included in the model formulation are described below.

Biological Conversion Processes

Biological processes such as mineralization, nitrification, denitrification, and plant uptake play a very important part in determining the concentration of nutrients in the soil. With the onset of precipitation, the amount of rainfall changes the nutrient concentration in the soil more than biological activity; however, biological activity between the storms not only deterministically changes the nutrient concentration in the soil but also affects the amount of nutrient loss during the storm.

Mineralization--

This process represents the change of the nutrient from organic material to inorganic nutrient species. For example, ammonification in the nitrogen cycle can convert the organic nitrogen into ammonium. The ammonification process is one of the mineralization processes. The term "mineralization potential" expresses the amount of organic material which is susceptible to mineralization. Large quantities of organic material such as litter may cover the soil surface in a forest watershed. Litter contributes significant amounts of inorganic nutrients to soil through the mineralization process.

Research by Stanford and Smith (1972), Stanford, Frere, and Schwaninger (1973), and Stanford and Epstein (1974) showed that the mineralization process in soil can be described by first-order kinetics and that temperature and moisture in the soil can significantly affect the mineralization process. It was proven that the reaction rate constant for mineralization could be corrected by Arrhenius' law. This reaction rate constant also has been determined experimentally as being proportional to the soil water content.

First-order kinetics means that the time change rate of a reactant is proportional to the amount of the reactant. The proportionality factor is the rate constant. For example, the biological conversion of compound A to compound B with reaction rate constant k can be expressed as:

$$A \xrightarrow{\quad k \quad} B$$

The rate of this reaction is expressed mathematically in terms of the rate of change in [A] and [B] with time as

$$-\frac{d}{dt}[A] = \frac{d}{dt}[B] = k[A]$$

In this modeling, the mineralization process is described by first-order kinetics and expressed by the following equation:

$$\frac{dc_1}{dt} = K_m \cdot c_1 \cdot (1 + x) \cdot e^{-K_1/T} \qquad (174)$$

where t = time

e = base of natural log

c_1 = concentration of organic nitrogen

T = temperature

K_m = reaction rate

x = percentage soil water content by weight

K_1 = temperature correction coefficient

It is apparent that the rate of mineralization tends to increase as temperature or soil water content is increased. Thus, the increased soil temperature and soil water content could potentially increase the amount of inorganic nutrients lost from the watershed.

Larsen (1967) reviewed the literature on soil phosphorus and did not present any findings on the mineralization rate constant. The mineralization process for phosphorus in this model was assumed to be of first-order kinetics.

Nitrification--

Nitrification is the oxidation of nitrogen from a reduced state to more oxidized states. Nitrosomonas in the soil can oxidize ammonium to nitrite and nitrobacter can oxidize the nitrite into nitrate. Both nitrosomonas and nitrobacter are nitrific bacteria.

Various equations have been proposed by different investigators to describe the nitrification process. Each equation is based upon different assumptions. For example, McLaren (1971) and Ardakami, Rehbock, and McLaren (1973) described the nitrification in terms of the Michaelis-Menton equation; however, this equation was applicable only under the condition that populations of nitrifiers are small compared to the carrying capacity of the environment, and the substrate concentration was high enough to yield a maximum specific growth rate. Therefore, the Michaelis-Menton equation can only be applied to batch culture and column profusion studies and not to the general conditions in the soil. Granthan (1950) and Gladstone (1946) proposed first-order kinetics and Miyake (1916) proposed second-order kinetics. Arrhenius' equation can interpret the change of nitrification rate constant with temperature.

Parker and Larson (1962) studied the effect of moisture on the nitrification rate. They found that production of nitrate nitrogen was retarded as soil moisture increased. Meanwhile, change of nitrate production was approximately exponential with soil moisture. Jenny (1930) found the humidity factor H to be a good indicator in relating soil nitrogen concentration with soil moisture. He showed that the relation between nitrogen concentration in the soil and the humidity factor was exponential.

Based on the investigations discussed above, the nitrification rate in this modeling is expressed as

$$\frac{dc_2}{dt} = k_n \cdot e^{-k_2/T} \cdot e^{-k_e \cdot H} \cdot c_2 \qquad (175)$$

where t = time

e = base of natural log

c_2 = ammonium concentration in the soil

k_n = nitrification rate constant

k_2 = temperature correction coefficient

k_e = exponential constant = 0.005

H = humidity factor

The humidity factor was expressed as (Jenny, 1930)

$$H = \frac{P}{(1 - \frac{RH}{100})\ SVPT} \qquad (176)$$

where P = average precipitation (mm/yr)

RH = relative humidity of air (percent)

$$SVPT = 10^{[9.2992 - 2360/(273 + T)]} \tag{177}$$

T = annual average temperature (°C)

RH is less than 100 percent.

Denitrification--

Similar to nitrification, various equations have been proposed to describe the denitrification process (Focht, 1974 and Nedwell, 1975). The denitrification process appears only under anaerobic or near-anaerobic conditions. Stanford, VanderPol, and Dzienia (1975a) studied this process under near-anaerobic conditions in 30 soils of diverse origin that differed widely in pH, organic carbon content, and other characteristics. They concluded that first-order kinetics could best describe the reduction from nitrate nitrogen to ammonium nitrogen. The apparent first-order rate constant ranged from about 0.024 to 0.96 day^{-1}. Stanford, VanderPol, and Dzienia (1975b) also showed that this first-order kinetics followed the temperature correction of Arrhenius' law.

In this nutrient modeling, nitrate reduction is expressed as

$$\frac{dc_3}{dt} = k_d \cdot I \cdot c_3 \tag{178}$$

where c_3 = nitrate concentration in the soil

k_d = reaction rate constant

$$I = e^{-k_3/T} \cdot e^{-k_e \cdot H} \tag{179}$$

k_3 = temperature correction coefficient

The remaining variables are as previously defined.

Plant Uptake--

Agricultural plant uptake is the primary mechanism for removal of nitrogen from soil. Van der Honert and Hooymons (1955) showed that the rate of nitrate uptake was a first-order process at nitrate concentrations less than 5 mg/ℓ. Many investigators (Broadbent and Reyes, 1971, Freid et al., 1957, and Mehran and Tanji, 1974) obtained similar results. Several studies have shown that the uptake of nutrients by plant roots is complex and still not well understood (Olsen and Kemper, 1968 and Barley, 1970; Liao and Bartholomew, 1974). In this paper, rate of nitrogen uptake by plants was assumed to be proportional to the concentration of nitrate nitrogen or ammonium nitrogen in the soil.

Mahtab et al. (1972) found that phosphorus uptake by plants was a function of clay and water in the soil and a function of applied phosphorus. However, phosphate concentration was found to be a predominant factor affecting the phosphate absorption rate and growth rate of plants (Loneragan and Asher, 1967, and Asher and Loneragan, 1967). Van der Honert and Hooymons (1955) showed that the rate of phosphate uptake is a first-order reaction at a phosphate concentration less than 1.0 mg/ℓ. This concentration is rarely exceeded for most soils at equilibrium. Freid et al. (1957), Nye (1966), and Bhat and Hye (1973) have studied the rate of phosphate uptake by plants. They found that the absorption rate was approximately proportional to the phosphate concentration in the soil solution. Therefore, rate of phosphorus uptake by plants was also assumed to follow first-order kinetics.

Adsorption-Desorption

Cation-exchange is a significant process existing in the soil. Clay particles in the soil always carry negative charges on their surface. Therefore, those cation ions in the soil solution are susceptible to adsorption on the soil particles. Ammonium ions are cations, and thus, the possibility of their being adsorbed by negatively charged soil particles is very high. On the other hand, acidic mineral soils contain significant amounts of adsorbed aluminum, iron, and manganese ions. These ions can combine with phosphate to form insoluble compounds. These compounds might be precipitated from the soil solution or adsorbed onto the surface of clay particles. The phosphorus can also be adsorbed onto the clay minerals by chemical bonding of the anions (orthophosphate) to positively charged exchangeable sites of the clay and substitution of phosphate for silicate in the clay structure. Phosphate compounds held by the soil may be loosely adsorbed and remain available to plants or may be firmly fixed and become unavailable. Those nutrient ions adsorbed on soil particles can be moved along with the eroded sediment. Hence, the adsorption-desorption process is still a significant process in the soil in determining the loss of nutrient with eroded soil.

Adsorption-Desorption for Ammonium--

Ammonium ions in the soil can exist in three different forms. They can be dissolved in soil water, adsorbed to surfaces of soil particles, or become interstitial to crystal lattices. No definite mechanism to describe the distribution of ammonium among these forms has been proposed (Mortland and Wolcott, 1965).

Donigian (1976) assumed the adsorption-desorption process for ammonium in the soil to be first-order kinetics. In this investigation this process is formulated to be

$$\frac{dc_4}{dt} = k_D \cdot c_4 \cdot e^{-k_4/T} \tag{180}$$

where c_4 = concentration of adsorbed or dissolved ammonium in the soil

k_D = reaction rate constant

k_4 = temperature correction coefficient

T = temperature

The remaining variables are as previously defined.

In general, most ammonium ions are adsorbed to soil particles. Thus, the reaction rate constant for adsorption is much greater than the desorption rate constant.

Adsorption-Desorption for Ortho-Phosphorus--

Similar to ammonium, ortho-phosphorus can also exist in three forms. It can be dissolved in soil solution, precipitate as Ca, Mg, Al, or Fe phosphates, or be adsorbed to surfaces of soil particles. Three different mechanisms were proposed to describe the transition of ortho-phosphorus between adsorbed and dissoved forms. They were the Langmuir equation (Harter, 1968, Humphreys and Pritchett, 1971, Kuo and Lotse, 1972, and Seyers et al., 1973), the Freundlich equation (Larsen, 1967, Gunary, 1970, and Kuo and Lotse, 1973), and the first-order equation (Freid et al., 1957 and Larsen, Gunary and Sutton, 1965).

The Langmuir equation was based on gas dynamics, whereas the Freundlich equation was based on experimental results. Thus, the Langmuir would have more accurate physical meaning than the Freundlich equation in interpreting the mechanism of the adsorption-desorption process. However, Harter (1968) tested the Langmuir equation with lake sediment, and found that this mechanism did not explain the entire adsorption isotherm. Larsen (1967) noted that the Langmuir equation was not strictly applicable to phosphorus adsorption by soil. Kuo and Lotse (1973) found that the Langmuir equation was not applicable when the adsorption-desorption process approached equilibrium, and proved that the Freundlich equation provided a better description; however, their experimental results were only suitable for bematite and gibbsite.

The adsorption-desorption reactions for phosphate were studied by Chen, Butler, and Stumn (1973). They found that the first-order rate equation best fits the experimental data for soil. In this study, first-order kinetics were adopted to describe adsorption-desorption processes for ortho-phosphorus.

Sediment as a Pollutant Transport Medium--

Erosion and sedimentation have important effects on water quality management. Water quality problems will not be solved solely by application of effluent controls to point sources of pollutant discharge; nonpoint source pollutants also play a significant role. In addition, many of the nonpoint source pollutants have been observed to be in proportion to eroded sediments.

In this study of nutrient losses, a simulation procedure using a sediment partition coefficient approach (Mulkey and Falco, 1978) was developed to evaluate the relative importance of sediments as a transport medium. Considering a daily volume of water-sediment-pollutant mixture from a surface runoff event, the following definitions apply:

V = total volume of water-sediment-pollutant mixture

M_w = mass of water in mixture volume

M_s = mass of sediment in mixture volume

ρ_w = density of water

ρ_s = sediment particle density

S = sediment concentration in the surface runoff water

c_s = concentration of pollutant attached to sediment

c_w = concentration of pollutant dissolved in water.

The mass of water and sediment in the mixture can be expressed as

$$M_w = V \rho_w \left(\frac{\rho_s}{\rho_s + S}\right) \tag{181}$$

and

$$M_s = V\ S\ (\frac{\rho_s}{\rho_s + S}) \tag{182}$$

Using concepts of pollutant adsorption to soil particles and dissolution in runoff water, the total pollutant, TP, in the mixture volume can be expressed as

$$TP = C_s\ M_s + C_w\ M_w \tag{183}$$

Substituting Equations (181) and (182) into Equation (183), it becomes

$$TP = V\ C_s\ S\ (\frac{\rho_s}{\rho_s + S}) + V\ C_w\ \rho_w\ (\frac{\rho_s}{\rho_s + S}) \tag{184}$$

Dividing both sides of Equation (184) by the total pollutant, a fraction equation can be written as:

$$\frac{VC_sS}{TP}\ (\frac{\rho_s}{\rho_s + S}) + \frac{VC_w\rho_w}{TP}\ (\frac{\rho_s}{\rho_s + S}) = 1.0 \tag{185}$$

The first item of Equation (185) represents the fraction of the total pollutant attached to the sediment particles, and the second item represents the fraction of the total pollutant dissolved in the runoff water. With a given volume of mixture, and the Freundlike isotherm function between concentrations of C_s and C_w, the fraction of pollutant associated with the soil particle and water can be determinated. The Freundlike empirical formula can be written as:

$$C_s = K_p\ C_w^{\ 1/\eta} \tag{186}$$

where K_p and η are constants whose values depend upon the pollutant and sediment properties. Equation (186) describes the equilibrium partitioning between the adsorption and solution phases. When η equal to one, Equation (186) will become a linear isotherm relationship with K_p the numerical value for the partitioning coefficient. Using the linear isotherm formula, the concentration value of C_s attached to the sediment particle can be derived as:

$$C_s = \frac{TP}{V\ [S(\frac{\rho_s}{\rho_s+S}) + \frac{\rho_w}{K_p}\ (\frac{\rho_s}{\rho_s+S})]} \tag{187}$$

and the concentration pollutant dissolved in water becomes

$$C_w = \frac{1}{K_p}\ C_s \tag{188}$$

Substituting Equation (187) into the first item of Equation (185), the fraction of the total pollutant associated with the sediment, defined as F_s, can be determined as:

$$F_s = \frac{1}{1 + \frac{\rho_w}{S\ K_p}} \tag{189}$$

The fraction of the total pollutant, F_s, is a function of sediment concentration in mixture volume and the partitioning coefficient. Equation (189) can be applied to demonstrate the importance of sediments as a pollutant transport medium for a range of sediment concentrations and partitioning coefficients. In the study of the nutrient loss simulation model, the partition coefficient method was used to evaluate the pollutant uptake by sediment and the pollutant dissolved in runoff water individually. In the simulated period, if a rainfall event occurs, the program first determines the amount of sedimentation to each size of sediment. Then the program converts the sediment weights into the corresponding volumes and combines the volume of surface runoff on a specific date to determine the volume of water-pollutant-sediment mixture. Once the total mixture volume is calculated, sediment concentrations for each size fraction of sediment are also determined for the specific simulating date, with the given partition coefficient constants and the total pollutant associated with the particular size of sediment, the partitioning method is used to determine the change of nutrient concentrations in different depth of layers of watershed plains. The variations of nutrient concentration are calculated for every two-hour time period in this simulation program. Tables 2 and 3 show the expressions of the nutrient loss attached to the sediment uptake processes being used in the partitioning procedure. A flow chart illustrating computation procedures by using the partitioning coefficient method in NITRO and PHOS subroutines is shown in Figure 18.

Nutrient Loading Function

When a substance is deposited in a body of water, it may become a pollutant. If the source of pollutant is a land-use area, this area can be treated as a potential unit for pollutant discharge. In evaluating the amount of pollutants loaded into a body of water, McElroy et al. (1976) proposed the loading function concept. The loading function is a simple mathematical expression. It can be applied in calculating the emission of a pollutant from a non-point source and discharge of the pollutant into waterways. The nutrient loading function for erosion loss is

$$Y(N)_E = Y(S)_E \cdot C_s(N) \cdot P_n \qquad (190)$$

where $Y(N)_E$ = nutrient loading

$Y(S)_E$ = sediment loading from soil erosion

$C_s(N)$ = nutrient concentration in soil

P_n = nutrient potency factor

P_n is defined as the ratio of nutrient concentration in sediment to nutrient concentration in soil.

Table 2. TOTAL POLLUTANT IN MIXTURE VOLUME FOR NITROGEN CYCLE

Pollutant Source Case	Nitrogen in Upper Layer	Nitrogen in Lower Layer	Ammonium in Soil
Litter	$\frac{\text{ROM*SSED*FR*XS(1)}}{\text{SGL}}$	$\frac{\text{ROM*SSED*FR**XS(4)}}{\text{SGL}}$	$\frac{\text{RSN*SSED*(1.0-FR)*XS(10)}}{\text{SGS}}$
No Litter	$\frac{\text{ROM*SSED*XS(1)}}{\text{SGS}}$	$\frac{\text{ROM*SSED*XS(4)}}{\text{SGS}}$	

Table 3. TOTAL POLLUTANT IN MIXTURE VOLUME FOR PHOSPHATE CYCLE

Pollutant Source Case	Organic Phosphate in Upper Layer	Organic Phosphate in Lower Layer	Inorganic Phosphate in Soil
Litter	$\frac{\text{ROR*SSED*FR*XT(1)}}{\text{SGL}}$	$\frac{\text{ROR*SSED*FR**XT(3)}}{\text{SGL}}$	$\frac{\text{RSP*SSED*(1.0-FR)*XT(7)}}{\text{SGS}}$
No Litter	$\frac{\text{ROR*SSED*XT(1)}}{\text{SGS}}$	$\frac{\text{ROR*SSED*XT(3)}}{\text{SGS}}$	

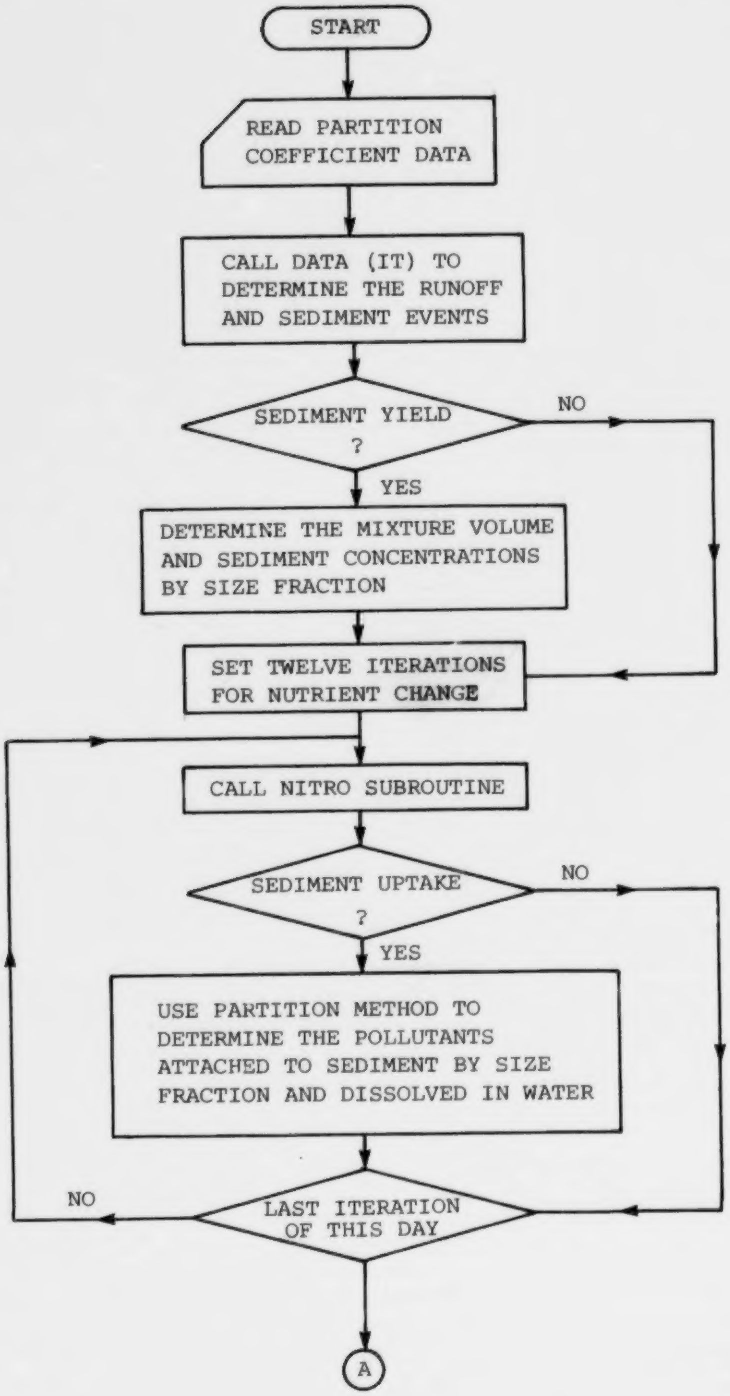
START
READ PARTITION COEFFICIENT DATA
CALL DATA (IT) TO DETERMINE THE RUNOFF AND SEDIMENT EVENTS
SEDIMENT YIELD ?
NO
YES
DETERMINE THE MIXTURE VOLUME AND SEDIMENT CONCENTRATIONS BY SIZE FRACTION
SET TWELVE ITERATIONS FOR NUTRIENT CHANGE
CALL NITRO SUBROUTINE
SEDIMENT UPTAKE ?
NO
YES
USE PARTITION METHOD TO DETERMINE THE POLLUTANTS ATTACHED TO SEDIMENT BY SIZE FRACTION AND DISSOLVED IN WATER
NO
LAST ITERATION OF THIS DAY
A

Figure 18. Partition coefficient procedure.

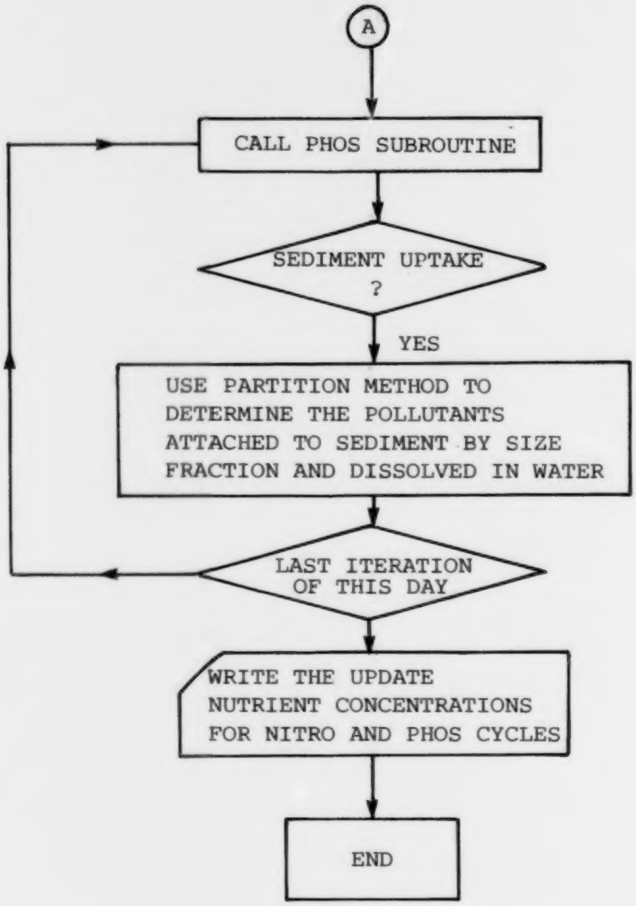
A
CALL PHOS SUBROUTINE
SEDIMENT UPTAKE ?
YES
USE PARTITION METHOD TO DETERMINE THE POLLUTANTS ATTACHED TO SEDIMENT BY SIZE FRACTION AND DISSOLVED IN WATER
LAST ITERATION OF THIS DAY
WRITE THE UPDATE NUTRIENT CONCENTRATIONS FOR NITRO AND PHOS CYCLES
END

Figure 18. Partition coefficient procedure (continued).

Similar to the nutrient loading function for soil erosion, the nutrient loading function for surface runoff and (adopted in this model) subsurface flow is

$$Y(N)_W = Q(W) \cdot C_s(N) \cdot R \qquad (191)$$

where $Y(N)_W$ = nutrient loading from water discharge

$Q(W)$ = discharge of water by surface runoff, interflow, and infiltration

$C_s(N)$ = nutrient concentration in soil

R = nutrient enrichment factor.

R is defined as the ratio of nutrient concentration in water to nutrient concentration in soil.

The loading function is a mathematical expression used to calculate the emission of a pollutant from a non-point source and discharge of the pollutant into surface waterways. This concept was developed by McElroy et al. (1976) and stated that

> "The rates and magnitudes of discharges of pollutants from non-point sources do not relate simply to source characteristics or source-related parameters. Evaluation of the severity of this problem is hampered by the lack of tools to quantify pollutant loads, and scanty and imprecise data on the interrelationships between control measures and pollutant loads are a deterrent to formulation of control or regulatory strategies...."

Due to the difficulty of relating the nutrient losses directly to the source characteristics, the loading function method was applied in this study.

Mass Balance Equations for Nutrient Model

The loading function and mass balance method are used throughout this nutrient model. In order to use the loading function method to evaluate nutrient releases, simulation of nutrient concentrations in the soil or litter is required. Mass balance forms the basic structure of the model calculations to simulate nutrient concentrations in the soil litter. The system of differential equations used to describe time variation of nutrient concentrations in the soil and litter is discussed below.

Coupled System of Differential Equations for Nitrogen--

Organic nitrogen, ammonium, and nitrate are the nutrient species found in the litter layer under discussion here. These three components with units kg/m^3 are expressed as [LON], [LA], and [LN], respectively. Ammonium, nitrate, plant nitrogen, and adsorbed ammonium are also considered in the soil layer (Figure 16). These four components with units kg/m^3 are expressed as [SA], [SN], [PN], and [AA], respectively.

The coupled system differential equations for the nitrogen components above are

$$\frac{d}{dt}\,[LON] = [LIT]/DL - k_m[LON] \tag{192}$$

$$\begin{aligned}\frac{d}{dt}\,[LA] = {} & k_m\,[LON] + PPTA/DL + k_{na}[LN] - k_{an} - k_r[LA]\;Q/ \\ & (A.\;DL) - k_1[LA]\;Q_1/(A.\;DL)\end{aligned} \tag{193}$$

$$\begin{aligned}\frac{d}{dt}\,[LN] = {} & PPTN/DL + k_{an} - k_r[LN]\;Q/(A.\;DL) - k_1\,[LN]\;Q_1/ \\ & (A.\;DL) - k_{na}\,[LN]\end{aligned} \tag{194}$$

$$\begin{aligned}\frac{d}{dt}\,[SA] = {} & k_{na}\,[SN] + k_1\,[LA]\;Q_1/(A.\;DS) + k_{as}[AA] - k_{an}[SA] \\ & - k_1[SA]\;Q_1/(A.\;DS) - k_{sa}[SA] - k_1[SA]\;Q_b/(A.\;DS) \\ & - k_p[SA]\end{aligned} \tag{195}$$

$$\begin{aligned}\frac{d}{dt}\,[SN] = {} & k_{an}[SA] + k_1[LN]\;Q_1/(A.\;DS) - k_{na}[SN] - k_p[SN] \\ & - k_1[SN]\;Q_b/(A.\;DS) - k_1[SN]\;Q_1/(A.\;DS)\end{aligned} \tag{196}$$

$$\frac{d}{dt}\,[PN] = k_p\,[SA] + k_p\,[SN] \tag{197}$$

$$\frac{d}{dt}\,[AA] = k_{sa}\,[SA] - k_{as}\,[AA] - k_s[AA]\;Q_s/(A.\;DS) \tag{198}$$

where A = area of watershed (ha)

DL = depth of litter (m)

DS = depth of soil (m)

[LIT] = litter input rate to the litter layer (kg/ha/yr)

PPTN,PPTA = nutrient input rate to the watershed from precipitation for nitrate and ammonium, respectively ($kg/m^2/day$)

Q = surface runoff (ft^3/sec)

Q_1 = infiltrated volume per unit time (ft^3/sec)

Q_b = subsurface flow (ft^3/sec)

Q_s = sediment discharge (lb/sec)

k_m = mineralization rate constant (day^{-1})

k_{an} = nitrification rate constant ($kg/m^3/day$)

k_{na} = denitrification rate constant (day^{-1})

k_{sa} = adsorption rate constant for ammonium (day^{-1})

k_{as} = desorption rate constant for ammonium (day^{-1})

k_p = nitrogen uptake rate by plant (day^{-1})

k_s = potency factor ammonium for sediment uptake

k_r = enrichment factor in surface runoff

k_1 = enrichment factor in seepage

Coupled System of Differential Equations for Phosphorus--

Organic phosphorus and ortho-phosphorus are the nutrient species in the litter layer examined in this study (Figure 17). These components, with units kg/m^3, are expressed as [LOP] and [LP], respectively. Orthophosphate, adsorbed orthophosphate, and plant phosphorus as illustrated in Figure 17 are those components considered in the soil layer, are in units kg/m^3, and are expressed as [SP], [AP], and [PP], respectively. The coupled system differential equations for the above phosphorus components are

$$\frac{d}{dt}[LOP] = [LIT]/DL - k_m[LOP] \qquad (199)$$

$$\frac{d}{dt}\,[LP] = PPTP/DL + k_m\,[LOP] - k_1\,[LP]\,Q_1/(A.\ DL) - k_r\,[LP]\,Q/(A.\ DL) \qquad (200)$$

$$\frac{d}{dt}\,[SP] = k_{dp}\,[AP] + k_1\,[LP]\,Q_1/(A.\ DS) - k_{ap}\,[SP] - k_{pp}\,[SP] - k_1\,[SP]\,Q_1/(A.\ DS) - k_1\,[SP]\,Q_b/(A.\ DS) \qquad (201)$$

$$\frac{d}{dt}\,[AP] = k_{ap}\,[SP] - k_{dp}\,[AP] - k_{sp}\,[AP]\,Q_s/(A.\ DS) \qquad (202)$$

$$\frac{d}{dt}\,[PP] = k_{pp}\,[SP] \qquad (203)$$

where PPTP = orthophosphate input rate to the watershed from precipitation ($kg/m^2/day$)

k_{dp} = desorption rate constant for orthophosphate (day^{-1})

k_{ap} = adsorption rate constant for orthophosphate (day^{-1})

k_{pp} = phosphorus uptake rate by plant (day^{-1})

k_{sp} = potency factor of orthophosphate for sediment uptake

The remaining variables were previously defined.

Model Structure

The nutrient model resulting from this research is composed of subroutines NITRO and PHOS. The flow chart which presents the relationship between subroutines and the main program was given in Figure 18. In this model, hydrologic data such as runoff volume, infiltrated volume, and sediment yield by size fraction, were first input. These hydrologic data were major inputs to subroutines NITRO and PHOS. After the hydrologic data and nutrient model parameters were read and the computation sequence was specified, subroutines NITRO and PHOS simulated the interaction of nutrients with water and sediment, the biological conversion processes among different nutrient species, and the adsorption-desorption mechanism of soil and plant uptake. In other words, subroutines NITRO and PHOS, after receiving the data input, were used to calculate change of nutrient concentration in the soil and amount of nutrient transported from the watershed into the stream.

Nutrient concentration in the litter or soil layer is assumed to be uniform. Amounts of nutrient leaving or entering the layer were proportional to the product of the water discharge or soil erosion and the existing nutrient concentrations in that layer. This scheme is a combination of the mass balance and the loading function concepts. Saxton, Schuman, and Burwell (1977) and Neilsen and Mackenzie (1977) used this scheme in simulating the nitrate movement in soils.

SECTION 5

TEMPERATURE AND DISSOLVED OXYGEN ROUTING

INTRODUCTION

Temperature and dissolved oxygen (DO) are important environmental parameters in aquatic ecosystems. Significant temperature change may alter the reproductive and growth habits of aquatic organisms. Increased water temperature can also be expected to influence the spawning habits of adult fish and the development and survival of juvenile fish in the stream. Sufficient dissolved oxygen in the water is necessary to maintain the normal metabolism of aquatic life. Low DO concentrations may lead to the deterioration of the living environment and eventually adversely affect the biota. For example, the concentration of dissolved oxygen in the water of small forest streams can significantly influence the character and productivity of the aquatic ecosystem in the stream. Fish and other aquatic organisms are dependent upon oxygen for survival, growth, and development.

Thermal energy content, dissolved oxygen, and biochemical oxygen demand (BOD) of runoff water can directly or indirectly affect the temperature and oxygen content in the stream. Based on mass and energy balance, the temperature and dissolved oxygen model is proposed in this study. This model is useful to evaluate the thermal and dissolved oxygen loading to the stream through surface runoff.

GOVERNING PROCESSES FOR TEMPERATURE AND DISSOLVED OXYGEN MODELING

Overland flows may transmit thermal and DO loading to the stream. Temperature and dissolved oxygen loading of the stream result from high temperature, high biochemical oxygen demand, and low dissolved oxygen in runoff water. Temperature and DO effects of subsurface flow are not included in this model.

Concept and Governing Factors for Thermal Loading

Thermal loading is determined by the temperature of overland flow. Due to heat transfer between soil and surface runoff, runoff temperature changes as water flows over the soil surface. Heat transfer depends on the temperature difference between soil and surface runoff. Soil temperature reflects the intensity and duration of solar irradiation prior to a runoff event (Duffie and Beckman, 1974 and TVA, 1972). Temperature distribution within the soil depends on soil properties such as mineral composition, porosity, and water content (De Vries, 1952, 1963).

There are three mechanisms of heat transfer: radiation, conduction, and convection. Each mechanism plays a role in the heat transfer process. It is appropriate to begin the discussion of mechanisms with radiation. Radiation transfers energy from the sun and thus, is the basic driving force of all hydrologic processes. All bodies at temperatures greater than absolute zero emit radiation. Radiation is a wave phenomenon with measurable presence at all wave lengths. It is usually explained on the basis of quantum or electromagnetic wave theory. At the microscopic level, radiation is governed by the Stephen-Boltzmann Law which expresses energy flux of an ideal radiator (black body) to the fourth power of its absolute temperature. Radiant energy is spread over various wave lengths depending on the nature of the emitting body.

The second fundamental heat transfer mechanism is conduction. Conduction is the passage of heat through a body or between bodies, as opposed to radiation, which transfers energy without medium. Conductive heat flux is attributed to molecular motion. Theory of conduction in solids distinguishes between electric conductors and nonconductors. In a dielectric, heat is conducted by lattice waves caused by molecular motion. In electrical conductors free electrons transfer additional energy. Macroscopic theory of heat conduction is based on experimental evidence which suggests a proportionality between heat flux and temperature gradient. Conduction is the only predominant mechanism for heat transfer in between soil layers and heat transmission between soil and surface flow.

The final heat transport mechanism is convection. Convective heat transport occurs because of relative motion between various parts of the heated body or fluid. Convection is classified as either free or forced. Free convection arises when a temperature difference causes density gradients with associated fluid movement. Forced convection occurs when a fan, pump, or other energy source provides the fluid motion. Convection plays an important role in heat transfer from water surfaces, particularly in evaporative processes.

In this model three basic physical processes governing thermal loading are considered: 1) atmospheric, 2) canopy-ground cover, and 3) surface runoff processes.

Concepts and Governing Factors for Dissolved Oxygen

Oxygen concentration in the stream water at any given time is determined by the solubility of oxygen in the water, the rate at which this oxygen is consumed by various biochemical processes (represented by biochemical oxygen demand), and the rate at which this depletion is replenished.

Deoxygenation of the water due to the bacterial decomposition of carbonaceous organic material and reaeration caused by the oxygen deficit and turbulence are the most fundamental processes occurring in natural water. The basic theory used to describe the deoxygenation and reaeration processes was proposed by Streeter and Phelps (1925). The rate at which the BOD is exerted was presumed to be identical to that observed while using the laboratory BOD test. A proportionality is assumed to exist between the reaeration rate and certain hydraulic parameters of flow. Numerous investigators have subsequently questioned the theory of Streeter and Phelps because the self-purification process in a small stream is not accurately presented by the model. An illustration of the discrepancy between field observations and their theory was published by Kittrell and Kochtitzky (1947). Dobbins (1964) suggested several other factors which contribute to the BOD and DO variations in flowing water. BOD effects include BOD removal by sedimentation and adsorption, and BOD addition of local runoff and scour of bottom deposits. The DO effects include concentration reductions due to purging action of gases rising from the benthal layer, plant respiration, diffusion into the benthal layer, and DO addition photosynthesis.

MODEL FORMULATION AND STRUCTURE

Available temperature and DO models generally simulate processes within a stream and not in overland flow. In the case of DO, similarity between instream and overland flow processes allows for the development of a suitable DO model from existing models. In the case of temperature, new modeling techniques are required.

Temperature Loading Modeling

Solar radiation is one of the predominant energy sources to the soil. Computation of the extra-terrestrial solar radiation is based on measured values of radiation emitted by the sun and the trigonometric relationship to express the direct solar beam intensity on a horizontal plane. With known extra-terrestrial radiation, clear sky solar radiation as received at the ground is a function of atmospheric transmittance and canopy-ground cover distribution. Attenuation of solar radiation by clouds is difficult to evaluate due to the types, distribution, and albedos of clouds and the lack of analytical parameters to express this combined effect on solar radiation. Three processes are considered in the temperature loading model: 1) atmospheric, 2) canopy-ground cover, and 3) surface runoff processes.

In order to obtain a set of formulas for computations of the heat flux to the top of the atmosphere and the attenuation of solar radiation on its path through the atmosphere, the Tennessee Valley Authority (1972) has made a survey of existing methods and combined them with field investigations by the TVA Engineering Laboratory.

At a given location and a certain time, solar radiation intensity on a horizontal plane at the top of the atmosphere is proposed by the TVA (1972) as

$$q_o = \frac{I_o}{r^2} (\sin \phi \sin \delta + \cos \phi \cos \delta \cos h) \qquad (204)$$

where

q_o = solar radiation intensity per unit area and unit time (KJ/(m^2 hr))

I_o = solar constant (4871 KJ/(m^2 hr))

r = radius vector

ϕ = latitude of the location (radians)

δ = declination of the sun (radians)

h = local hour angle of the sun (radians)

Declination of the sun δ can be found from the equation proposed by Cooper (1969)

$$\delta = 23.45 \sin [360 \cdot \frac{284 + n}{365}] \tag{205}$$

where n = the day of the year.

Solar radiation received at the top of the atmosphere is attenuated on its path through the atmosphere by scattering and adsorption on encountering gas molecules, water vapor, and dust particles. The solar radiation received at the ground per unit area per unit time (q_s) is:

$$q_s = q_o [\frac{a'' + 0.5 (1 - a' - d) - 0.5 d_a}{1 - 0.5 R_g (1 - a' + d_s)}] \tag{206}$$

where

a' = mean atmospheric transmission coefficient for cloudless, dust free, moist air after scattering only

a'' = mean atmospheric transmission coefficient for cloudless, dust free, moist air after scattering and adsorption

d_a = depletion coefficient of the direct solar beam by dust adsorption

d_s = depletion coefficient of the direct solar beam by dust scattering

$d = d_a + d_s$

R_g = total reflectivity of the ground in the vicinity of the site

The items a' and a'' in Equation (206) were expressed as functions of optical mass and water content by

$$a' = e^{-(0.465 + 0.134 W) (0.129 + 0.171 e^{-0.880 M_p}) M_p} \tag{207}$$

$$a'' = e^{-(0.465 + 0.134 W)} (0.179 + 0.421 e^{-0.721 M_p}) M_p \qquad (208)$$

where

W = mean monthly precipitable water content

M_p = local optical air mass

W and M_p can be expressed in terms of optical air mass, local evaluation, and monthly mean dew point temperature.

$$W = e^{(-0.1981 + 0.0341 O_d)} \qquad (209)$$

$$M_p = [(288 - 0.0065z)/288]^{5.256} M \qquad (210)$$

where

O_d = mean monthly surface dew point temperature (°F)

z = local elevation (meter)

M = optical air mass

Kasten (1964) established an empirical formula for the optical air mass M

$$M = 1/[\sin \alpha + 0.15 (\alpha + 3.885)^{-1.253} \qquad (211)$$

where $\sin \alpha = \sin \phi \sin \delta + \cos \phi \cos \delta \cos h$.

The remaining variables are previously defined.

Radiation data expressed in langleys are the best source of information to calculate energy input after atmospheric processes. Lacking these, it is possible to use those relationships mentioned above to estimate net solar radiation following transmission through the atmosphere.

Canopy-Ground Cover Processes--

Solar radiation, after passing through the atmosphere, can be reflected and absorbed, or transmitted to the canopy and ground cover over the soil surface. The complex stochastic nature of the canopy-ground cover system precludes deterministic modeling of the passage of radiation. Most models of light transmission rely heavily on regression of measured data. Wellner

(1948), Brooks (1959), Byran (1948), Kittredge (1962), Lull and Reigner (1967), and Reifsnyder and Lull (1965) have investigated the processes and presented useful data.

An easily derived estimate of light intensity under normally stocked mature conifer stands has been proposed by Roussel (1948). The relation proposed is

$$ER = k/N \tag{212}$$

where

ER = the ratio of light intensity inside a given stand to the simultaneous intensity in the open

k = constant which depends on the species of tree

N = number of trees per hectare

For example, for mixed spruce and fir stands $k = 20$. In this model, both the regression relation and published data were adopted to predict the solar radiation transmitted through the canopy-ground cover because the effect of forest canopy on the thermal regime of a watershed is difficult to simulate deterministically.

Surface Runoff Processes--

Water flowing over the soil surface is expected to transfer heat between soil surface and water itself. Several investigators (Brooks and Rhoades, 1954, McKenzie, 1924, and Box, et al., 1963) have presented their studies. They found that irrigation can significantly change the temperature of surface soil through soil-heat transfer. The heat flow per unit time between surface water layer and soil can be expressed by a first-order differential equation relating conduction exchange to thermal conductivity, proportional surface area, and vertical temperature gradient (Gates, 1968a,b).

The analytical expression is

$$\frac{dQ}{dt} = \frac{Asw}{\frac{1}{k_s} Y_s + \frac{1}{kw} Y_w} \cdot (Tw - Ts) \qquad (213)$$

where

$\frac{dQ}{dt}$ = heat flow unit time (cal/day)

Asw = area of soil layer (m^2)

k_s = thermal conductivity of soil (cal day^{-1} m^{-1} $°C^{-1}$)

Y_s = depth of soil at which Ts is taken (m)

kw = thermal conductivity of water (cal day^{-1} m^{-1} $°C^{-1}$)

Y_w = thickness of the water from water-soil interface to the midpoint of water layer

Ts = temperature of the soil layer (average at a specific time) (°C)

Tw = temperature of the water (average at a specific time) (°C)

The mathematical model most often used to describe the heat transfer by conduction between the soil surface and the different soil layers is the one-dimensional heat flow equation (Hanks, Austin, and Ondrechan, 1971, Carson, 1961, 1963, Penrod and Steward, 1967, Lee, 1970, and Wieranga, Hagan, and Gregory, 1971). The equation describing heat transfer in a one-dimensional homogeneous soil with constant apparent thermal diffusivity can be expressed by

$$\frac{\partial T}{\partial t} = \alpha \frac{\partial^2 T_1}{\partial Z^2} \qquad (214)$$

where

$\alpha = \frac{\lambda}{C}$ = apparent thermal diffusivity

λ = thermal conductivity (cal $\cdot$ day^{-1} $\cdot$ cm^{-1} $\cdot$ $°C^{-1}$)

C = volumetric heat capacity (cal cm^{-3} $°C^{-1}$)

T_1 = average temperature of the soil layer (°C)

Z = distance from soil surface in ther vertical direction (cm)

t = time (day)

Once Equation (214) has been solved, the soil temperature profile as a function of time and depth will be found.

Dissolved Oxygen Loading Model

Dissolved oxygen may be the most important water quality parameter in fisheries management. Because water contains less than one percent oxygen by volume at normal temperatures, the aquatic environment is critically sensitive to the oxygen demands of the organisms that inhabit it.

Solubility of oxygen in water (saturation concentration) is inversely proportional to water temperature. As water warms, its ability to hold oxygen declines. Churchill, Buckingham, and Elmore (1962) have provided an empirical regression equation for calculating the temperature effect

$$C_1 = 14.652 - 0.41022\ T + 0.0079910\ T^2 - 0.000077774\ T^3 \qquad (215)$$

where

C_1 = the solubility of oxygen in water (mg/ℓ)

T = water temperature (°C)

The DO concentration in a stream is the net result of oxygen fluxes into and out of water. Fluxes into the water are primarily from atmospheric reaeration across the water surface and oxygen production by photosynthetic organisms in the water. Oxygen primarily leaves the water due to consumption of organic substrates (BOD) and ammonia (nitrification) by bacteria during their oxidation.

The Streeter-Phelps equation (1925) has long been accepted in describing the oxygen deficit (D) in the stream. Oxygen deficit is defined as $C_s - C$

in which C_s is the saturated dissolved oxygen in the water and C_1 is the dissolved oxygen in the water. The equation is expressed as

$$D = \frac{K_1 L_a}{K_2 - K_1} (e^{-K_1 t} - e^{-K_2 t}) + D_a e^{-K_2 t} \tag{216}$$

$$= C_s - C_1$$

where

K_1 = BOD rate constant (day^{-1})

K_2 = reaeration rate constant (day^{-1})

L_a = initial BOD (mg/ℓ)

D_a = initial dissolved oxygen deficit at time t (mg/ℓ)

This equation considered two major processes, deoxygenation and reaeration in determining the DO in the stream.

The BOD material will consume the dissolved oxygen in the water, whereas the oxygen in the air will supplement oxygen by reaeration process. When water flows over the land surface, it will pick up BOD material from the surface. At the same time, the BOD material may also be removed by sediment.

The oxygen budget method proposed by Dobbins (1964) is adopted to simulate the dissolved oxygen in the surface runoff water. This method has considered the deoxygenation, reaeration, and sediment uptake processes. The equations used to describe the BOD and DO profiles are based on the following assumptions

1. Stream flow is steady and uniform.
2. The process for the stretch as a whole is a steady-state process, the conditions at every cross section being unchanged with time.
3. Removal of BOD by both the bacterial oxidation and sedimentation or adsorption or both are first order reactions; the rates of removal at any section being proportional to the amount present.
4. Removal of oxygen by the benthal demand and by plant respiration, the addition of oxygen by photosynthesis, and the addition of BOD from the benthal layer or the local runoff are uniform along the stretch.

5. The BOD and oxygen are uniformly distributed over each cross section, thus permitting the equations to be written in the usual one-dimensional form.

The equations derived are based on the oxygen budget and these assumptions are expressed as

$$L = L_a e^{-(K_1 + K_3)t} + \frac{L_a}{K_1 + K_3} (1 - e^{-(K_1 + K_3)t}) \qquad (217)$$

$$D = \frac{K_1 (L_a - \frac{L_a}{K_1 + K_3}) (e^{-(K_1 + K_3)t} - e^{-K_2 t})}{K_2 - (K_1 + K_3)}$$

$$+ D_a e^{-K_2 t} + (\frac{D_B}{K_2} + \frac{K_1 L_a}{K_2 (K_1 + K_3)}) (1 - e^{-K_2 t}) \qquad (218)$$

$$D_B = \frac{K_2 (D - D_a e^{-K_2 t})}{1 - e^{-K_2 t}} - K_1 L \qquad (219)$$

where

K_3 = rate constant for BOD removal by sedimentation or adsorption

D_B = rate of removal of dissolved oxygen along the stretch

L = BOD along the stretch (mg/ℓ)

The remaining variables are as previously defined.

This dissolved oxygen simulation model is designed to evaluate the average dissolved oxygen concentration in the overland flow during a storm event. The loadings of dissolved oxygen (DO) and biochemical oxygen demand (BOD) through surface runoff directly affect the concentration of DO in the stream. Therefore, the average concentration of dissolved oxygen in the overland flow may be one of the important factors which relate to the study of water quality in the stream.

Model Structure

In simulating the thermal loading from rainfall events, three physical processes should be considered. First, energy input to the watershed from solar radiation must be evaluated. Solar radiation can be scattered and absorbed by water vapor, air mass, and dust particles. Gross solar energy input also depends on the average hour angle, radius vector, number of days in the year, solar irradiation time, and altitude of the watershed. Second, vegetation distribution and type of vegetation can affect the net solar energy input to the watershed surface. Different vegetation has different effects on reflecting, absorbing, and shielding the solar radiation. Net solar energy input to the soil can be estimated only after the processes occurring in the atmosphere and watershed surface have been considered. Third, as runoff occurs, heat transfer between soil and flowing water determines the thermal loading through runoff water to the water body.

In the thermal loading model, these three important processes have been incorporated. Three different subroutines are used to simulate these processes. The subroutines can estimate the net solar energy input to the watershed, temperature distribution in the soil, and amount of heat transported by surface runoff. In order to perform the thermal routing, an accurate hydrograph is required. Hydrographs from each watershed for each storm event can be obtained from a multiwatershed hydrological model developed by Simons, Li, and Spronk (1978).

The dissolved oxygen routing model can be used to calculate average dissolved oxygen concentration in the runoff water. In this model, modified Streeter-Phelps theory has been adopted to calculate oxygen deficit and biological oxygen demand. Dissolved oxygen in the runoff water can be calculated after the temperature and oxygen deficit in the runoff are determined. Temperature data can be obtained from the thermal routing model, where the oxygen deficit can be calculated by running the dissolved oxygen subroutine in the model. The flowchart for the thermal and dissolved oxygen model is shown in Figure 19.

In summary, the thermal and dissolved oxygen model may be used to predict thermal loading and dissolved oxygen concentration in the runoff water from a multiwatershed drainage for each storm event. This model can evaluate the thermal loading and the dissolved oxygen concentration only when the water hydrograph for each watershed is supplied. Simulated total thermal loading and average dissolved oxygen concentration from each storm event can provide the important information that may be used in evaluating the impact of thermal pollution from land use on the water quality.

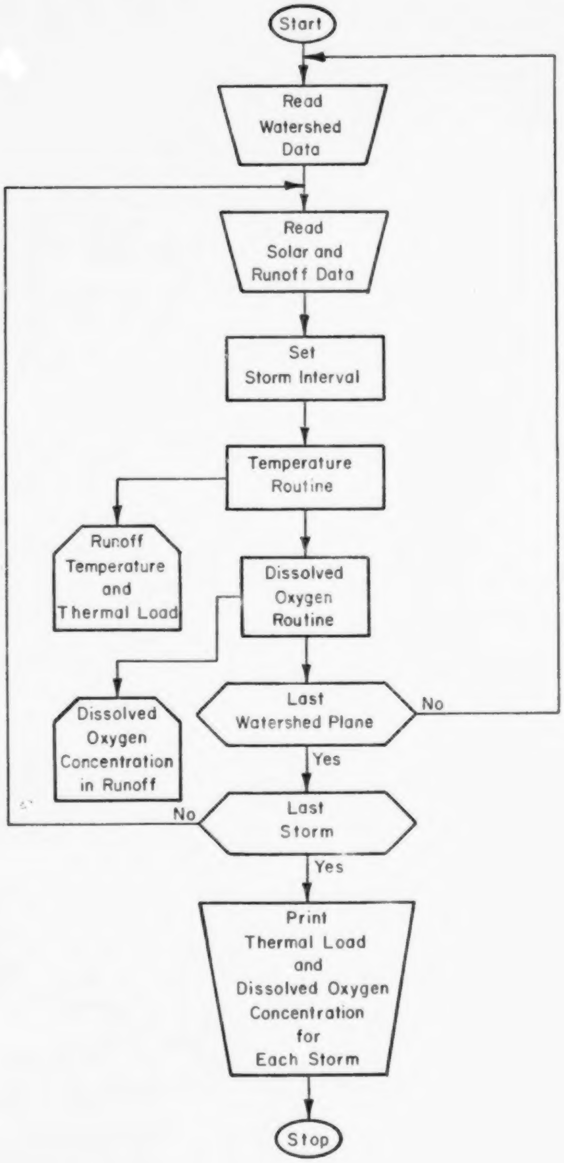
Start
Read Watershed Data
Read Solar and Runoff Data
Set Storm Interval
Temperature Routine
Runoff Temperature and Thermal Load
Dissolved Oxygen Routine
Dissolved Oxygen Concentration in Runoff
Last Watershed Plane
No
Yes
Last Storm
No
Yes
Print Thermal Load and Dissolved Oxygen Concentration for Each Storm
Stop

Figure 19. Flow chart for thermal and dissolved oxygen model.

SYMBOLS FOR SECTION 5

Symbol	Description
a'	Mean atmospheric transmission coefficient for cloudless, dust free, moist air after scattering only
a"	Mean atmospheric transmission coefficient for cloudless, dust free, moist air after scattering and adsorption
Asw	Area of soil layer (m^2)
C	Volumetric heat capacity $(\mathrm{cal} \cdot \mathrm{cm}^{-3} \cdot {}^{\circ}\mathrm{C}^{-1})$
C_s	Saturated dissolved oxygen at given temperature (mg/ℓ)
C_1	Dissolved oxygen in the water (mg/ℓ)
D	Oxygen deficit (mg/ℓ)
D_a	Initial dissolved oxygen deficit at time t (mg/ℓ)
D_B	Rate of removal of dissolved oxygen along the stretch
d	$d_a + d_s$ = total depletion coefficient
d_a	Depletion coefficient of the direct solar beam by dust absorption
d_s	Depletion coefficient of the direct solar beam by dust scattering
ER	Ratio of light intensity inside a given stand to the simultaneous intensity in the open
h	Local hour angle of the sun (radians)
I_o	Solar constant (4871 KJ/m^2 hr)
K_1	BOD rate constant (day^{-1})
K_2	Reaeration rate constant (day^{-1})
K_3	Rate constant for BOD removal by sedimentation or adsorption

Symbol	Description
k	Constant which depends on the species of tree
k_s	Thermal conductivity of soil (cal day^{-1} m^{-1} °C^{-1})
kw	Thermal conductivity of water (cal day^{-1} m^{-1} °C^{-1})
L	BOD along the stretch (mg/ℓ)
L_a	Initial BOD (mg/ℓ)
M	Optical air mass
M_p	Local optical air mass
N	Number of trees per hectare
n	Day of the year
O_d	Mean monthly surface dew-point temperature (°F)
Q	Heat (cal)
q_o	Solar radiation intensity at the top of atmosphere (KJ/(m^2-hr))
q_s	Solar radiation intensity on the ground (KJ/(m^2 hr))
R_g	Total reflectivity of the ground in the vicinity of the site
r	Radius vector
T_1	Average temperature of soil layer (°C)
T	Water temperature (°C)
t	Time (day)
Ts	Temperature of the first soil layer (average at a specific time) (°C)
Tw	Temperature of the water (average at a specific time) (°C)
W	Mean monthly precipitable water content (cm)
Y_s	Depth of soil at which Ts is taken (m)
Y_w	Thickness of the water from water-soil interface to the midpoint of water layer (m)

Symbol	Description
Z	Distance from soil surface in the vertical direction (cm)
z	Local elevation (m)
α	Apparent thermal diffusivity (cm^2/day)
δ	Declination of the sun (radians)
λ	Thermal conductivity (cal day^{-1} cm^{-1} $°C^{-1}$)
ϕ	Latitude of the location (radians)

SECTION 6

STREAMBANK EROSION

INTRODUCTION

Areal growth of drainageways is a common feature of landscape evolution in semiarid and subhumid areas. This growth is initiated and sustained by the erosive force of concentrated runoff. Erosion rates are controlled by the hydraulic characteristics of the flow and by the erosion resistant soil properties at the flow boundary. The source of the eroded material is either the stream bank (channel widening or channel migration) or the streambed (degradation).

Depending on the geographic location, streambank erosion may or may not be a major nonpoint source pollutant of U.S. waterways. The amount of sediment entering U.S. waterways from this source has been estimated to be 500 million tons/year (Barnes, 1968). For the 300,000 miles of channels in the drainage system, this figure results in an average of 1670 tons/mile/year. In general, the erosion rate as measured by bank recession depends on the characteristics of the streamflow and bank materials. Recession of stream banks can occur by direct or indirect action of flowing water, such as flow impingement, toe undermining, or seepage forces. Additional factors contributing to streambank erosion are freeze-thaw and wet-dry cycles, wave action, ice flows, sudden changes in stage, debris, and sediment load.

A special report on streambank erosion problems (U.S. Congress, 1969) has attributed the inadequate performance of some streambank erosion control projects to the lack of understanding of the cause-effect relationships in streambank erosion. On this basis, it is clear that an inquiry into the nature of these relationships is necessary in order to bridge the widening gap between the accelerated landscape evolution and the environmental constraints regarding nonpoint source pollution.

The model developed in this report represents a step in this direction. Emphasis is on the development of a predictive method to assess the impact of streambank erosion as a nonpoint source pollutant. At the outset, it is recognized that the spatial and temporal variability of the stream environment precludes the formulation of the model on purely theoretical grounds. On the other hand, models with a strict empirical basis tend to be highly site-specific, their applicability being limited by the available amount of supportive data. Therefore, a semi-empirical model is suggested that retains a predictive capability by virtue of its phenomenological structure.

STREAMBANK EROSION

The term streambank erosion is commonly used in connection with channel widening and straightening tendencies in perennial streams. These morphological processes are understood in a qualitative sense. For straight alluvial reaches, Leopold and Maddock (1953) showed that water discharge fluctuations have channel widening tendencies. In meandering rivers, periods of high flow cause the channel to straighten its thalweg and attack the convex bank. Some combination of channel widening and straightening is likely to prevail in any particular location. Furthermore, the problem is compounded by the spatial variability of the physical environment, especially with regard to soils, vegetation, and land use patterns.

Interaction between streambank erosion and streambed erosion is also an important component of alluvial channel morphology. Alluvial channels are constantly moving the sediment on their beds. This sediment moves downstream at the prevailing transport rate. During low flows, the local transport rate is such that meandering channels have the tendency to erode the crossings and deposit sediment in the pools. During high flows this trend is reversed. Erosion occurs at the pools and deposition in the crossings. Thus, while low flows have stabilizing tendencies, high flows act in the opposite way, eroding the convex bank in the pool, scouring the deep sections, impinging on the concave bank, and depositing sediment in the crossings.

Swift changes in channel morphology caused by short high flow periods are followed by long periods of low flow in which the channel starts anew in the reconstruction of its original thalweg. This is an inherent self-stabilizing tendency of alluvial channels that can be upset if the hydrologic balance of the contributing watershed is altered, i.e., by an increase in surface runoff at the expense of subsurface runoff.

Researchers have sought to approach the problem of streambank erosion from the standpoint of channel morphology. According to this concept, channel cross-sectional shape, as expressed by a width-to-depth ratio, is likely to be a function of the prevailing hydraulic and soil conditions. Deterministic models that describe physical processes are absent, although there has been some recent progress in relation to the morphology of streams in small watersheds (Li, Simons, and Stevens, 1976). More often, statistical models (Schumm, 1960) have substituted for the lack of the proper analytical tools, but their widespread applicability still remains to be established.

STREAMBANK EROSION BY CHANNEL WIDENING

Channel widening is directly related to an increase in stream power (the product of boundary shear stress and mean velocity). In general, alluvial channels tend to vary their cross-sectional characteristics as a function of water and sediment discharge. Since both water and sediment discharge vary in time and space in a random fashion, alluvial streams are constantly striving to change their cross-section to adjust to the changing flow conditions.

In alluvial streams, quantities such as area, depth, width, and velocity increase with water discharge. Considering the unsteadiness of the flow, these relations are certainly not unique on a short-term basis. On a long-term basis, however, equilibrium (steady-state) relations describing channel morphology can be postulated. Under equilibrium conditions, a certain channel width is associated with certain values of water and sediment discharge. These are referred to as "threshold" discharges. "Channel forming" discharge (a discharge in excess of the threshold discharge) causes a channel to depart from an equilibrium to a nonequilibrium condition, thus imposing an imbalanced stress on the system. The sequence of events following the departure from equilibrium may be described as follows. At the threshold discharge, the channel is in equilibrium with the appropriate area, depth, width, and depth/width ratio. As the discharge increases to a channel forming discharge, there is a disproportionate increase in depth since the width is kept almost constant due to the lag between the hydrologic excitation and the morphological channel response. This disproportionate increase in depth at constant channel width causes a corresponding increase in velocity (hydraulic effect) and depth/width ratio (morphological effect). Both the hydraulic and morphological effects start to work correcting the imbalance. Increase in flow depth causes an increase in the boundary shear stress τ_o , and the increase in velocity V causes an increase in the eroding capacity of the flow. Stream power ($\tau_o V$) is also increased, enabling the channel to increase its sediment transport capacity. The additional sediment transported can either originate in the channel bed or be detached from the channel banks. Usually, the channel bed is formed of sands and the banks are composed of finer particles such as silt and clay. Silts and clays are more resistant to detachment than the sand particles, but once detached they are easily transported. The question is then: Can the soil particles in the channel bank be detached? The answer lies in the amount of increase in the boundary shear stress and flow velocity, and consequently, in their product--the stream power. Bank erosion will occur when the stream power is such that it is able to detach the silt and clay particles in the banks. When this happens, the channel slowly begins to carve its banks to accommodate the new discharge conditions.

Rate of bank erosion will depend on the amount and duration of the channel-forming discharge. Equilibrium (in the long-term sense) is reestablished when increase in width causes a decrease in depth, depth/width ratio, average boundary shear stress, velocity, and stream power. The newly formed channel will remain in equilibrium from the morphological standpoint until another channel forming discharge is imposed on the system.

From the above description, it can be concluded that amount of streambank erosion is directly related to stream power of the channel forming discharge. Since stream power is equal to the product of boundary shear stress and mean velocity, it follows that

$$\tau_o V = \gamma_w d S_o V = \gamma_w q \; S_o \qquad (220)$$

in which d is flow depth, γ_w is specific weight of water, S_o is bed slope, and q is water discharge per unit of channel width. Since S_o can only be subjected to slight, if any, changes it follows that the increase in stream power is associated with an increase in discharge per unit width. The amount of streambank erosion by channel widening can, therefore, be related to the channel forming unit width discharge.

MODELING STREAMBANK EROSION BY CHANNEL WIDENING

Morphology of alluvial channels can be described empirically by hydraulic geometry relations. These relations specify variation of channel width, depth, and velocity with discharge both at a station (for discharges of different frequencies) and downstream (for discharges of the same frequency). Relations at a station are applicable for the study of channel widening. The hydraulic geometry relation for the channel width is

$$w = aQ^b \tag{221}$$

in which w is channel width, Q is water discharge, and a and b are the empirical coefficient and exponent, respectively.

Since Q is equal to qw, Equation (221) can be expressed as

$$w = a_1 \, q^{b_1} \tag{222}$$

in which

$$a_1 = a^{\frac{1}{1-b}} \tag{223}$$

and

$$b_1 = \frac{b}{1-b} \tag{224}$$

Equation (222) expresses the relationship between channel width and unit-width discharge. Under geomorphic equilibrium, channel width remains unchanged under a unit-width discharge smaller than the "threshold" discharge. When the unit-width discharge exceeds this threshold value, flow will slowly begin carving the channel bank to accommodate the increase in discharge. Mathematically, the rate of change of channel width can be expressed as

$$\frac{\partial w}{\partial t} = \frac{\partial w}{\partial q}\frac{\partial q}{\partial t} \tag{225}$$

in which $\partial w/\partial q$ is change in channel width with respect to a change in unit-width discharge, and $\partial q/\partial t$ is the rate of change of unit-width discharge.

Change in channel width due to a change in unit-width discharge is

$$\frac{\partial w}{\partial q} = a_2\, q^{b_2} \tag{226}$$

in which

$$a_2 = a_1 b_1 \tag{227}$$

and

$$b_2 = b_1 - 1 \tag{228}$$

Expressed in terms of increments

$$\frac{\Delta w}{\Delta q} \cong a_2\, q^{b_2} \tag{229}$$

where Δw is the change in channel width due to a change Δq in unit-width discharge. If this change in unit-width discharge is associated with a time interval Δt then

$$\frac{\Delta w}{\Delta t} = \frac{\Delta w}{\Delta q}\frac{\Delta q}{\Delta t} \tag{230}$$

The process of channel widening may occur by detachment of individual soil particles from the banks (microprocess) or by massive bank failure (macroprocess). The total amount of material eroded from the banks and available for transportation (as bed load or suspended load) is

$$\Delta W_T = (\Delta w)\ (\Delta x)\ (\bar{H})\ [(1-p)\ G\gamma_w] \tag{231}$$

in which ΔW_T is the weight (lbs) of soil material eroded from the banks of a channel, Δw is the change in channel width (ft), Δx is the channel reach length (ft), $\bar{H}$ is the average channel depth (ft), p is porosity of the material in the banks, G is specific gravity of the material in the banks, and γ_w is the density of water (lbs/cu ft).

From Equations (229) and (231)

$$\Delta W_T = (a_2\ q^{b_2}\ \Delta q)\ (\Delta x)\ (H)\ [(1-p)\ G\gamma_w] \tag{232}$$

by which the total amount of material ΔW can be calculated from a knowledge of the hydraulics (q), hydrology (Δq), morphology (a_2, b_2), geometry (Δx, H), and soil characteristics (p, G).

Eroded material becomes available for transportation either as bed load or suspended load. Coarser particles will join the bed load and move slowly by rolling and sliding along the bed. Finer particles will join the suspended load and be readily transported by the sustaining medium. The suspended load fraction can be calculated by the following formula

$$P_s = \frac{50 + (-1)^n\ 34 \left(\dfrac{d_{10} - d_{50}}{d_\gamma - d_{50}}\right)}{100} \tag{233}$$

in which d_{10} is the diameter for which 10 percent is finer in the bed material size distribution, d_{50} is the median diameter of the bank material, and d_γ is either d_{16} or d_{84} in the bank material size distribution. For $d_{10} > d_{50}$, n equals 2 and d_γ equals d_{84}. For $d_{10} < d_{50}$, n equals 1 and d_γ equals d_{16}.

LIMITATIONS OF THE MODEL

As formulated, the streambank erosion model estimates total amount of erosion that is likely to occur in transition from a condition of geomorphic equilibrium to another condition of equilibrium. As such, it does not provide information on the rate of streambank erosion. Rather, it gives a total figure assuming the new equilibrium condition is eventually reached. In practice, however, rate of streambank erosion is a function of the time history of the hydrologic excitation which is not explicitly considered in the present model. Therefore, calculated values are to be regarded as estimates of the total amount of streambank erosion that is associated with a certain level of hydrologic excitation. Further refinements will need to be implemented if the model is to provide information on the rate of streambank erosion.

SUMMARY

In this section, a mathematical empirical model of the process of streambank erosion by channel widening was presented. The predictive capability of the model is enhanced by its phenomenological structure, although empirical data are needed in the stream morphology component. The model estimates the total amount of streambank erosion and the fraction of it that goes into suspension. Threshold channel conditions, bank characteristics, and the hydrologic excitation are input to the model. Further refinements are needed if the model is to predict the rate of streambank erosion.

SYMBOLS FOR SECTION 6

Symbol	Description
a	Coefficient in width-discharge relationship
a_1	$a^{(1/(1-b))}$
a_2	$a_1 b_1$
b	Exponent in width-discharge relationship
b_1	$b/(1-b)$
b_2	b_1-1
d	Flow depth
d_i	Sediment diameter for which i percent of the grain sizes are finer
G	Specific gravity of material in banks
$\bar{H}$	Average channel depth (ft)
P_s	Suspended load fraction
p	Porosity
Q	Discharge (cfs)
q	Discharge per unit width
S_o	Channel bed slope
t	Time
V	Average stream velocity (ft/sec)
w	Channel width (ft)
x	Dimension in downstream direction (ft)

Symbol	Description
ΔW_T	Weight of soil material eroded from the banks of a channel (lbs)
γ_w	Specific weight of water (lbs/cu ft)
τ_o	Boundary shear stress

SECTION 7

THE RILLING PROCESS AND FOREST LITTER

INTRODUCTION

Forest litter is among the major nonpoint source pollutants in upland watersheds. With current emphasis on nonpoint source pollution control, there is an urgent need for an increased understanding of the mechanics of forest litter loading to the streams. A literature search has revealed the virtual nonexistence of forest litter loading models. While some measurements have been made regarding quantity of organic debris delivered to a stream (Swanson and Lienkaemper, 1975), there has been no attempt to develop a comprehensive forest litter loading model.

Movement of forest litter is a complex process involving the interaction of hydrologic, topographic, and vegetative elements of the landscape. In developing a phenomenological model of forest litter loading, a considerable simplification can be implemented if the forest litter movement can be linked to the amount of concentrated flow in the watershed. Concentrated flow is defined as rill flow (as opposed to interrill flow).

A first approximation to the rill formation and the loading of forest litter is presented in this section. The model is based on the assumption that the amount of forest litter loading is directly proportional to the areal extent of rilling. This is a reasonable assumption in view of the demonstrated effectiveness of concentrated flow in transporting sediment and debris through upland watershed drainage networks. This approach allows the conversion of the forest litter loading problem into that of determining the areal extent of rilling (rilling density) given a set of topographic, hydrologic, and morphologic conditions.

RILL AND INTERRILL FLOW

Overland flow is defined as that part of surface runoff uniformly distributed over an area with no readily recognizable flow concentrations. On many soil surfaces, however, overland flow eventually concentrates in numerous small channels. These flow concentrations are due to topographic irregularities or differences in soil erodibility. Their size is related to the amount of flow and to the factors causing the flow to concentrate. In the early stages of development, channels formed by surface erosion may be 3 to 4 inches wide and 1 to 2 inches deep. As erosion progresses, channels deepen and widen at a rate that is a function of slope steepness, runoff characteristics, and soil conditions. Such erosion-formed channels are called rills. If left uncontrolled, rills may eventually develop into large incisions that cannot be obliterated by normal tillage. These overgrown rills are commonly called gullies.

Interrill flow refers to that part of surface runoff that occurs between rills with no significant flow concentration. Velocities and flow depth in interrill flow are small compared to those of rill flow. Therefore, the sediment or organic material transport capacity of interrill flow is considerably less than that of rill flow.

Influence of rilling in the sediment transporting capacity of runoff from upland areas was documented by Meyer, Foster, and Romkens (1975). They showed that differences in erodibility between two experimental plots could be explained in terms of the greater rilling density of the more erodible plot. Therefore, it can be concluded that the transporting capacity of runoff (sediment and organic debris) is highly related to the areal extent of rilling.

Rill Development

The process of rill development was described by Leopold, Wolman, and Miller (1964). Initially, rilling develops as tiny incisions following a parallel pattern bite into a slope without materially affecting the gradient. The head of a rill system may not extend the entire way to the watershed divide, and a zone near the divide may remain essentially unchanneled.

Processes by which parallel shoestring rills become integrated into a drainage network are cross-grading and micropiracy (Horton, 1945). Micropiracy is a consequence of the overtopping and breaking down of ridges that initially separate adjacent rills. Two parallel and adjacent rills are generally slightly different in elevation and depth. One will be slightly deeper or at a lower elevation than the other. As water is drawn away from the rill of a higher elevation to the rill of a lower elevation, the interrill divide is progressively broken down and a component of flow toward the main rill develops. This phenomenon is referred to as cross-grading.

Rill Density

Rill development is a complex physical process. For simplicity in modeling, it is assumed that the vegetation distribution is uniform and does not significantly affect rill development. This assumption implies that the most influencing physical process is that of soil erosion. Under this condition, a mathematical formulation of rill density in upland watersheds can be obtained from a knowledge of stream morphology. Hydraulic geometry relations derived by Li, Simons, and Stevens (1976) are used in this report as the basis of the formulation.

Open channel uniform flows can be expressed by a low of resistance to flow of the type

$$S_o = f \frac{Q_o^2}{8gR_oA_o^2} \tag{234}$$

in which S_o is bed slope, f is the Darcy-Weisbach friction coefficient, Q_o is discharge, R_o is hydraulic radius, A_o is cross-sectional area, and g is the acceleration of gravity.

In laminar flow or flow that behaves like laminar, friction factor f can be related to the Reynolds number R_e by

$$f = \frac{K_1}{R_e} \tag{235}$$

in which K_1 is a constant and

$$R_e = \frac{Q_oR_o}{\nu A_o} \tag{236}$$

Value ν is the kinematic viscosity of water. Hydraulic radius R_o is by definition

$$R_o = \frac{A_o}{P_o} \tag{237}$$

in which P_o is the wetted perimeter corresponding to A_o. Usually, P_o can be approximated by a relationship of the form

$$P_o = a\ A_o^{0.5} \tag{238}$$

in which a is an empirical coefficient.

Substituting Equations (235) through (238) into Equation (234) yields

$$Q_o = \frac{8gS_oA_o^2}{K_1\ \nu\ a^2} \tag{239}$$

Equation (239) relates discharge Q_o to area A_o and bed slope S_o in laminar flow or flow with resistance characteristics similar to laminar.

Assuming that an overland flow plane of length L, width W, and slope S_o (in the direction of L) is subjected to a rainfall excess of intensity i, after equilibrium is attained, the total discharge in a cross section at a distance X from the top of the plane is (Figure 20).

$$Q_T = iXW \tag{240}$$

Interaction of the flow and the loose boundary leads to the development of a rilling pattern oriented in the direction of the flow. Bankful water discharge in each rill at the threshold of geomorphic equilibrium is Q_o and bankful cross-sectional area is A_o. Therefore,

$$Q_T = n\ Q_o = iXW \tag{241}$$

in which n is the number of rills developed after attainment of geomorphic equilibrium. From Equations (239) and (241)

$$n = \frac{K_1\ a^2\ v\ iXW}{8g\ S_o\ A_o^{\ 2}} \tag{242}$$

Each rill has a top width T_o. Therefore, rilling density R_D expressed as a percentage of the plane width is

$$R_D = 100\ \frac{n\ T_o}{W} \tag{243}$$

or

$$R_D = 100\ \left(\frac{K_1\ a^2\ v\ iX}{8g\ S_o}\right)\left(\frac{T_o}{A_o^{\ 2}}\right) \tag{244}$$

Quantity $T_o/A_o^{\ 2}$ can be related to stream morphology using the hydraulic geometry relations developed by Li, Simons, and Stevens (1976) as

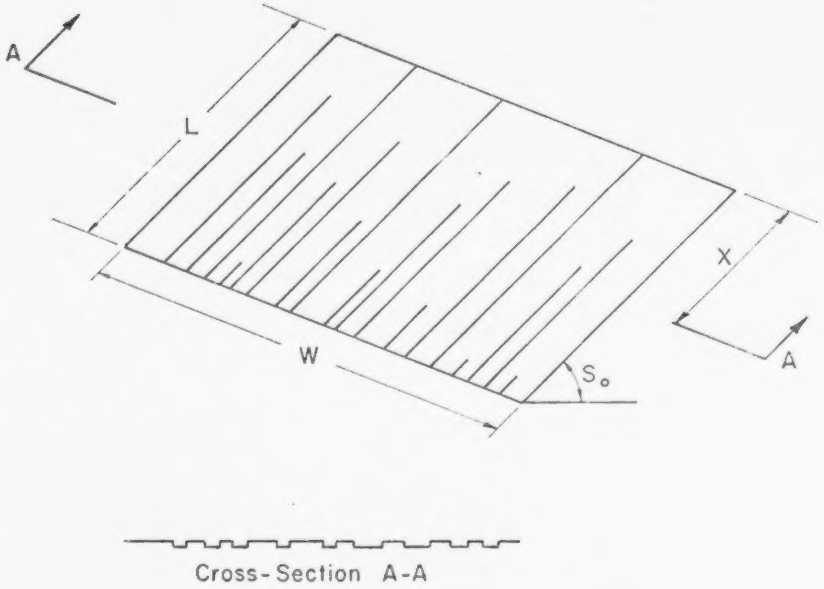
A
L
X
W
S₀
A
Cross-Section A-A

Figure 20. Schematic of rill pattern model.

$$T_o = C_t \, y_o \tag{245}$$

and

$$A_o = C_a \, T_o \, y_o \tag{246}$$

in which y_o is the equilibrium depth of flow, and C_a and C_t are coefficients depending on the angle of friction ϕ of the particles at the boundary and the ratio of lift to drag forces β. For $\beta = 0.85$ (Bhowmik, 1968), the following relationships between ϕ , C_a , and C_t were obtained (Li, Simons, and Stevens, 1976).

$$C_a = 0.61 \, \phi^{0.021} \tag{247}$$

$$C_t = 210 \, \phi^{-1.038} \tag{248}$$

Substituting Equations (245) and (246) into Equation (244) gives

$$R_D = 100 \left(\frac{K_1 \, a^2 \, v \, iX}{8g \, C_a{}^2 \, C_t} \right) \left(\frac{1}{S_o \, y_o{}^3} \right) \tag{249}$$

At hydraulic and geomorphic equilibrium, particles at the rill boundary are at the threshold of motion. Therefore, the Shield's criterion for incipient motion (ASCE, 1975) can be used to relate the boundary shear stress to the soil particle diameter assuming an armoring diameter of D_{84} as

$$\tau_* = \frac{\gamma_\omega \, y_o \, S_o}{(\gamma_s - \gamma_\omega) D_{84}} \tag{250}$$

in which τ_* is the dimensionless critical shear stress, γ_s is the density of particles, and γ_ω is density of water which yields

$$y_o S_o = K_2 D_{84} \tag{251}$$

in which

$$K_2 = \frac{\gamma_s - \gamma_\omega}{\gamma_\omega} \, \tau_* \tag{252}$$

Substituting Equation (251) into Equation (249) gives

$$R_D = 100\left[\frac{K_1 a^2}{C_a{}^2 C_t K_2{}^3}\right]\left(\frac{\nu}{8g\ D_{84}{}^3}\right)\left(iXS_o{}^2\right) \tag{253}$$

Equation (253) expresses rilling density in laminar flow or flow behaving like laminar as a function of slope of the plane S_o measured along distance X, threshold rainfall intensity i, armoring diameter D_{84}, and several friction (K_1), transport (K_2), and morphological constants (a, C_a, and C_t). For a subsequent rainfall event with intensity smaller than threshold intensity, rilling density would most likely remain unchanged.

For turbulent flow, an alternate expression to Equation (253) can be derived considering that f is independent of R_e. For this case

$$Q_o = \left(\frac{8g\ S_o}{fa}\right)^{1/2} A_o{}^{5/4} \tag{254}$$

instead of Equation (239), that leads to the following expression for rilling density in turbulent flow

$$R_{D_t} = 100\left[\frac{a^{1/2}}{C_a{}^{5/4} C_t{}^{1/4} K_2{}^{3/2}}\right]\left(\frac{f}{8g\ D_{84}{}^3}\right)^{1/2}\left(iXS_o\right) \tag{255}$$

Equation (255) expresses rilling density in turbulent flow as a function of the slope of the plane S_o measured along the distance X, threshold rainfall intensity i, armoring diameter D_{84}, and several friction (f), transport (K_2), and morphological constants (a, C_a, and C_t).

According to Meyer, Foster, and Romkens (1975), extent of rilling depends on the runoff rate, slope steepness, and soil properties. Equations (253) and (255) depict the effect of these variables on rill density: the greater threshold runoff rate (iX) and slope (S_o), and the smaller the particle diameter D_{84}, the greater rilling density.

FOREST LITTER LOADING

Quantity of forest litter delivered to a stream is a direct function of the areal extent of rilling and the amount of forest litter production. The areal extent of rilling will, in general, be determined by large events. Smaller subsequent events will not entirely fill established rill network. Therefore, litter washed out of the rill network will be detached from the area defined by the top width of the flowing water. This top width may be obtained from an 'at a station' equation provided by Li, Simons, and Stevens (1976). Ratio of stream top width to the channel top width established by the previous large event is given by

$$\frac{T}{T_o} = \left(\frac{Q}{Q_o}\right)^{0.24} \qquad (256)$$

As before, $Q = (iXW)/n$, however, the number of rills n is determined by the large event and remains the same for all smaller flows. Therefore, Equation (256) becomes

$$\frac{T}{T_o} = \left(\frac{\frac{iXW}{n}}{\frac{i_oXW}{n}}\right)^{0.24} = \left(\frac{i}{i_o}\right)^{0.24} \qquad (257)$$

Since yearly litter production data is usually the most precise data available, forest litter loading is calculated on an annual basis. Excess rainfall intensities for the year are searched to yield the largest intensity. If this intensity is smaller than the previous large event, then litter loading is determined from

$$F_L = \frac{\bar{R}_{D_o}}{100} A \eta F_p \qquad (258)$$

where F_L is the litter loading for the simulated year, $\bar{R}_{D_o}$ is the rill density corresponding to the previous large event, A is the watershed area, η is the ratio T/T_o, and F_p is the annual forest litter production. If the largest excess intensity is greater than the previous large event, then a new rill density $\bar{R}_D$ is calculated and the litter loading is given by

$$F_L = \frac{\bar{R}_D}{100} A F_p \qquad (259)$$

where η is now equal to 1.

From a practical standpoint, it is necessary to establish a minimum rilling area below which the forest litter loading would be likely to be insignificant. This minimum value is arbitrarily set at the rainfall rate for which the rilling density is less than 5 percent. Therefore, Equations (258) and (259) are applicable for calculating amount of forest litter loading to a stream if the following is known: 1) a threshold rainfall event with a rate for which the rilling density is greater than 5 percent, 2) the area of plane, 3) forest litter production rate, and 4) a previous excess intensity which is assumed to establish an existing rill density.

SYMBOLS FOR SECTION 7

Symbol	Description
A	Plane area
A_o	Equilibrium cross-sectional area
a	Fitted coefficient in wetted perimeter--flow cross-sectional area equation
C_a	Coefficient in at-a-station expression for cross-sectional flow area
C_t	Coefficient in at-a-station expresstion for channel top width
D_{84}	Diameter for which 84% is finer
F_L	Forest litter loading
F_p	Forest litter production
f	Darcy-Weisbach friction coefficient
g	Acceleration of gravity
i	Rainfall intensity
K_1	Constant in Darcy-Wiesbach friction factor equation
K_2	Constant, Eq. 244
L	Plane length
n	Number of rills
P_o	Equilibrium wetted perimeter
Q_o	Equilibrium discharge
Q_T	Total discharge
R_e	Reynolds number, Eq. 227

Symbol	Description
R_o	Equilibrium hydraulic radius
R_D	Rill density, in percentage
R_{D_t}	Rill density in turbulent flow
$\bar{R}_D$	Average rill density, in percentage
S_o	Bed slope
T	Stream top width
T_o	Equilibrium top width
W	Plane width
X	Distance from top of plane
y_o	Equilibrium flow depth
β	Ratio of lift to drag forces
γ_s	Density of particles
γ_w	Density of water
ϕ	Angle of friction
ν	Kinematic viscosity of water
τ_*	Dimensionless critical shear stress
η	Ratio T/T_o

SECTION 8

A PLANNING MODEL USING INTERACTIVE SEQUENTIAL GOAL PROGRAMMING

INTRODUCTION

Basin evolution is a complex process affected by many natural and man-made events especially those related to land-use and forest management practices. The problem of management of a basin depends upon the selection of the best land-use strategy to optimize specified socio-economic objectives under certain constraints on water and sediment transport conditions in the stream channels and on water quality standards in the basin. The quality of a basin management plan depends on the quality and the availability of data. However, efficiency of planning depends on the optimization tool to be selected and accuracy of simulation models used to project future basin-system response. A review and evaluation of multi-objective programming techniques used to solve basin planning problems has been conducted by Loucks (1975) and later by Cohon and Marks (1975). One technique of increasing popularity often encoutered in water resources literature is goal programming. It is designed to evaluate (possibly conflicting) goals as well as goals of differing priorities. Goal programming for linear systems was introduced by Charnes and Cooper (1961) and was thoroughly developed by Lee (1972).

The goal programming (GP) algorithm seeks to minimize deviations from specified goals and can be described as

$$\text{Minimize } Z = \sum_{i=1}^{k} (w_i^+ y_i^+ + w_i^- y_i^-) \quad (260)$$

$$\text{subject to } f_i(\underline{x}) - y_i^+ + y_i^- = g_i \quad (i = 1, 2, \ldots k) \quad (261)$$

where $f_i(\underline{x})$ is an objective function,

y_i^+ is the deviation above (overachievement of) the specified goal level,

y_i^- is the deviation below (underachievement of) the specified goal level,

w_i^+ and w_i^- are penalties attached to the above goal deviations, and

g_i is the goal attainment desired for objective function i.

Usually a priority factor is assigned to each positive and/or negative deviational variable such that the product of the deviation and the priority factor must be greater at all times for the more important goal or goals. Goals with a higher priority are then satisfied before a lower priority goal can be satisfied.

The main drawback of the GP algorithm is that policy decisions are necessary to define desired goal levels g_i and relative penalty weights w_i with the corresponding priority factors. Direct application of the GP algorithm to a large complex basin system also presents some difficulties because of the different types of spatial and temporal information that are used with various process models in the simulation phase after each course of action has been selected. For example, land-use process models are based on a soil-vegetation classification, while water and sediment models are tied to hydrologic response units which do not necessarily correspond to soil-vegetation response units. In addition, more complex models (i.e., water and sediment yields) usually require shorter time-steps for computational stability.

CONCEPTUAL DESIGN OF THE SEQUENTIAL MULTI-LEVEL GOAL PROGRAMMING MODEL

To avoid the difficulties discussed above and to reduce computational cost, the planning model is designed as multi-level. The lower level is used to select optimal land-use strategies based on different alternative management practices and subject to some specified land-use constraints. In this level, elements of the resource response matrix are calculated by various land-use process models which use the same type of spatial and temporal information (i.e., same soil-vegetation units and time-step). After selecting a set of optimal strategies for land-use management, the upper level is then used to select best management strategy for the whole basin system based on different land-use strategies selected from the first level and the outcomes of hydrologic and water quality component processes, subject to some specified socioeconomic constraints. In this level, complex models of water and sediment yields and water quality are used to calculate the elements of the process response matrix which then serves as the necessary input for the selection of the best basin management strategy. The flowchart of the overall structure of the proposed planning model is presented in Figure 21. Detail description of level 1 resource estimation models and level 2 process simulation models can be found in Bartlett, Boxmeyer, and Ponce (1978) and the previous chapters of this report, respectively.

The preliminary version of the model is based on a linear GP package developed by Bartlett, Bottoms, and Pope (1976). This version does not have great flexibility for future expansion and requires too much effort from the user to input the necessary information according to some pre-specified formats. Therefore, the following improvements have been implemented in the present model.

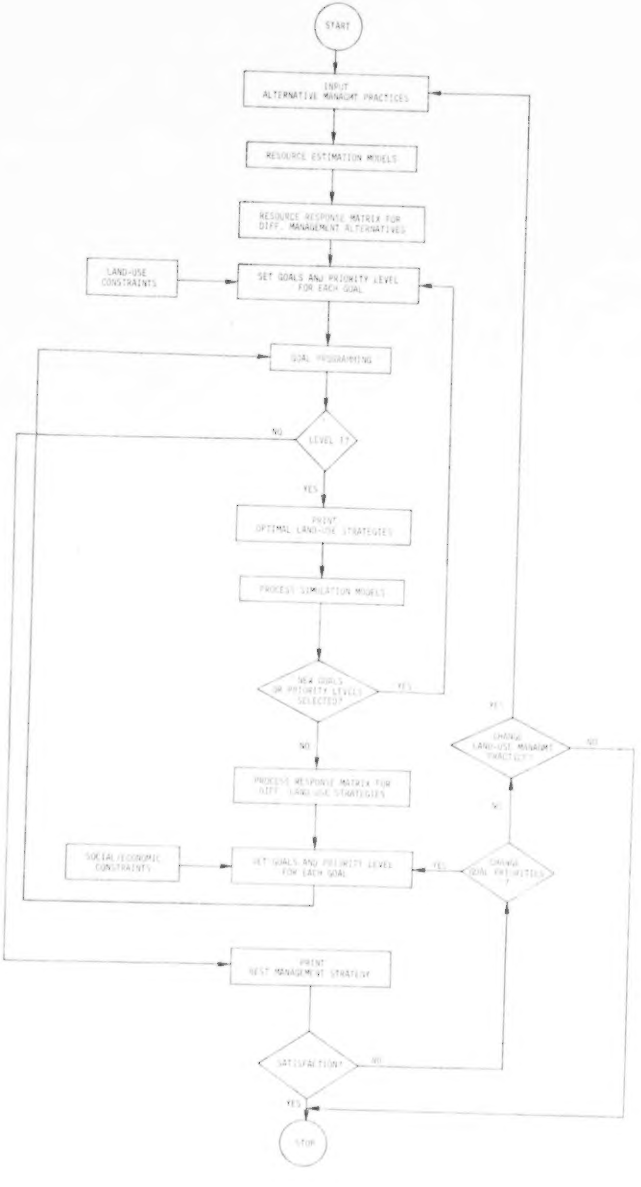
START
INPUT
ALTERNATIVE MANAGMT PRACTICES
RESOURCE ESTIMATION MODELS
RESOURCE RESPONSE MATRIX FOR
DIFF. MANAGEMENT ALTERNATIVES
LAND-USE
CONSTRAINTS
SET GOALS ANJ PRIORITY LEVEL
FOR EACH GOAL
GOAL PROGRAMMING
NO
LEVEL 1?
YES
PRINT
OPTIMAL LAND-USE STRATEGIES
PROCESS SIMULATION MODELS
NEW GOALS
OR PRIORITY LEVELS
SELECTED?
YES
NO
YES
CHANGE
LAND-USE MANAGMT
PRACTICE?
NO
PROCESS RESPONSE MATRIX FOR
DIFF. LAND-USE STRATEGIES
NO
SOCIAL/ECONOMIC
CONSTRAINTS
SET GOALS AND PRIORITY LEVEL
FOR EACH GOAL
YES
CHANGE
GOAL PRIORITIES
?
PRINT
BEST MANAGEMENT STRATEGY
SATISFACTION?
NO
YES
STOP

Figure 21. Overall structure of proposed planning model.

1. The iterative approach to goal programming suggested by Dauer and Krueger (1977) has been used to enable one to solve linear, nonlinear, integer, and other goal programming problems using the corresponding optimization technique in an iterative manner. Although the present model is set up to solve only linear GP problems, the new formulation does offer the users a possibility to adapt the model to other types of planning and management problems involving goals which are no longer linear. Further discussion on the implementation of this approach will be presented in the next section.

2. The model is set up to run on interactive mode. All necessary input information will be key-in by the user according to instructions appearing on the computer terminal's screen. Format-free input certainly helps average users. Detail description on the input requirement and output options of the model and its programming logic will be provided in a separate user's manual.

An Iterative Approach to Goal Programming

The following is a summary of the approach suggested by Dauer and Krueger (1977) to solve a general goal programming problem iteratively. The fundamental premise of goal programming is that we seek to attain each goal i without regard to the attainability of the goals with lower priority level j, where $i < j$. Thus all goals will be listed according to the order in which we wish to achieve these goals. We then define the attainment problem for goal 1 as follows.

Suppose $\underline{f}^i(\underline{x})$ and $\underline{g}^i$ are p_i vectors for $1 \leq i \leq k$. Setting

$$\underline{y}^i = (y_1^i, y_2^i, \ldots, y_{p_i}^i)^T \tag{262}$$

then the GP problem for goal 1 (GP1) can be written as

$$\text{Minimize} \quad s_1 = y_1^1 + y_2^1 + \ldots + y_{p_1}^1 \tag{263}$$

subject to some constraints (in vector notation)

$$\underline{f}^1(\underline{x}) - \underline{y}^1 \leq \underline{g}^1 \tag{264}$$

$$h(\underline{x}) \leq g^{o} \tag{265}$$

$$\underline{x} \varepsilon \Omega, \ \underline{y}^{1} \geq 0 \tag{266}$$

If s_1^* denotes the solution of this problem, we then say that s_1^* is the maximum degree of attainment for goal 1. Now the attainment problem for goal 2 is equivalent to problem GP2

$$\text{Minimize} \quad s_2 = y_1^2 + y_2^2 + \ldots + y_{P_2}^2 \tag{267}$$

subject to the constraints

$$\underline{f}^{2}(\underline{x}) - \underline{y}^{2} \leq \underline{g}^{2} \tag{268}$$

$$\underline{f}^{1}(\underline{x}) - \underline{y}^{1} \leq \underline{g}^{1} \tag{269}$$

$$y_1^1 + y_2^1 + \ldots + y_{P_1}^1 = s_1^* \tag{270}$$

$$h(\underline{x}) \leq g^{o} \tag{271}$$

$$\underline{x} \varepsilon \Omega, \ \underline{y}^{1} \geq 0, \ \underline{y}^{2} \geq 0 \tag{272}$$

Constraints (269) and (270) imply that in trying to attain goal 2 we will not sacrifice our previously determined maximum degree of attainment of goal 1. Let s_2^* be the solution of the problem GP2; we can then proceed to goal 3, etc. Thus, the sequential goal attainment algorithm can be summarized as follows

Step 1 Solve problem GP1 using the appropriate optimization technique and thus obtain s_1^*.

Step 2 Set $j = 2$.

Step 3 Using $s_1^* \ldots s_{j-1}^*$ solve problem GP_j using the appropriate optimization technique. Let s_j^* denote the optimum.

Step 4 If $j \neq k$ (the number of goals), set $j = j + 1$ and go to step 3; otherwise proceed to step 5.

Step 5 Let $\underline{x}^* = (x_1^*, x_2^*, \ldots, x_n^*)$ denote the solution(s) of problem GP_k associated with the optimum s_k^*. The optimal solution(s) of the goal programming problem is given by $\underline{x}^*$. Values s_j^*, $1 \leq j \leq k$, designate the degree to which the j^{th} goal can be attained given the priority structure and constraints of the problem.

The above algorithm makes use of whatever optimization technique is available for each iterative optimization problem. Actual implementation of this algorithm for the linear GP problems can be described by the flowchart in Figure 22.

Approach to Model Simplification for Practical Use

At the present stage of research, simulation models developed for hydrologic, hydraulic, biological, and chemical processes which are described in the previous chapters of this report are quite complex and cumbersome and therefore not suitable to be incorporated into the iterative algorithm of the GP/Level 2 when various management strategies are to be investigated. One way to overcome this difficulty is to replace complex models with simpler ones which are derived from the accurate simulation results of the former by some suitable interpolation scheme. In the present planning model, Aitken's approach has been used for this purpose.

CONCLUSIONS AND SUGGESTIONS FOR FUTURE RESEARCH

A prototype planning model for the evaluation of alternative forest management practices based on a multi-level iterative goal programming approach is described. This model is of modular structure and set up to operate on interactive mode. Further refinement is necessary for the model to become a useful, working aid for decision makers. The following areas of research are of particular importance.

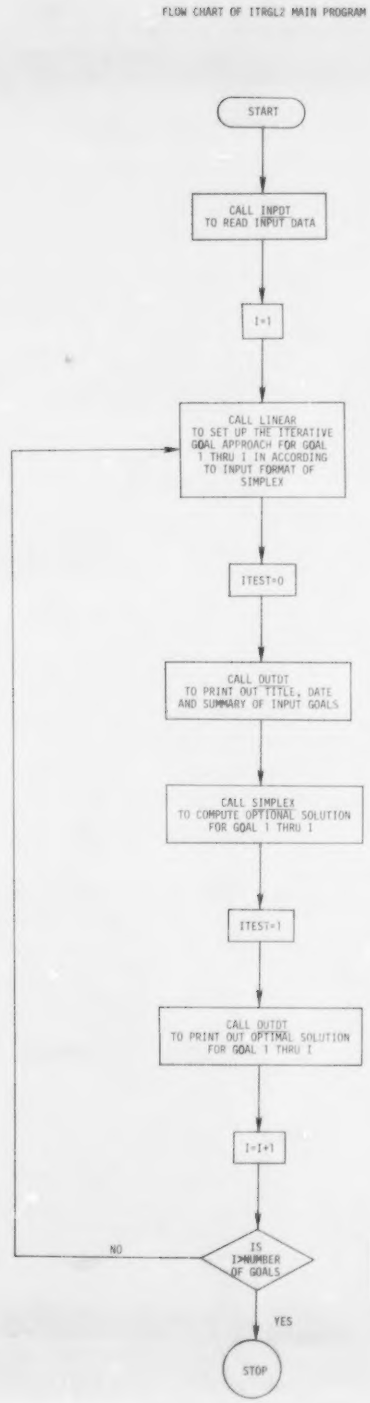
FLOW CHART OF ITRGL2 MAIN PROGRAM
START
CALL INPDT TO READ INPUT DATA
I=1
CALL LINEAR TO SET UP THE ITERATIVE GOAL APPROACH FOR GOAL 1 THRU I IN ACCORDING TO INPUT FORMAT OF SIMPLEX
ITEST=0
CALL OUTDT TO PRINT OUT TITLE, DATE AND SUMMARY OF INPUT GOALS
CALL SIMPLEX TO COMPUTE OPTIONAL SOLUTION FOR GOAL 1 THRU I
ITEST=1
CALL OUTDT TO PRINT OUT OPTIMAL SOLUTION FOR GOAL 1 THRU I
I=I+1
NO
IS I>NUMBER OF GOALS
YES
STOP

Reproduced from best available copy.

Figure 22. Flow chart for linear goal planning algorithm.

FLOW CHART FOR INPDT SUBROUTINE

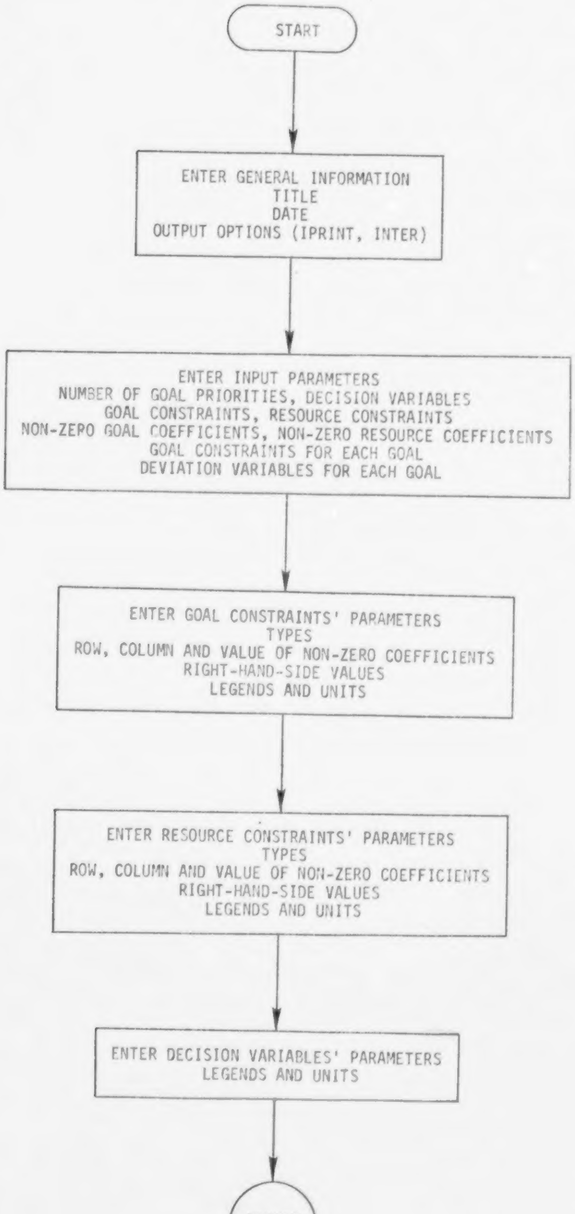
START
ENTER GENERAL INFORMATION
TITLE
DATE
OUTPUT OPTIONS (IPRINT, INTER)
ENTER INPUT PARAMETERS
NUMBER OF GOAL PRIORITIES, DECISION VARIABLES
GOAL CONSTRAINTS, RESOURCE CONSTRAINTS
NON-ZEPO GOAL COEFFICIENTS, NON-ZERO RESOURCE COEFFICIENTS
GOAL CONSTRAINTS FOR EACH GOAL
DEVIATION VARIABLES FOR EACH GOAL
ENTER GOAL CONSTRAINTS' PARAMETERS
TYPES
ROW, COLUMN AND VALUE OF NON-ZERO COEFFICIENTS
RIGHT-HAND-SIDE VALUES
LEGENDS AND UNITS
ENTER RESOURCE CONSTRAINTS' PARAMETERS
TYPES
ROW, COLUMN AND VALUE OF NON-ZERO COEFFICIENTS
RIGHT-HAND-SIDE VALUES
LEGENDS AND UNITS
ENTER DECISION VARIABLES' PARAMETERS
LEGENDS AND UNITS
RETURN

Figure 22. Continued.

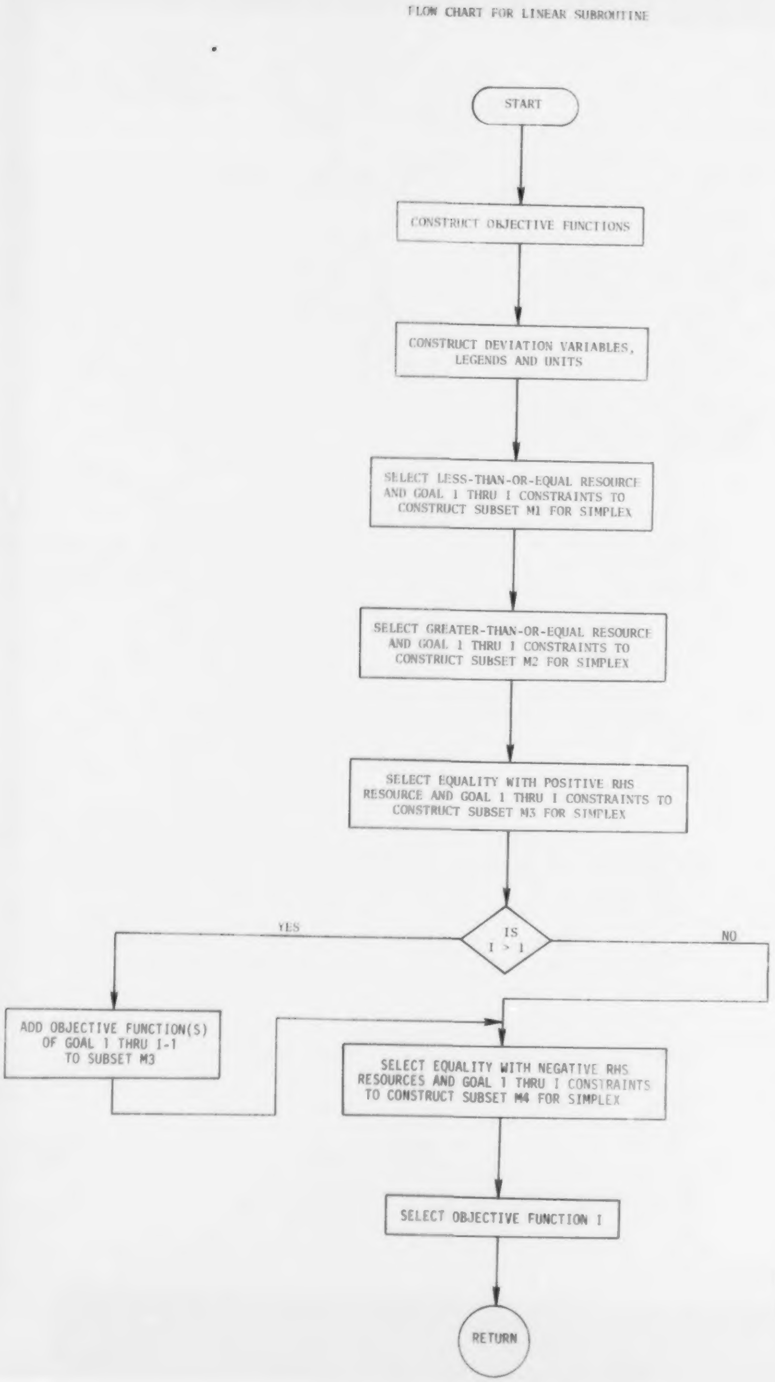
FLOW CHART FOR LINEAR SUBROUTINE
START
CONSTRUCT OBJECTIVE FUNCTIONS
CONSTRUCT DEVIATION VARIABLES, LEGENDS AND UNITS
SELECT LESS-THAN-OR-EQUAL RESOURCE AND GOAL 1 THRU I CONSTRAINTS TO CONSTRUCT SUBSET M1 FOR SIMPLEX
SELECT GREATER-THAN-OR-EQUAL RESOURCE AND GOAL 1 THRU I CONSTRAINTS TO CONSTRUCT SUBSET M2 FOR SIMPLEX
SELECT EQUALITY WITH POSITIVE RHS RESOURCE AND GOAL 1 THRU I CONSTRAINTS TO CONSTRUCT SUBSET M3 FOR SIMPLEX
IS I > 1
YES
NO
ADD OBJECTIVE FUNCTION(S) OF GOAL 1 THRU I-1 TO SUBSET M3
SELECT EQUALITY WITH NEGATIVE RHS RESOURCES AND GOAL 1 THRU I CONSTRAINTS TO CONSTRUCT SUBSET M4 FOR SIMPLEX
SELECT OBJECTIVE FUNCTION I
RETURN

Reproduced from best available copy.

Figure 22. Continued.

Flow Chart of OUTDT Subroutine

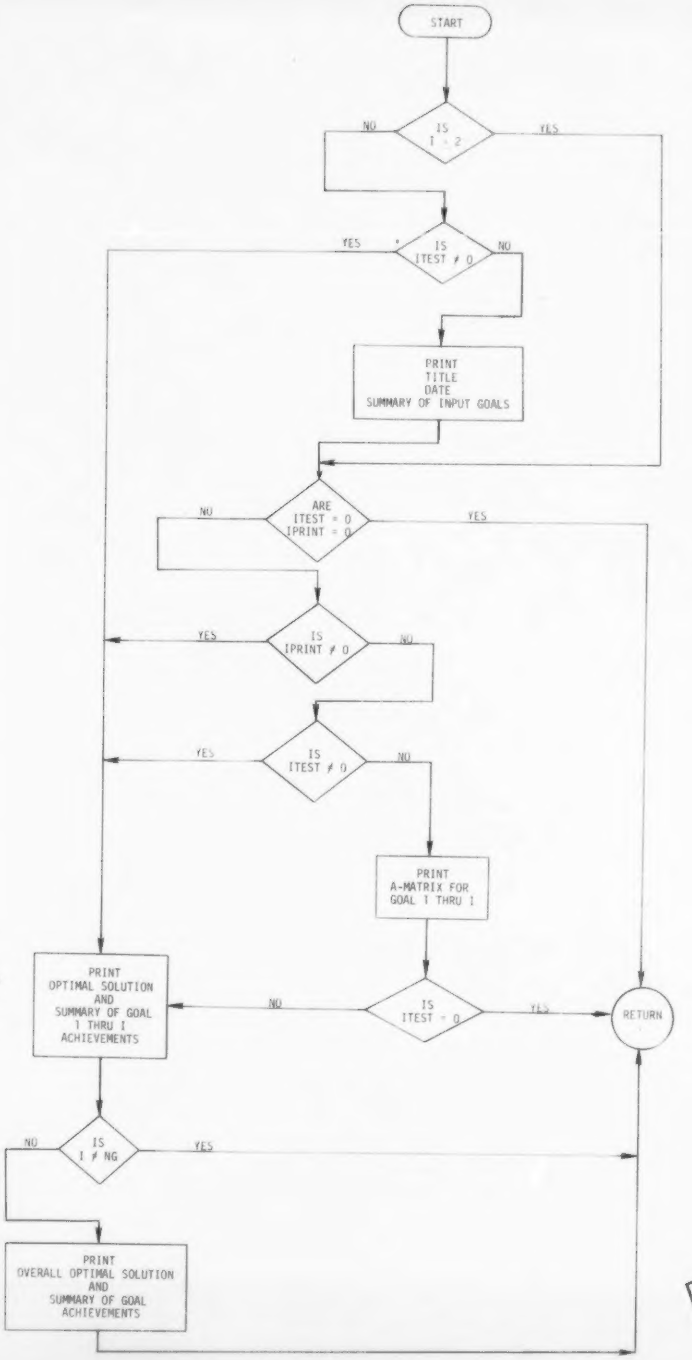
START
IS
I ≥ 2
NO
YES
IS
ITEST ≠ 0
YES
NO
PRINT
TITLE
DATE
SUMMARY OF INPUT GOALS
ARE
ITEST = 0
IPRINT = 0
NO
YES
IS
IPRINT ≠ 0
YES
NO
IS
ITEST ≠ 0
YES
NO
PRINT
A-MATRIX FOR
GOAL 1 THRU I
PRINT
OPTIMAL SOLUTION
AND
SUMMARY OF GOAL
1 THRU I
ACHIEVEMENTS
NO
IS
ITEST = 0
YES
RETURN
IS
I ≠ NG
NO
YES
PRINT
OVERALL OPTIMAL SOLUTION
AND
SUMMARY OF GOAL
ACHIEVEMENTS

Reproduced from
best available copy.

Figure 22. Continued.

1. Incorporation of a search package to the model to help in solving some nonlinear optimization problems which may appear in the management process is desirable.

2. A simple and efficient query language is needed to help decision makers interface with the GP model and various process simulation models. Further study of this query language should lead to an efficient linkage of the planning model to an ecosystem data base. It is only at this stage that one may claim that the planning model is truly operational.

SYMBOLS FOR SECTION 8

$f_i(x)$	An objective function
$\underline{f}^i(\underline{x})$	ρ_1 vectors for $1 < i < k$
g_i	Goal attainment desired for objective function i
$\underline{g}^i$	ρ_1 vectors for $1 < i < k$
s_1^*	Maximum degree of attainment for goal 1
w_i^+, w_i^-	Penalties attached to goal deviations
y_i^+	Deviation above (overachievement of) the specified goal level
y_i^-	Deviation below (underachievement of) the specified goal level

SECTION 9

SNOWMELT

INTRODUCTION

In many watersheds the most significant contribution to runoff is from snowmelt. Often the most severe erosion and sedimentation events occur as combinations of high intensity spring rainfall and snowmelt runoff. This aspect of the hydrologic cycle is particularly important in high altitude watersheds of the western United States and in northern latitudes. After examining available snowmelt models, it was felt that a modified version of the model developed by Leaf and Brink (1973a) would provide the best approach for incorporation into the generalized planning model.

The Leaf and Brink (1973a) model is a simulation originally developed for snowmelt prediction in Colorado subalpine watersheds. It is a mechanistic approach with data requirements consistent with previously described planning model components, in particular, evapotranspiration and water balance components. The snowmelt model as formulated is designed to provide daily runoff water yields and therefore, it requires modification to interface with the water and sediment routing components. This snowmelt model has been expanded by the authors into a general hydrologic simulation at subalpine forests (Leaf and Brink, 1973b) and into a land use simulation applicable to similar locations (Leaf and Brink, 1975).

In its expanded form, the Leaf and Brink approach to some degree parallels the mission of the present planning model. However, the snowmelt process model dominates the approach, and the process formulations for water and sediment runoff are insufficient for the purpose of simulating nonpoint source pollutant transport. Snowmelt portions of the simulation are a sound formulation of the mechanics of snowmelt in a homogeneous pack. The model contains some empirical relations that make a given formulation regionally specific. These expressions will be discussed in order to aid in application to regions other than the Colorado Rocky Mountains. The modifications necessary to merge this snowmelt model with the previously described planning model routines are also discussed. Although adequately described in the above cited references (Leaf and Brink, 1973a, 1973b, 1975), the basic mechanics will be reviewed below for completeness.

SNOWMELT PROCESSES

General

The Leaf and Brink model is a combination of the fundamental laws of conservation of mass (water balance) and conservation of energy. The thermal state of the snowpack is described by the calorie deficit of the pack on any given day. The calorie deficit is defined to be the number of calories (per unit area) required to bring the pack to an isothermal state at 0°C. It is assumed that no melt can occur until the pack has reached this state. The general scheme of computing snowpack accumulation, temperature change, and melt begins with an assessment of the effects of the day's precipitation if any, on the pack. This includes the effect of the snow or rain introduced to the pack at the average air temperature, as well as the addition of water to the pack as snow or as rainfall. After the effect of rainfall has been assessed, an energy balance calculation is begun with a determination of the net radiation input (or loss) to the snow pack. Depending of the thickness of the snowpack and the amount of free water existing in the pack. The new pack temperature is calculated using either a thermal diffusion model or the radiation balance directly. Based on the new temperature, a new calorie deficit or melt is calculated, and the simulation proceeds to the next day's precipitation and radiation data. Water balance relations are adjusted daily based on the above outcome.

THERMAL DIFFUSION MODEL

The core of the Leaf and Brink (1973) model is the thermal diffusion model. The unsteady heat flow equation as presented has the following form

$$k_s \frac{\partial^{\partial} T_s}{\partial z^2} = c_s \rho_s \frac{\partial T_s}{\partial T} \qquad (273)$$

where T_s is the temperature of the snowpack (a function of space and time), z is depth in the pack, t is time, c_s is specific heat of snow, ρ_s is density of snow, and k_s is thermal conductivity of snow. If Equation (273) is written

$$\frac{\partial T_s}{\partial t} = \frac{1}{K_v} \frac{\partial^2 T_s}{\partial z^2} \qquad (274)$$

the constant K_v is called the thermal diffusivity of snow and is defined of course as

$$K_v = \frac{c_s \rho_s}{k_s} \qquad (275)$$

Thermal diffusivity at the pack is more useful expressed as a function of ice properties and snow density. Schwerdtfegar (1963) proposed

$$K_v = \frac{2k_i}{(3\rho_i - \rho_s)c_i} \qquad (276)$$

where k_i is the thermal conductivity of ice (0.005 cal/°C cm sec), ρ_i is the density of ice (0.917 g/cm^3), and c_i is the specific heat of ice (0.48

cal/°C g). Density of snow is taken as a bulk property of the entire pack. In this formulation it appears as an empirical function of pack water equivalent; that is,

$$\rho_s = f(W) \tag{277}$$

where W is pack water equivalent. This expression is a source of regional specificity in the model. It is intuitive that the snowpack in the dry Colorado mountains would have a lower bulk density than one would expect to be found in a pack of equivalent water content in the Pacific Northwest. The current formulation uses the expression that Leaf and Brink (1973) derived from data taken in the Fraser Experimental Forest in Colorado.

Equation (274) is solved in finite difference form by reference to the difference grid appearing in Figure 23. This formulation uses only three spatial nodes. One representing the pack-air interface, one the middle and one the pack pack-ground interface. With reference to Figure 23, Equation (274) in forward difference form becomes

$$\frac{T_{i,j+1}-T_{i,j}}{\Delta t} = \frac{T_{i+1,j}-2T_{i,j}+T_{i-1,j}}{\Delta z^2} \tag{278}$$

where $z = i\Delta z$

$t = j\Delta t$

Rewriting Equation (278) and noting that there are only three space nodes

$$T_{2,j+1} = T_{2,j} + \frac{\Delta t K_v}{\Delta z^2} (T_{1,j} - 2T_{2,j} + T_{3,j}) \tag{279}$$

From Equation (279) it is seen that the diffusion model is used to calculate only the temperature in the middle of the pack. Upper and lower boundary conditions are the average air temperature and the ground temperature, respectively. Ground temperature is assumed to be constant on a given day.

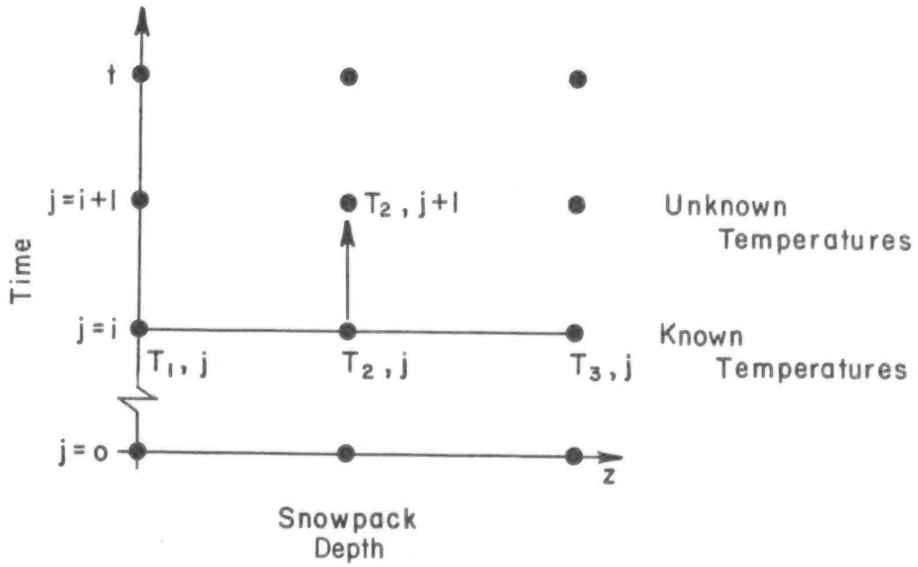
t
j=i+1
j=i
j=o
Time
T₂ , j+1
Unknown Temperatures
Known Temperatures
T₁ , j
T₂ , j
T₃ , j
z
Snowpack Depth

Figure 23. Finite difference grid for snowpack temperature.

The solution for Equation (274) may be shown to have a stability requirement of

$$\frac{K_v}{\Delta z^2} < 0.5 \tag{280}$$

Therefore, the snowpack must be greater than a specific depth for a given density to insure stability. The pack water balance routines use snowpack water equivalent rather than depth to represent snow accumulation. Therefore, the diffusion model is only used when the pack has a water equivalent greater than, in this case, 4.7 inches. When there is less water available, the thermal status of the pack is completely determined by precipitation and radiation balance. Temperature at the middle of the pack as calculated by the diffusion model is used to calculate the calorie deficit of the pack when the diffusion model is in use. If a descrepency in pack temperature exists between the values calculated by the diffusion model and that calculated by the radiation balance, the longwave radiation component is adjusted to equalize the temperatures.

The diffusion model performs the daily calculations in two twelve hour steps. As stated earlier, the model uses the average air temperature on upper boundary conditions. The average temperature is assumed to represent the integration at all of the important processes acting at the snowpack surface. In order to allow for better representation of temperature fluctuations during the day, a "high" average and a "low" average are calculated and used during the twelve hour periods.

In addition to low water equivalents, the diffusion model is also not used when the pack reaches isothermal conditions. This condition is normally reached prior to the onset of melt. Once the pack reaches the isothermal state, additional net energy inputs will result in the formation of free water. The pack is assumed to have a holding capacity for free water of 4% of its water equivalent. When the pack reaches the isothermal state and its free water holding capacity is satisfied it is termed "primed". Additional net energy inputs will result in runoff. During the time when the pack is isothermal, but still thick enough for diffusion model stability, the model is held in a "standby mode", so that if the pack cools again, it will be reinitialized and used again to calculate temperature and calorie deficit. Pack energy calculations are performed by the radiation balance routine during melt periods.

In the closing discussion of the diffusion model, it should be noted that the model will predict thermal status of the pack given environmental and initial condition data. However, observed values of pack temperature may be input during the winter on any given day in order to reinitialize the state of the pack. Such introduction of observed data, while not necessary, can measurably improve the accuracy of spring melt and runoff computations.

ENERGY BALANCE

As discussed above, thermal status of the pack may be calculated through either the diffusion model or radiation and energy balance techniques. Energy balance is used exclusively during times of melt due to the isothermal state of the pack, and during the recommendation period prior to reaching a pack thickness sufficient to insure stability of next transfer calculation.

SHORTWAVE RADIATION

Radiation inputs to the snowpack may be grouped into two classes, shortwave radiation and longwave or black body radiation. Shortwave energy is available to the snowpack directly from the sun. This energy is assumed to be directly measured by a horizontal radiometer somewhere in the vicinity of the site of interest. It is of course possible to calculate the solar radiation incident on the top of the atmosphere as a function of latitude and time of the year. However, as mentioned in the earlier section on evapotranspiration, transmissivity of the atmosphere is highly variable depending on cloud cover, humidity, suspended particulate, photo-chemical matter, and among other factors difficult to measure. Therefore, direct measurement of incoming shortwave energy is the most feasible method of estimating this input.

Shortwave input is highly dependent on slope and aspect of the irradiated slope. South facing slopes, receive much more energy during the day than a north facing slope. Most radiometers are placed in the open in a horizontal orientation. Therefore, for more precise estimates of available radiation, a correction should be made.

Correction equations are for radiation on the top of the atmosphere. It is assumed that the correction on these slopes has the same effect on ground surfaces at the same latitude. Declination angle of the sun S is a function at the time of year. It is given by

$$\delta = \mathrm{Sin}^{-1}(\sin(\delta_{max})\sin(\sigma) \tag{281}$$

where

$$\delta_{max} = 23.44(\frac{\pi}{180}) \tag{282}$$

$$\begin{aligned}\sigma = \frac{2\pi}{360}\ (279.9348 + \frac{360}{2\pi}\ d + 1.914827\ \sin(d)\\ - 0.079525\cos(d) + 0.019938\sin(2d)\\ - 0.001620\cos(24))\end{aligned} \tag{283}$$

and

$$d = \frac{2\rho}{365.242}\ (D-1) \tag{284}$$

where D is the Julian date or day number of the year.

The equation for instantaneous insolation at the top of the atmosphere q_o may be found (TVA, 1972) as

$$q_o = \frac{I_o}{r^2} \sin(\alpha) \tag{285}$$

where I_o is the solar constant 1.94 cal/cm^2 min, r is the ratio of the instantaneous earth-sun distance to the mean value of that distance, and α is the solar altitude angle given by

$$\sin(\alpha) = \sin(\phi)\ \sin(\delta) + \cos(\phi)\ \cos(\delta)\ \cos(\omega t) \tag{286}$$

Here, ϕ is the latitude of the point of interest and $\omega\tau$ is the hour angle. The value of r may be expressed as a function of day number by

$$r = 1 + 0.017 \cos\left(\frac{2\pi}{365}\ (186 - D)\right) \tag{287}$$

If Equation (285) is integrated over the illuminated portion at the day, the total insolation at that point at the top of the atmosphere may be obtained. If t represents the time in hours from solar noon, then this integration is given by

$$I_t = \frac{I_o}{r^2}\ (2t\sin(\phi)\sin(\delta) + \frac{2}{\omega}\cos(\phi)\cos(\delta)\sin(\omega\tau)) \tag{288}$$

where I_t is the total daily extraterrestrial isolation, and ω is the angular velocity of the earth. Time t may be found by calculating the times of sunrise and sunset. This is accomplished by setting $g_o = 0$ in Equation (285) and solving for t which yields

$$\cos(\omega t) = -\tan(\phi)\tan(\delta) \tag{289}$$

Frank and Lee, 1966, presented a tabular method for obtaining irradiation on slopes. This method was included in the Leaf and Brink model. However, the latitudes were somewhat limited and since the above equations were needed to shape the melt runoff to be discussed later, it was decided to implement the expression derived in the Frank and Lee paper directly. The overall approach is to determine a correction factor for horizontally measured irradiation. The technique used involves locating a slope of the earth that is equivalent to the surface of interest, but in a horizontal orientation. Okanowe (1957) presented the following equation for the adjusted latitude ϕ' and the change in longitude α (or hour angle) between the slope and its equivalent horizontal surface.

$$\phi' = \mathrm{Sin}^{-1}\ (\sin(k)\cos(h)\cos(\phi) + \cos(k)\sin(\phi)) \qquad (290)$$

and

$$\alpha = \mathrm{Tan}^{-1}\ [(\sin(h)\sin(k))/(\cos(k)\cos(\phi) - \cos(h)\sin(k)\sin(\phi))] \qquad (291)$$

where h is the slope azimuth and k is the slope inclination. When this new location is used to compute instantaneous insolation, the result is given by

$$q_o = \frac{I_o}{r^2}\ (\sin(\phi)\sin(\delta) + \cos(\phi)\cos(\delta)\cos(\omega t')) \qquad (292)$$

where

$$\omega t' = \omega \tau + \alpha \qquad (293)$$

The adjusted sunrise and sunset angles are given by

$$\cos(\omega t') = -\tan(\phi')\tan(\delta) \qquad (294)$$

Total adjusted daily radiation I_t' is given by

$$I_t' = \frac{I_o}{r^2}\ [(t_2 - t_1)\ \sin(\phi')\sin(\delta) + \frac{12}{\pi}\ \cos(\phi')\cos(\delta)(\sin(\alpha t_2') - \sin(\omega t_1'))] \qquad (295)$$

It should be noted that $\frac{12}{\pi}$ is $\frac{1}{\omega}$ in radians.

The ratio of adjusted extra terrestrial irradiation to local extraterrestrial irradiation is the correction factor for that day. As each set of correction factors is compiled for each slope in the watershed, these factors are multiplied times the measured radiation to give the corrected shortwave radiation for each slope.

LONGWAVE RADIATION

Longwave radiation is calculated by assuming that the source behaves as a black body. The basic equation for this phenomena is the Stephan-Boltzmann function

$$L_p = \sigma \, T_A{}^4 \tag{296}$$

where L_p is the potential longwave radiation for a body with absolute temperature T_A in langleys/day, σ is the Stephan-Boltzmann constant for a 24 hour period 1.17×10^{-7} langleys/day °K^4, and T_A is the absolute temperature of the radiator in °K. The Leaf-Brink model addresses four types of longwave radiation exchange. First from the sky to the snow. Here,

$$L_{SS} = \alpha(1-C_D) \, \sigma \, T_A{}^4 \tag{297}$$

where L_{SS} is the longwave input to the pack from the sky in langleys/day, C_D is the canopy cover density, and α is a longwave energy transmissivity constant for the atmosphere. The second transfer occurs from the forest cover to the snowpack. Here the transmissivity of the air may be ignored and

$$L_F = \sigma \, C_D \, T_F{}^4 \tag{298}$$

where T_F is the absolute temperature of the foliage. The snowpack itself radiates longwave energy and the transfer from the snow to the canopy L_{SF} is given by

$$L_{SF} = \sigma \, C_D \, T_S{}^4 \tag{299}$$

where T_S is the absolute temperature of the snow. Finally the snowpack also radiates to the sky and this radiation may be described by

$$L_{SS} = (1-C_D) \, \sigma \, T_S{}^4 \tag{300}$$

If, of course the thermal budget of the canopy is not being monitored, Equations (299) and (300) may be combined to give the total longwave radiation omitted by the pack as

$$L_S = \sigma T_S^4 \qquad (301)$$

However, under usual winter conditions, temperature of the snow is taken to be approximately equal to temperature of the forest canopy and the energies calculated by Equations (298) and (299) are equal and therefore balanced out. Thus, the only significant longwave energies are the transfers between the pack and sky described by Equations (297) and (299). When net radiation is computed, the program uses either the diffusion model or the result of the radiation balance to compute the new thermal status of the pack.

WATER BALANCE

Overall integration of the snowmelt model into the generalized planning model is guided by the concept that in locations where snowmelt is important and during cold times of the year the snowpack processes are the dominant hydrologic phenomena. Therefore a switch is made during the colder months to the Leaf and Brink model, returning to the PROSPR approach discussed earlier during the growing season. As discussed earlier the Leaf and Brink (1973b) model is intended to function as a hydrologic simulation in subalpine forests. Therefore, the model contains many components already discussed in the sections on evapotranspiration and water balance. Processes included here are potential evapotranspiration, soil months recharge, interception of snowfall, evaporation of snow and snowmelt.

POTENTIAL EVAPOTRANSPIRATION

One of the simplest approaches to estimating potential evapotranspiration (PET) is by the Hamon (1961) method. The expression used is as follows

$$E_p = C_h D^2 \bar{e}* \tag{302}$$

where C_h is the empirical constant introduced by Hamon (equal to 0.0055 in the units discussed below), D is the number of periods of 12 hour continuous sunshine in the month, $\bar{e}*$ is average daily value of saturation vapor pressure in g/m^3 at mean daily temperature, and E_p is the PET in inches/day. Since Equation (302) is an average expression for the United States, some adjustment of C_h may be made based on historical data to regionalize the expression. Leaf and Brink, 1973b, further adjusted the PET calculation to compensate for differences in observed and potential radiation. The final expression resulting from these adjustments is

$$E_t = \frac{R_s}{I_t'} C_h' D^2 \bar{e}* \tag{303}$$

where R_s is measured shortwave solar energy, C_h' is the adjusted Hamon constant, and I_t' is the total adjusted daily extraterrestrial radiation as defined earlier. The expression of adjusted Hamon PET is used to estimate evapotranspiration during the dormant part of the plant's annual growth cycle. For the present, a somewhat arbitrary decision is made to use this expression until a date corresponding to the beginning of the growth season is reached, and begin to use it again when a similar date ending the growth season is reached in the autumn. During the growing season, the approach described in Section 2 is utilized.

SOIL MANTLE RECHARGE

During the growing season, soil water balance is determined by the approach discussed in Section 2. However, this approach is inconsistent with the conditions prevailing during snow cover. Reduced ET and the possibility of frozen soil surfaces indicate that soil moisture movement will be severely limited during the colder months. Therefore, the simple soil mantle recharge method used by Leaf and Brink (1973b) is adapted. It is assumed that when the snowpack has reached isothermal conditions and is producing melt water runoff, the soil will accept water at the hydraulic conductivity adjusted for low temperatures. So long as there is a snowpack present, the infiltration rate is assumed to be constant. After the melt is complete the Green-Ampt approach as described in Section 2 is used.

Before the growing season has begun, any melt produced must satisfy the first layer recharge volume before runoff may be produced. This process is begun by adjusting the soil water content of the first layer based on the final value at the end of the growing season and any melt that may have occurred during the winter months. The resulting unfilled pore space is the volume that must be removed from the melt water before runoff. The value of soil water content immediately prior to the onset of the growth season becomes the initial moisture content of the upper soil layer for the methods of Section 2.

MELT WATER RUNOFF

The Leaf and Brink (1973a) snowmelt model was designed to produce daily runoff water yields. This type runoff description is inadequate for prediction of the water hydrographs required for simulation of nonpoint source pollution transport. A means for transforming the melt water volume into a snowmelt hyetograph is required. Since the melt occurs in response to the input of solar energy, it seems reasonable to approximate the snowmelt hyetograph by distributing the melt over the sunshine period using the hourly insolation divided by the total daily insolation as a weighting function. Since hourly measurements of insolation at the snowpack are not usually available it is assumed that the corresponding ratio of hourly extraterrestrial to total extraterrestrial radiation will suffice. This insolation weighted meltwater runoff function is subjected to infiltration of the saturated hydraulic conductivity, and the resulting excess runoff is treated by the routing models in the same manner as the excess rainfall described in Section 3.

SYMBOLS FOR SECTION 9

Symbol	Description
C_i	Specific heat of ice (cal/g °C)
C_s	Specific heat of snow (cal/g °C)
C_D	Canopy cover density
C_n	Hamon coefficient 0.0055
C'_n	Adjusted Hamon coefficient
D	Julian day of year
	Number of 12 hours periods of sunshine in a month
$\bar{e}*$	Average daily saturation vapor pressure (g/m^3)
E_p	Potential evapotranspiration (in/mon)
E_t	Adjusted potential evapotranspiration (in/mon)
h	
i	Space index
I_o	Solar constant (1.94 cal/cm^2 min)
I_t	Total daily insolation at top of atmosphere (langleys/day)
j	Time index
k	Slope inclination angle day
k_i	Thermal conductivity of ice (cal/°C cm sec)
k_s	Thermal conductivity of snow (cal/°C cm sec)
K_v	Thermal diffusivity of snow (cm^2/sec)
L_F	Longwave energy from foliage to air (langleys/day)

Symbol	Description
L_P	Longwave radiation (langleys/day)
L_S	Longwave energy loss from peak (langleys/day)
L_{SF}	Longwave energy from snow to foliage (langleys/day)
L_{SS}	Longwave energy from sky to snow (langleys/day)
q_o	Instantaneous insolation (langleys/min)
q_o	Instantaneous insolation at top of atmosphere (langleys/min)
r	Raio of instantaneous sun distance to mean value of that distance
R_s	Measured shortwave energy (langleys/day)
t	Time (sec)
T	Temperature (°C)
T_A	Absolute temperature (°K)
T_F	Temperature of foliage (°K)
T_s	Temperature of snowpack (°C)
W	Snowpack water content (in.)
z	Depth (cm)
α	Solar altitude angle (deg)
α	Longwave energy transmissity
δ	Declination angle of sun (deg)
δ_{max}	Maximum declination angle of sun (deg)
ρ_i	Density at ice (g/cm^3)
ρ_s	Density of snow (g/cm^3)
σ	Stephan-Boltzmann constant, $1.17x10^{-4}$ (langleys/day°K^4)
ϕ	Latitude (deg)
ϕ'	Latitude corrected for slope and aspect
ω	rotational velocity of earth (degs/sec)

REFERENCES

American Society of Civil Engineers. 1975. Task Committee on Sedimentation. Sedimentation Engineering. ASCE, New York.

Ardakami, M. S., J. T. Rehbock, and A. D. McLaren. 1973. Oxidation of Nitrate to Nitrate in a Soil Column. Soil Sci. Soc. Amer. Proc. 37:53-56.

Asher, C. J., and J. F. Loneragan. 1967. Response of Plants to Phosphate Concentration in Solution Culture: I. Growth and Phosphorus Content. Soil Sci. 103:225-233.

Barley, K. P. 1970. The Configuration of the Root System in Relation to Nutrient Uptake. Adv. Agron. 22:159-202.

Barnes, R. C., Jr. 1968. Streambank Erosion. Soil Conservation 33(6):126-128.

Bartlett, E. T., K. E. Bottoms, and R. P. Pope. 1976. GOAL--Multiple Objective Programming. Range Science Series No. 21, College of Forestry and Natural Resources, Colorado State University, Fort Collins, Colorado.

Bartlett, E. T., K. Boxmeyer, and S. L. Ponce. 1978. Planning Model for Evaluation of Alternative Forest Management Practices: The Allocation Model. Final Report submitted to the Environmental Protection Agency, Contract-Grant No. R80-5-13101.

Bhat, K. K. S., and P. H. Nye. 1973. Diffusion of Phosphate to Plant Roots in Soil: I. Quantitative Autoradiography of the Depletion Zone. Plant and Soil 38:161-175.

Box, J. E., W. H. Sletten, J. H. Kyle, and A. Pope. 1963. Effects of Soil Moisture, Temperature, and Fertility on Yield and Quality of Irrigated Potatoes in the Southern Plains. Agronomy Journal 55:482-484.

Broadbent, F. E., and O. C. Reyes. 1971. Uptake of Soil and Fertilizer Rice in Some Phillipine Soils. Soil Sci. 112:200-205.

Brooks, T. A. 1959. An Introduction to Physical Microclimatology. University of California, Davis.

Brooks, T. A., and D. G. Rhoades. 1954. Daytime Partition of Irradiation and the Evaporation Chilling of the Ground. Trans. American Geophysical Union 35:145-152.

Burwell, R. E., D. R. Timons, and R. F. Holt. 1975. Nutrient Transport in Surface Runoff as Influenced by Soil Cover and Seasonal Period. Soil Sci. Soc. Amer. Proc. 39:523-528.

Byran, S. M. 1948. Terrestrial Radiation and its Importance in Some Forestry Problems. Journal of Forestry 46(9):653-658.

Carson, J. E. 1963. Analysis of Soil and Air Temperature by Fourier Techniques. J. Geophys. Res. 68:2217-2232.

Carson, J. E. 1961. Soil Temperature and Weather Conditions. Agronne. Nat. Lab., ANL-6470. p. 244.

Charnes, A., and W. W. Cooper. 1961. Management Models and Industrial Applications of Linear Programming, Vol. 1. John Wiley, New York.

Chen, C. L. 1976. Flow Resistance in Broad Shallow Grassed Channels. Journal of the Hydraulics Division, ASCE, Vol. 102, No. HY3, March.

Chen, Y. R., J. N. Butler, and W. Stumn. 1973. Kinetic Study of Phosphate Reaction with Aluminum Oxide and Kaolinite. Environ. Sci. Tech. 7:327-332.

Churchill, N. S., R. S. Buckingham, and H. C. Elmore. 1962. The Prediction of Stream Reaeration Rates. Tennessee Valley Authority, Division Rates. Tennessee Valley Authoirty, Division of Health and Safety, Chattanooga. p. 98.

Cohon, J. L., and D. H. Marks. 1975. A Review and Evaluation of Multiobjective Programming Techniques. Water Resources Research 11(2):208-220.

Cooper, P. I. 1969. The Absorption of Solar Radiation in Solar Stills. Solar Energy, Vol. 12, No. 3.

Cowan, I. R. 1965. Tranpsort of Water in the Soil-Plant-Atmosphere System. J. Appl. Ecol. 2:221-239.

Cowan, I. R., and F. L. Milthorpe. 1968. Plant Factors Influencing the Water Status of Plant Tissues. In: Water Deficits and Plant Growth, Vol. 1. T. T. Kozlowski (Ed.). Academic Press, New York. pp. 137-193.

Dauer, J. P., and R. J. Krueger. 1977. An Iterative Approach to Goal Programming. Apl. Res. Q. 28(3), ii, pp. 671-681.

DeVries, D. A. 1952. The Thermal Conductivity of Soil. Meded. Landbouwhogeschool, Wageningen 52:72.

DeVries, D. A. 1963. Thermal Properties of Soils. In: Physics of Plant Environment, Van Wijk, W. R., (Ed.). North-Holland Publishing Co., Amsterdam. pp. 210-235.

Dobbins, W. E. 1964. BOD and Oxygen Relationships in Streams. J. San. Eng. Div., ASCE 90:53-78.

Donigian, A. S., Jr. 1976. Modeling Pesticides and Nutrients on Agricultural Lands. Environmental Protection Agency Technology Series. EPA-600/2-76-043.

Duffie, J. A., and W. A. Beckman. 1974. Solar Energy Thermal Process. John Wiley and Sons, New York City, New York.

Eggert, K. G. 1976. Modeling the Unsteady Infiltration Process, unpublished M.S. Thesis, Dept. of Civil Engineering, Colorado State University, Fort Collins.

Einstein, A. H. 1950. The Bed Load Function for Sediment Transportation in Open Channel Flows. U. S. Department of Agriculture Technical Bulletin No. 1026.

Frank, E. C. and R. Lee. 1966. Potential Solar Beam Irradiation on Slopes. Tables for 30° to 50° latitude, USDA, Forest Service Research Paper RM-66. Rocky Mountain Forest and Range Experiment Station, Fort Collins, Colorado.

Focht, D. D. 1974. The Effect of Temperature, pH, and Aeration on the Production of Nitrous Oxide and Gaseous Nitrogen-A Zero-Order Kinetic Model. Soil Sci. 118:173-179.

Freid, M., C. E. Hagen, J. F. Saize Del Rio, and J. E. Leggett. 1957. Kinetics of Phosphate Uptake in the Soil-Plant System. Soil Sci. 84:427-437.

Gates, D. M. 1968a. Energy Exchange between Organism and Environment. In: Biometeorology, W. P. Lowry (Ed.). Proc. 28th Annu. Bio. Colloquium. Oregon State University Press, Corvallis. 122 pp.

Gates, D. M. 1968b. Toward Understanding Ecosystems. Advanced Ecol. Res. 2:1-35.

Gladstone, S. 1946. Elements of Physical Chemistry. D. Van Norstrand Company, Inc., New York, New York.

Goldstein, R. A., and J. B. Mankin. 1972. PROSPER: A Model of Atmosphere-Soil-Plant Water Flow. Proceedings, Summer Simulation Conference, Los Angeles, pp. 1176-1181.

Goldstein, R. A., J. B. Mankin, and R. J. Luxmoore. 1974. Documentation of PROSPER, A Model of Atmosphere-Soil-Plant Water Flow. Oak Ridge National Laboratory, EDFB-IBP-73-9, Oak Ridge, Tennessee.

Granthan, G. R. 1950. Progress Report on Trickling Filter Studies. Sewage and Industrial Waste 22:867-874.

Green, R. E., and I. C. Corey. 1971. Calculation of Hydraulic Conductivity: A Further Evaluation of Some Predictive Methods. Soil Sci. Soc. Amer. Proc. 35:3-8.

Green, W. H., and G. A. Ampt. 1911. Studies on Soil Physics Part I: The Flow of Air and Water Soils. J. Agricultural Science, May.

Gunary, D. 1970. A New Adsorption Isotherm for Phosphate in Soil. J. Soil Sci. 21:72-77.

Haith, D. A. 1973. Optimal Control of Nitrogen Losses from Land Disposal Areas. J. Environmental Engr. Div. ASCE (EE6):923-937.

Hamon, W. R. 1961. Estimating Potential Evapotransporation. ASCE, Journal of the Hydraulics Division, Vol. 87, No. HY3.

Hanks, R. J., D. D. Austin, and W. T. Ondrechan. 1971. Soil Temperature Estimation by a Numerical Method. Dept. of Soils Meteorol., College of Agr., Utah State University, Logan. 9 pp.

Harley, B. M., F. E. Perkins, and T. S. Eagleson. 1970. A Modular Distributed Model of Catchment Dynamics. Massachusetts Institute of Technology, Department of Civil Engineering, Hydrodynamics Laboratory Report No. 133, June.

Harter, R. D. 1968. Adsorption of Phosphate by Lake Sediment. Soil Sci. Soc. Amer. Proc. 32:514-518.

Horton, R. E. 1945. Erosional Development of Streams and Their Drainage Basins; Hydrophysical Approach to Quantitative Morphology. Bulletin of the Geological Society of America 56:275-370.

Huang, C., and N. E. Hopson. 1974. Nitrification Rate in Biological Processes. J. Environmental Engr. Div., ASCE 110:409-422.

Humphreys, F. R., and W. L. Pritchett. 1971. Phosphorus Adsorption and Movement in Some Sandy Forest Soils. Soil Sci. Soc. Amer. Proc. 35:485-500.

Jenny, H. 1930. A study on the Influence of Climate upon the Nitrogen and Organic Matter Content of the Soil. Missouri Agricultural Experimental Station Research Bulletin.

Johnson, A. H., D. R. Bouldin, E. A. Gayette, and A. M. Hedges. 1976. Phosphorus Loss by Stream Transport form a Rural Watershed: Quantities, Processes, and Sources. J. Environ. Qual. 5:148-157.

Kibler, D. F., and D. A. Woolhiser. 1970. The Kinematic Cascade as a Hydrologic Model. Hydrology Paper No. 39, Colorado State University, Fort Collins.

Kissel, D. E., S. J. Smith, W. L. Hargrove, and D. W. Dillov. 1977. Immobilization of Fertilizer Nitrate Applied to a Swelling Clay Soil in the Field. Soil Sci. Soc. Amer. Proc. 41:346-349.

Kittredge, J. 1962. The Influence of the Forest on the Weather and Other Environmental Factors. Forest Influence, FAD 15:81-137.

Kittrell, F. W., and O. W. Kochtitzky. 1947. Natural Purification Characteristics of a Shallow Turbulent Stream. Sewage Works Journal 19(6).

Kuo, S., and E. G. Lotse. 1972. Kinetics of Phosphate Adsorption by Calcium Carbonate and Ca-Kaolinite. Soil Sci. Soc. Amer. Proc. 36:725-729.

Kuo, S., and E. G. Lotse. 1973. Kinetics of Phosphate Adsorption and Desorption by Hematite and Gibbsite. Soil Sci. 116:400-406.

Larsen, S. 1967. Soil Phosphorus. Adv. Agron. 19:151-210.

Larsen, S., D. Gunary, and C. D. Sutton. 1965. The Rate of Immobilization of Applied Phosphate in Relation to Soil Properties. J. Soil Sci. 16:141-148.

Leaf, C. F. and G. E. Brink. 1975. Land Use Simulation Model of the Subalpine Coniferous Forest Zone. USDA Forest Service Research Paper RM-135, Rocky Mountain Forest and Range Experimental Station, Fort Collins, Colorado.

Leaf. C. F. and G. E. Brink. 1973b. Hydrologic Simulation Model of Colorado Subalpine Forest. USDA Forest Service Research Paper RM-107, Rocky Mountain Forest and Range Experiment Station, Fort Collins, Colorado.

Leaf, C. F. and G. E. Brink. 1973a. Computer Simulation of Snowmelt within a Colorado Subalpine Watershed. USDA Forest Service Research Paper RM-99, Rocky Mountain Forest and Range Experiment Station, Fort Collins, Colorado.

Lee, C. B. 1970. Kentucky Air-Soil Temperature Climatology. U.S. Dept. of Commerce, Weather Bur.--Central Region, Kansas City, Missouri. ESSA Tech. WBTMCR-33. 15 pp.

Lee, S. M. 1972. Goal Programming for Decision Analysis. Auerbach.

Leopold, L. B., and T. Maddock. 1953. The Hydraulic Geometry of Stream Channels and Some Physiographic Implications. U.S. Geological Survey, Professional Paper 252, Washington, D.C.

Leopold, L. B., M. G. Wolman, and J. P. Miller. 1964. Fluvial Processes in Geomorphology. W. H. Freeman and Company, San Francisco, California.

Li, R. M. 1974. Mathematical Modeling of Response from Small Watersheds. Ph.D. Dissertation, Department of Civil Engineering, Colorado State University, Fort Collins.

Li, R. M., D. B. Simons, and M. A. Stevens. 1975. Nonlinear Kinematic Wave Approximation for Water Routing. Water Resources Research 11(2).

Li, R. M., D. B. Simons, and M. A. Stevens. 1976. Morphology of Cobble Streams in Small Watersheds. J. Hydraul. Div., ASCE, 12(HY8):1101-1112.

Liao, C. F. H., and W. V. Bartholomew. 1974. Relation between Nitrate Absorption and Water Transpiration by Corn. Soil Sci. Amer. Proc. 38:472-476.

Lindsay, W. L. 1978. Chemical Equilibria in Soil. John Wiley and Sons, Inc., New York, New York.

Loneragan, J. F., and C. J. Asher. 1967. Response of Plants to Phosphate Concentration in Solution Culture: II. Rate of Phosphate Absorption and its Relation to Growth. Soil Sci. 103:311-317.

Loucks, D. P. 1975. Conflict and Choice: Planning for Multiple Objectives. In: Economy Wide Models and Development Planning, edited by C. Blitzer, P. Clark, and L. Taylor, Oxford University Press, New York.

Lull, H. W., and I. C. Reigner. 1967. Radiation Measurements by Various Instruments in the Open and in the Forest. U.S. Forest Service. Northeast Forest Experiment Station Research Paper No. NE-84. 21 pp.

Luxmoore, R. J., D. J. Van Roagen, F. D. Hale, J. B. Mankin, and R. A. Goldstein. 1977. Field Water Balance and Simulated Water Relations of Prairie and Oak-Hickory Vegetation on Deciduous Forest Soils. Soil Sci. 123(2):77.

Mahtab, S. K., A. R. Swoboda, C. L. Godfrey, and G. W. Thomas. 1972. Phosphorus Diffusion in Soil: II. The Effect on Phosphorus Uptake by Plants. Soil Sci. Soc. Amer. Proc. 36:55-57.

McElroy, A. D., S. Y. Chiu, J. W. Nebgen, A. Aleti, and F. W. Bennett. 1976. Loading Functions for Assessments of Water Pollution from Nonpoint Sources. Environmental Protection Agency Technology Series. EPA-600/2-76-151.

McKenzie, T. E. 1924. The Effect of Irrigation upon Soil Temperature. Technical and Scientific Service Bulletin 53. Department of Agriculture, Egypt. 10 pp.

McLaren, A. D. 1971. Kinetics of Nitrification in Soil: Growth of the Nitrifiers. Soil Sci. Soc. Amer. Proc. 35:91-95.

Mehran, M., and K. K. Tanji. 1974. Computer Modeling of Nitrogen Transportations in Soil. J. Environ. Qual. 3:391-396.

Mein, R. G., and C. L. Larson. 1973. Modeling Infiltration During a Steady Rain. Water Resources Research 9(2).

Meyer, L. D. 1971. Soil Erosion by Water on Upland Areas. River Mechanics, Vol. II, edited by H. W. Shen, Fort Collins, Colorado.

Meyer, L. D., G. R. Foster, and M. J. M. Römkens. 1975. Source of Soil Eroded by Water from Upland Slopes. USDA, Agricultural Research Service Publication ARS-S-40, June.

Miyake, K. 1916. On the Nature of Ammonification and Nitrification. Soil Sci. 2:481-492.

Mortland, M. M. and A. R. Wolcott. 1965. Sorption of Inorganic Nitrogen Compounds by Soil Materials. Soil Nitrogen, Madison, Wisc., Amer. Soc. Agron., Agronomy Monography No. 10, pp. 150-197.

Nedwell, D. B. 1975. Inorganic Nitrogen Metabolism in Eutrophicated Tropical Mangrove Estuary. Water Resources 9:221-231.

Neilsen, G. H., and A. F. Mackenzie. 1977. Soluble and Sediment Nitrogen Losses as Related to Land Use and Type of Soil in Eastern Canada. J. Environ. Qual. 6:318-321.

Nye, P. H. 1966. The Effect of the Nutrient Intensity and Buffering Power of a Soil, and the Absorbing Power, Size and Root Hairs of a Root on Nutrient Absorption by Diffusion. Plant and Soil 25:81-105.

Okanoue, M. 1957. A Simple Method to Compute the Amount of Sunshine on a Slope. Journal of Japanese Forests, Nov., pp. 435-437.

Olsen, S. R., and W. D. Kemper. 1968. Movement of Nutrients to Plant Roots. Adv. Agron. 20:91-152.

Parker, D. T., and W. E. Larson. 1962. Nitrification as Affected by Temperature and Moisture Content of Mulched Soils. Soil Sci. Soc. Amer. Proc. 26:238-242.

Penrod, F. B., and O. W. Steward. 1967. Determining Thermal Properties of a Soil and the Periodic Transfer of Solar Energy in the Earth. Soc. Agr. Eng. Trans. 10(3):359-363.

Reifsnyder, W. E., and H. W. Lull. 1965. Radiant Energy in Relation to Forest. U.S. Department of Agriculture, Forest Service, Technical Bulletin No. 1344, 111 pp.

Roussel, L. 1948. Canopy and Photometry. Bull. Soc. For. Franche-Comté 25(8):313-326. (In French).

Saxton, K. E., G. E. Schuman, and R. E. Burwell. 1977. Modeling Nitrate Movement and Dissipation in Fertilizer Soil. Soil Sci. Soc. Amer. Proc. 41:265-271.

Schumm, S. A. 1960. The Shape of Alluvial Channels in Relation to Sediment Type. U.S. Geological Survey, Professional Paper 352-B, Washington, D.C. pp. 17-30.

Schwerdtfeger, P. 1963. Theoretical Derivation of the Thermal Conductivity and Diffusivity of Snow. UGGI, International Association of Scientific Hydrology Commission Publication 61.

Seshu, S., and N. Belabanian. 1963. Linear Network Analysis. John Wiley and Sons, London. 571 pp.

Seyers, J. K., M. G. Browman, G. W. Smillie, and R. B. Corey. 1973. Phosphate Sorption by Soils Evaluated by the Langmuir Adsorption Equation. Soil Sci. Soc. Amer. Proc. 37:358-363.

Sharma, R. C., and A. B. Ghosh. 1976. A Note on the Leaching Behavior of Urea and Ammonium Nitrate. J. India Soil Sci. 24:238-239.

Simons, D. B., R. M. Li, and K. G. Eggert. 1976. Storm Water and Sediment Runoff Simulation for Upland Watersheds Using Analytical Routing Technique, Volume I-Water Routing and Yield, Colorado State University, Engineering Report CER77-78DBS-RML-KGE16, Prepared for USDA Forest Service, Rocky Mountain Forest and Range Experiment Station, Flagstaff, Arizona, April.

Simons, D. B., R. M. Li, and B. E. Spronk. 1978. Storm Water and Sediment Runoff Simulation for a System of Multiple Watersheds. Vol. I, Water Routing and Yield. Prepared for Forest Service, Rocky Mountain Forest and Range Experiment Station, Flagstaff, Arizona. CSU No. CER77-78DBS-RML-BES47. April.

Simons, D. B., R. M. Li, and M. A. Stevens. 1975. Development of Models for Predicting Water and Sediment Routing and Yield from Storms on Small Watersheds, prepared for USDA Forest Service, Rocky Mountain Forest and Range Experiment Station, Flagstaff, Arizona.

Simons, D. B., R. M. Li, and T. J. Ward. 1977. Estimation of Parameters for Describing Channel Geometry for Watershed Modeling, Colorado State University, Engineering Report CER77-78DBS-RML-TJW12, prepared for USDA Forest Service, Rocky Mountain Forest and Range Experiment Station, Flagstaff, Arizona, December.

Stanford, G., and E. Epstein. 1974. Nitrogen Mineralization-Water Relations in Soils. Soil Sci. Soc. Amer. Proc. 38:103-197.

Stanford, G., M. H. Frere, and D. H. Schwaninger. 1973. Temperature Coefficient of Soil Nitrogen Mineralization. Soil Sci. 115:321-323.

Stanford, G., and S. J. Smith. 1972. Nitrogen Mineralization Potentials of Soils. Soil Sci. Soc. Amer. Proc. 36:465-472.

Stanford, G., R. A. Vander Pol, and S. Dzienia. 1975a. Denitrification Rates in Relation to Total and Extractable Soil Carbon. Soil Sci. Soc. Amer. Proc. 39:284-289.

Stanford, G., R. A. Vander Pol, and S. Dzienia. 1975b. Effect of Temperature on Denitrification Rate in Soils. Soil Sci. Soc. Amer. Proc. 39:867-870.

Streeter, H. W., and E. B. Phelps. 1925. A Study of the Pollution and Natural Purification of the Ohio River. Public Health Bulletin 146, U.S. Public Health Service, Washington, D.C.

Swanson, F. J., and G. W. Lienkaemper. 1975. The History and Physical Effects of Large Organic Debris in Western Oregon Streams. In: Workshop: Logging Debris in Streams, Department of Forest Engineering, Oregon State University, Corvallis, Oregon, September 9-10.

Swift, L. W., W. T. Swank, J. B. Mankin, R. J. Luxmoore, and R. A. Goldstein. 1975. Simulation of Evapotranspiration and Drainage from Mature and Clear-Cut Deciduous Forests and Young Pine Plantations. Water Resources Research 11(5):667.

Tanner, C. B. and W. C. Pelton. 1960. Potential Evapotranspiration Estimates by the Approximate Energy Balance Method of Penman. Geophys. Res. 65:3391-3414.

Tennessee Valley Authority, Division of Water Control Planning, Engineering Laboratory. 1972. Heat and Mass Transfer between a Water Surface and the Atmosphere. Water Resources Research, Laboratory Report No. 14, Norris, Tennessee.

U.S. Bureau of Reclamation. 1960. Investigation of Meyer-Peter, Müller Bedload Formulas. Sedimentation Section, Hydrology Branch, Div. of Project Investigation, U.S. Department of Interior.

U. S. Congress, House of Representatives. 1969. A Study of Streambank Erosion in the United States. Army Corps of Engineers. Report to Committee on Public Works, Washington, D.C.

Van der Honert, T. H., and J. J. M. Hooymons. 1955. On the Absorption by Maize in Water Culture. Acta Bot. Neerlandria 43:376-384.

Van Wijk, W. R., and D. A. DeVries. 1966. The Atmosphere and the Soil. In Physics of Plant Environment, W. R. Van Wijk (Ed.). North-Holland Publishing Co., Amsterdam. pp. 17-61.

Wellner, C. A. 1948. Light Intensity Related to Stand Density in Natural Stands of the Western White Pine Type. Journal of Forestry 46(1):16-18.

Wierenga, P. J., R. M. Hagan, and E. J. Gregory. 1971. Effects of Irrigation Water Temperature on Soil Temperature. Agron. J. 66:33-36.

Wong-Chong, G. M., and R. C. Loehr. 1975. The Kinetics of Microbial Nitrification. Water Research 9:1099-1106.

Wooding, R. A. 1965. A Hydraulic Model for the Catchment-Stream Problem: I. Kinematic Wave Theory. Journal of Hydrology 3(3).

Woolhiser, D. A. 1975. Simulation of Unsteady Overland Flow. In: Unsteady Flow in Open Channels, edited by K. Mahmood and V. Yevjevich, Water Resources Publications, Fort Collins, Colorado.